Monitoring land cover change with LiDAR and aerial imagery in Christchurch, New Zealand

---

A thesis submitted in partial fulfilment

of the requirements for the Degree of

Master of Geographical Information Science (GIS)

by

Zhao Haotian

Department of Geography

University of Canterbury

2018

Contents

List of Figure

List of Table

Abstract

Land cover change information in urban areas supports decision makers in dealing with public policy planning and resource management. Remote sensing has been demonstrated as an efficient and accurate way to monitor land cover change over large extents. The Canterbury Earthquake Sequence (CES) caused massive damage in Christchurch, New Zealand and resulted in significant land cover change over a short time period. This study combined two types of remote sensing data, aerial imagery (RGB) and LiDAR, as the basis for quantifying land cover change in Christchurch between 2011 – 2015, a period corresponding to the five years immediately following the 22 February 2011 earthquake, which was part of the CES.

An object based image analysis (OBIA) approach was adopted to classify the aerial imagery and LiDAR data into seven land cover types (bare land, building, grass, shadow, tree and water). The OBIA approach consisted of two steps, image segmentation and object classification. For the first step, this study used multi-level segmentation to better segment objects. For the second step, the random forest (RF) classifier was used to assign a land cover type to each object defined by the segmentation.

Overall classification accuracies for 2011 and 2015 were 94.0% and 94.32%, respectively. Based on the classification result, land cover changes between 2011 and 2015 were then analysed. Significant increases were found in road and tree cover, while the land cover types that decreased were bare land, grass, roof, water. To better understand the reasons for those changes, land cover transitions were calculated. Canopy growth, seasonal differences and forest plantation establishment were the main reasons for tree cover increase. Redevelopment after the earthquake was the main reason for road area growth. By comparing the spatial distribution of these transitions, this study also identified Halswell and Wigram as the fastest developing suburbs in Christchurch. These results provided quantitative information for the effects of CES, with respect to land cover change. They allow for a better understanding for the current land cover status of Christchurch.

Among those land cover changes, the significant increase in tree cover aroused particularly interest as urban forests benefit citizens via ecosystem services, including health, social, economic, and environmental benefits. Therefore, this study firstly calculated the percentages of tree cover in Christchurch's fifteen wards in order to provide a general idea of tree cover change in the city extent. Following this, an automatic individual tree detection and crown delineation (ITCD) was undertaken to determine the feasibility of automated tree counting. The accuracies of the proposed approach ranged between 56.47% and 92.11% in thirty different sample plots, with an overall accuracy of 75.60%. Such varied accuracies were later found to be caused by the fixed tree detection window size and misclassifications from the land cover classification that affected the boundary of the CHM. Due to the large variability in accuracy, tree counting was not undertaken city-wide for both time periods. However,

directions for further study for ITCD in Christchurch could be exploring ITCD approaches with variable window size or optimizing the classification approach to focus more on producing highly accurate CHMs.

Acknowledgements

Firstly, I want to express my sincere gratitude to my senior supervisor, Dr. Justin Morgenroth. He consistently steered me in the right the direction whenever he thought I needed it and always available to answer questions. I could not have imagined having a better advisor and mentor for my Masters research.

Secondly, I want to thank my co-supervisor Dr. Xu Cong for her insightful comments and encouragement. She also taught me many practical skills which enabled me to better finish my research.

Thirdly, I want to thanks everyone in the remote sensing and geospatial analysis lab. It was a great experience to work with them for the past year. Discussing and chatting with them can always provide me with new ideas and new skills.

Last but not least, I must express my very profound gratitude to my parents for providing me with strong support and continuous encouragement throughout my study and through the process of researching and writing this thesis. Thank you.

Chapter 1- Introduction

1.1 Land cover classification

Land cover is the biophysical description of the Earth's surface (Lambin et al., 2001). With the continued growth of productivity and the increase in world population density, land covers in different areas are experiencing significant changes in a very short period. Compared with natural areas, 54.3% of the world's population live in urban areas, which only account for less than 2% of the Earth's land surface (The World Bank, 2016). Despite the relatively small extent of the urban areas, intensive human activities have resulted in land cover changes within and outside these areas. Effective and accurate monitoring of these changes is important because it provides valuable information for assessing the environmental effects and supporting better planning.

Remote sensing technologies collect electromagnetic energy (e.g. visible lights, radio waves, laser pulses) that is reflected off objects on Earth's land surfaces, ocean or atmosphere (Short, 2010). Acquisition of remotely sensed data is undertaken by sensors carried on different platforms such as satellite and aerial crafts. The high altitudes of these platforms allow a sensor to efficiently observe a large area with limited costs (Khorram, 2012). Consequently, remote sensing is well suited for monitoring land cover for large extents such as a city or a region (Xiubin, 1996). Remote sensing sensors can be divided into two types: passive sensors and active sensors. The former type collects reflected or emitted electromagnetic energy generated by natural sources (e.g. sunlight), while the latter generate and emit their own source of energy (e.g. laser lights) and then collects the reflected energy.

Multispectral sensors are commonly used passive sensors and the multispectral imagery collected by them is one of the primary sources of data for land cover classification (Haack & Mahabir, 2018). Some remote sensing platforms that collect multispectral imagery have been continuously run for decades and provide valuable historical data for land cover change comparison (Marshall & Thenkabail, 2015; Phiri & Morgenroth, 2017). Using only multispectral imagery, land cover classification accuracies exceeding 75% have been achieved in cities (Alqurashi, Kumar, & Sinha, 2016; Lu, Hetrick, & Moran, 2010; Myint, Gober, Brazel, Grossman-Clarke, & Weng, 2011; Shackelford & Davis, 2003; Yuan, Sawaya, Loeffelholz, & Bauer, 2005). When surveying land surfaces, multispectral sensors measure spectral reflectance as the sun's radiation reflects off the surface of the Earth. As a result, it is highly affected by surrounding conditions such as weather and cloud cover. Besides, distinguishing land covers with similar spectral characteristics can be problematic for multispectral data. Common examples are road and river gravels (Stefanov, Ramsey, & Christensen, 2001), road and buildings, trees and grass (Zhang, Huang, Huang, & Li, 2006), as well as crop fields and wetlands (Yuan et al., 2005).

Urban land cover features are heterogeneous and complex, using spectral information alone generally fails to yield accurate land cover classification. Combining multispectral data with other remotely-sensed data like LiDAR (light detection and ranging) data is one solution for improving the classification accuracy (Li, Gu, Han, & Yang, 2007). LiDAR is an active remote sensing technology which can accurately measure changes in the vertical profile of the surface of the Earth or objects on it (Jensen, 2007). Despite limited spectral information, LiDAR has been widely used for specific urban land cover identification, such as buildings (Wang & Schenk, 2000) and trees (Zhang, Zhou, & Qiu, 2015) and also for general land cover classifications (Chen & Gao, 2014; Singh, Vogler, Shoemaker, & Meentemeyer, 2012; Zhu & Toutin, 2013). Fusing LiDAR data with multispectral data can take advantage of the benefits of each sensor. Many studies which integrated LiDAR and multispectral data for urban land cover classifications have shown improvements in overall accuracy, ranging from 5% to 32% (Kim, 2016; Koetz, Morsdorf, Van der Linden, Curt, & Allgöwer, 2008; Singh et al., 2012).

1.2 Land cover classification in Christchurch, New Zealand

The Canterbury Earthquake Sequence (CES) of 2010-2011 caused significant damage to the city of Christchurch in New Zealand. Environmental effects of the CES included surface rupture and deformation, river avulsion and flooding, liquefaction, mass movement of soil, hydrological changes, as well as damage to urban trees and other flora and fauna (Quigley et al., 2016). In addition, buildings and other infrastructures were also affected by the earthquakes (Cole, Dhakal, & Turner, 2012). In response to these effects, the government made a series of rebuilding and recovery plans. For example, the Canterbury Earthquake Recovery Authority (CERA) divided the city into four different zones according to the levels of damage. The worst damaged zones involved 7,857 properties whose buildings needed to be demolished to ensure public safety; these areas have been re-zoned and newly built structures are not presently permitted (LINZ, 2017). As a result of the effects from the CES, land cover in Christchurch experienced dramatic changes in a short period of time.

Tree cover was one of the land covers which was affected by the CES. Localized studies of small-scale areas within Christchurch determined that trees were lost due to changes in the soil environment and the redevelopment processes (Morgenroth & Armstrong, 2012; Morgenroth, O'Neil-Dunne, & Apiolaza, 2017). This is of particular concern as trees, and urban forests as a whole, benefit citizens via a large number of ecosystem services, including health, social, economic, and environmental benefits (Roy, Byrne, & Pickering, 2012). A multi-temporal land cover classification could provide a greater understanding of the land cover changes, including changes in tree cover that occurred in Christchurch following the CES.

1.3 Research objectives

The main objective of this research is to qualify and quantify the land cover change in the 4 year period (2011-2015) immediately following the February 2011 earthquakes in Christchurch, using LiDAR and aerial imagery data. To achieve this, the research also explores some methodological questions for processing remote sensing data for land cover classification. Specifically, the objectives are as follows:

1. To explore the optimum methodological steps for the land cover classification of Christchurch. These options including algorithms for LiDAR surfaces interpolation, classification techniques, classifiers and their parameter settings
2. To describe the land cover change in Christchurch by quantifying land cover in 2011 and 2015 by describing land cover transitions, and by describing the spatial distribution of transitions.
3. To determine the net change in the number of trees between 2011 and 2015, using individual tree crown delineation (ITCD).

1.4 Thesis structure

Chapter 1 provides a general introduction on the background information of urban land cover, remote sensing data classification, and individual tree crown detection and delineations (ITCD). It also outlines the objectives and the structure of the research.

Chapter 2 reviews literature related to urban land cover change, classification techniques for multispectral imagery and LiDAR data, urban forests, as well as, ITCD.

Chapter 3 presents the land cover classification using LiDAR and aerial imagery fusion and land cover changes between 2011 and 2015 at Christchurch city. Assessment of classifications and reasons for land cover changes are also discussed in this chapter.

Chapter 4 presents ITCD using LiDAR data. This study was conducted after deriving tree covered areas with land cover classification results from the previous chapter.

Chapter 5 discusses the combined results of chapter 3 and 4 in the context of the CES and the research objectives listed above. It concludes by suggesting areas for future research.

Chapter 2 - Literature review

2.1 Urban land cover analysis with multispectral data

Urban land cover information provides important input data for a wide range of fields such as environmental science, urban management, and sociology studies (Stefanov et al., 2001). Results from those studies provide not only assessments of the environmental effects caused by land cover change in the past (Chen & Stow, 2002; Dewan & Corner, 2012; Rastandeh, Pedersen Zari, & Brown, 2018) but also predictions of future changes in terms of urban sprawl pattern (López, Bocco, Mendoza, & Duhau, 2001), biodiversity (Hepinstall-Cymerman, 2011), urban runoff (Berezowski, Chormański, Batelaan, Canters, & Van de Voorde, 2012) and so forth.

With the development of remote sensing technology, deriving accurate land cover information from remote sensing data becomes possible (Yang, Xian, Klaver, & Deal, 2003). Among different types of data, multispectral imagery is one of the most commonly used data for land cover classification (Haack & Mahabir, 2018). Multispectral data can be acquired from different platforms such as satellite and aerial planes. When surveying land surfaces, multispectral sensors measure spectral reflectance as the sun's radiation reflects off the surface of the Earth. Land cover types can then be distinguished according to their spectral reflectance differences (Khorram, 2012).

For satellite platforms, the cycle of acquiring data could range from around three days (Quickbird) to more than several weeks (Landsat, SPOT) depending on operation orbits (Gao, Masek, Schwaller, & Hall, 2006; Sifakis & Deschamps, 1992). Some platforms equipped with multispectral sensors have been run for decades and provide continuous data that enables land cover change detection over a long time span (Marshall & Thenkabail, 2015). Yuan et al. (2005) analysed the land cover change in a metropolitan area of Minnesota, USA, using multispectral images between 1986 and 2002 from Landsat satellite platforms. The images have a spatial resolution of 30 m and the overall classification accuracies ranged from 93.5% to 95.5%. Alqurashi et al. (2016) also used Landsat images to compare the land cover change of five cities in Saudi Arabia within 30 years. The accuracy ranged was 82% to 96%. In another study conducted by Yuan (2008), high-resolution imagery (2.4 m resolution) from Quickbird satellite was used for detecting land cover change in the Greater Mankato area, USA. The accuracy reached approximately 93%.

Compared with satellite imagery, aerial imagery usually contain less spectral information because the sensors for aerial imaging have a narrow spectral capture range (Cox, 1992). However, the low acquisition altitude provides aerial imagery with a much higher spatial resolution than satellite imagery, which can allow for a more detailed land cover classification (Wentz, Stefanov, Gries, & Hope, 2006).

Aerial imagery is also more flexible with respect to acquisition time. This enables observations of land cover change for specific purposes and periods, for example, earthquake damage and recovery assessment. A study conducted by Al-Kofahi, Steele, VanLeeuwen, and Hilaire (2012) used aerial imagery to classify land cover in Albuquerque, New Mexico, the USA into trees, shrubs, grass, and non-greenspace. With only spatial and textural variables derived from true-colour aerial photos, they received an overall accuracy of 89%. Caccetta et al. (2016) used aerial imagery with red, green, blue and near-infrared bands to classify land cover as vegetation and non-vegetation areas for parts of Perth, Australia. By comparing with ground reference data for three sites, the overall accuracies ranged from 94% to 98%. Multi-temporal aerial imagery with only RGB bands (red, green and blue) was used in a study by Walker and Blaschke (2008), who classified land cover in the Phoenix metropolitan area, USA, into four types: soil, grass, woody building, sealed surfaces. The overall accuracy reached 84%. Zhang et al. (2018) conducted a similar study in an urban district of Wuhan, China. They classified the aerial RGB imagery into five classes, water, building, vegetation, bare land and road, and received overall accuracies with a range from 86.29% to 96.35% (Moskal, Styers, and Halabisky (2011)).

Despite wide-spread application, acquisition of multispectral data is highly affected by illumination conditions because it collects reflected energy generated from sunlight (Khorram, 2012). For both satellite and aerial spectral imagery, factors such as cloud cover and shadow will cause poor data quality and lead to misclassification (Dare, 2005). In addition, distinguishing land covers with similar spectral characteristics can be problematic when using only multispectral data. Common examples are road and river gravels (Stefanov et al., 2001), roads and buildings, trees and grass (Zhang et al., 2006), as well as crop fields and wetlands (Yuan et al., 2005).

2.2 Urban land cover analysis with LiDAR data

LiDAR is an active remote sensing technology which describes features by calculating the travel time between the transmission of a laser pulse from a sensor and subsequent receipt of the pulse after it has reflected off the ground or above-ground feature (Jensen, 2007). Due to the high-resolution and accuracy in both horizontal and vertical directions, airborne LiDAR is widely used in digital elevation model generation, building extraction and tree modelling (Bandyopadhyay, van Aardt, & Cawse-Nicholson, 2013; Li et al., 2007; López et al., 2001). Using this information, researchers have achieved high accuracy in classifying urban land cover types (Table 2-1).

LiDAR-derived height features such as digital elevation model (DEM), digital surface model (DSM) and normalized digital surface model (nDSM) are the most commonly used surfaces for urban land cover classification. These digital models are interpolated from LiDAR points and then analysed with classification methods comparable to those for raster imagery interpretation. Charaniya, Manduchi, and

Lodha (2004) classified raster images which were interpolated by LiDAR data into 4 classes using a supervised parametric classification algorithm (Gaussian mixture models). The overall accuracy was in the range of 66%-84% depending on the combination of features. Shaker and El-Ashmawy (2012) classified land cover in a small urban area (part of the British Columbia Institute of Technology located in the Burnaby, British Columbia, Canada) with different feature combinations generated from LiDAR data. They found that by integrating those LiDAR-derived features, the overall classification accuracy ranged between 43.1% and 77.2%. Apart from the common urban land cover types, Zhou (2013) extracted high-voltage-electric wires by analysing the elevation and slope features in nDSM derived from LiDAR data. The overall classification accuracy including other five land cover types reached 89.37%.

Compared with classifying LiDAR-derived raster surfaces, some studies directly classified LiDAR point clouds. Alexander, Tansey, Kaduk, Holland, and Tate (2010) used decision trees to classify points into different urban land cover types and resulted in 73%-92% classification accuracy. Tang, Dong, and Buckles (2012) used two features, height and normal variation, derived from LiDAR data to extract buildings and trees points in a downtown area at New Orleans, State of Louisiana, USA. The classification accuracy for these two land cover types reached 92%.

In addition to the DEM, DSM and nDSM, returns of LiDAR pulse can be a supplementary source for identifying land cover types, especially for differentiating roof and trees. Most LiDAR pulses which hit on surface objects such as trees or vegetation often have more than one return. For land covers such as roads and roofs, LiDAR could have a single return. Nordbo, Karsisto, Matikainen, Wood, and Järvi (2015) made a land cover classification with six LiDAR-derived variables for a part of the capital city of Finland, Helsinki. Returns of each LiDAR pulse was one of the variables that proved useful in effectively distinguishing high-rise buildings and trees. The classification accuracy for these two land cover types ranged 88.9%-93.3% and 89.2%-92.6%, respectively. Brennan and Webster (2006) interpolated a return per pulse surface to assist classification after adding echo information attributes for point clouds. They finally received a 94.31% overall accuracy for an area including building structures and vegetation in the Annapolis Valley, Nova Scotia, Canada.

Intensity information of LiDAR pulses was also considered by many studies (Samadzadegan, Bigdeli, & Ramzi, 2010; Shaker & El-Ashmawy, 2012; Zhou, 2013). Intensity data usually contain noise and require correction. Yoon, Shin, and Lee (2008) discussed the influence of radiometric correction and data noise of intensity on land type classification. The results showed that LiDAR intensity data cannot be used for identifying vegetation. Yan, Shaker, Habib, and Kersting (2012) discussed the effects of geometric and radiometric corrections on LiDAR intensity data for land cover classification. The correction process required detailed configuration information from a LiDAR sensor and survey routine data. The results showed the classification accuracy improved by 9.4–12.8%. Considering that some

corrections are unfeasible and unsustainable quality, intensity data is not suitable for studies with limited time and resources.

Table 2-1: A list of studies using LiDAR and fusion data for urban land cover classification

Source	Data Type	Land Cover Type	Classification method	Overall accuracy
Charaniya et al. (2004)	LiDAR	Tree, grass, road, roof	pixel-based; Gaussian mixture models	66% to 84%
Brennan and Webster (2006)	LiDAR	Bright structures, coniferous; deciduous; dark structures; lush low vegetation; non-saturated intertidal; roads; saturated intertidal; saturated or stressed low vegetation; water.	object-based; rule-based	nearly 94%
Lodha, Fitzpatrick, and Helmbold (2007)	LiDAR	Buildings, trees, road, grass	object-based; support vector machines	90% to 92%
Alexander et al. (2010)	LiDAR	Building, grass, road, tree, shrubs	pixel-based; decision trees	73% to 92%
Shaker and El-Ashmawy (2012)	LiDAR	Buildings, grass, bare soil, roads	pixel-based	43% to77%
Walker and Blaschke (2008)	RGB	Soil, grass, woody building, sealed surfaces	object-based	84%
Moskal, Styers, and Halabisky (2011): case study 1	RGB	Buildings, grass, impervious surface, shrub, tree, water, ground, other	object-based	71%
Moskal, Styers, and Halabisky (2011): case study 3	RGB+near-infrared	Bare ground, grass, impervious surface, shrub, tree, water, other	object-based	83%
Al-Kofahi, Steele, VanLeeuwen, and Hilaire (2012)	RGB+near-infrared	Trees, shrubs, grass and non-greenspace	object-based	89%
W. Zhang et al. (2018)	RGB	Water, building, vegetation, bare land and road	object-based	86% to 96%
Li et al. (2007)	LiDAR + RGB	Road, building, tree, grass, bare land.	object-based; support vector machines	83%to95%
Guan, Li, and Chapman (2011)	LiDAR + RGB	Building, tree, bare ground, unclassified	object-based; maximum likelihood	85% to 92%
Buján et al. (2012)	LiDAR + RGB	High vegetation, low vegetation, buildings, bare earth, pavements and roads	object-based; decision trees	nearly 96%
Bandyopadhyay et al. (2013)	LiDAR + RGB	Building, vegetation, others	object-based; decision tree	89% to 93%
Xie, Cheng, and Guan (2013)	LiDAR + RGB	Buildings, woodland, grassland, road,	object-based; decision trees	89% to 95%
Rastiveis (2015)	LiDAR + RGB	Buildings, trees, asphalt roads, concrete roads, grass, cars	pixel-based; Bayes classification	nearly 95%

2.3 LiDAR and multispectral fusion

Urban landscapes are complex and using LiDAR data or multispectral imagery alone may yield errors when classifying features with similar structural or spectral characteristics. Many studies which integrated LiDAR and multispectral data have shown improvement in overall accuracy, ranging from 5% to 32% (Kim, 2016; Koetz et al., 2008; Singh et al., 2012) . The fusion of data can compensate for the shortcomings of both datasets and improve the classification accuracy in urban environments.

Some LiDAR platforms acquire LiDAR data and aerial images simultaneously. As a result, researchers use the spectral information derived from aerial images to improve classification accuracy. Bartels and Wei (2006) combined LiDAR-derived features with additional co-registered spectral bands. The result showed that the overall accuracy improvement ranged between 13.31% and 33.33% with different feature combinations. Rastiveis (2015) integrated LiDAR data and aerial imagery based on the Bayesian theory in a three-level fusion algorithm for urban land cover classification. The study applied the fusion of two datasets at both pixel-level and object-level. The author also made a comparison between the results generated by a single data source and the fusion of data sources. Compared with single-source LiDAR data, a fusion of LiDAR and RGB images significantly improved the classification in terms of overall accuracy (from 88% to 95%) and kappa coefficient (from 84% to 93%). Gan, Zhong, Li, and Guan (2015) derived three groups of features calculated based on information from LiDAR data, RGB bands and the combination of both. The result showed that the combination feature group yielded the highest accuracy, with 86.52%, compared with 59.8% (RGB only) and 80.52% (LiDAR only). Hartfield, Landau, and Van Leeuwen (2011) tested combinations with features derived from aerial multispectral imagery and LiDAR data for land cover classification at the city of Tucson, Arizona, USA. The fusion of 4 multispectral bands, NDVI (normalized difference vegetation index) and LiDAR-derived CHM (canopy height model) has the highest overall classification accuracy (89.2%), compared with using only the multispectral data (82.5%). Bandyopadhyay et al. (2013) presented a feature-level fusion approach between LiDAR and aerial imagery to separate urban vegetation and buildings from other urban land cover classes. They derived a vegetation index by combining LiDAR intensity data with the red band and a reflectance index using blue and green bands. The overall classification accuracies for two study areas reached 89.98% and 93.96%, respectively. Importantly this study noted some classification errors due to misalignment between the aerial images and LiDAR data, which addresses the importance of image co-registration.

A key strength of fusion of aerial imagery and LiDAR data is that it can compensate for the drawbacks of using single dataset. For LiDAR data, it contains accurate height information but lacks spectral information which is useful in distinguishing vegetation. By comparison, aerial imagery can provide more detailed texture and reflectance information but lacks the ability to provide a vertical assessment of features.

2.4 Object base image analysis (OBIA)

2.4.1 PBIA vs. OBIA

In addition to the sources of data used for land cover classification, the use of pixel-based image analysis (PBIA) and object-based image analysis (OBIA) techniques can have an impact on the classification

result. PBIA has been traditionally widely used for imagery classification. PBIA considers spectral differences between pixels using various classification techniques (Casals-Carrasco, Kubo, & Madhavan, 2000). As the spatial relationships are not included in this method, adjacent pixels could be assigned to different classes, resulting in a so-called salt-and-pepper effect (Yu et al., 2006). Besides, PBIA is also largely affected by data acquiring conditions such as season and weather change, as the spectral responses for a same land cover class could be different (Walker & Blaschke, 2008). OBIA, by comparison, groups similar neighbouring pixels into objects with a process called segmentation, and then classifies each object based on not only spectral, but also textural, structural and contextual characteristics (Benz, Hofmann, Willhauck, Lingenfelder, & Heynen, 2004). Therefore, OBIA can address the shortcomings of PBIA and the classification accuracy can be improved.

When analysing high-spatial resolution images for urban land cover classification, the limitations of PBIA are more obvious. Firstly, land covers in urban area are complex and therefore the spectral variation of pixels within a class becomes larger. This introduces more noise and increases the difficulty of classification (Schiewe, Tufte, & Ehlers, 2001). Secondly, a single land entity (such as a single tree or a roof) is much larger than the pixel size, which means sampling by pixel units does not well represent the characteristics of a land cover class (Blaschke, 2001; Walker & Blaschke, 2008). In contrast, the advantages of OBIA with high-resolution images have been reported in many studies. Casals-Carrasco et al. (2000) compared PBIA with OBIA by classifying land covers in an urban-rural area at Napa County, California (USA) using aerial RGB images of 15 cm spatial resolution. Their result indicated that the accuracy for the built-up class using OBIA increased by 41.73%. Myint et al. (2011) compared PBIA and OBIA using multispectral Quickbird. The dataset covers the central city area of the Phoenix city, Arizona (USA) and has 4 spectral bands with spatial resolutions of 2.4 m. Their result showed that the overall accuracy improved from 67.6% to 90.4% after changing PBIA to OBIA. Shafri and Hamedianfar (2015) conducted a land cover classification for an urban area at a part of Kuala Lumpur, Malaysia with high spatial resolution hyperspectral images (0.68 m spatial resolution). Compared with PBIA, the overall accuracy of OBIA improved by 14.54%.

OBIA shows better performance than PBIA on analysing urban land cover with LiDAR data. Firstly, LiDAR-derived images have limited bands compared with multispectral images which consist of 4 to dozens of bands (Chen & Gao, 2014). When classifying pixels, values from different bands are used to distinguish different land cover types. Fewer bands mean less information could be used for identification. Secondly, LiDAR data provide accurate elevation information which allows precise delineation of small land entities such as private yards and roofs (Blaschke, 2010). Many studies have reported high accuracies for a specific land cover extraction such as buildings (Miliaresis & Kokkas, 2007) and trees (MacFaden, O'Neil-Dunne, Royar, Lu, & Rundle, 2012; Ossola & Hopton, 2018); and for general urban land cover classification with different numbers of classes. There are four studies in Table 2-1 which used only LiDAR data and OBIA for land cover classification. All accuracies of these

studies have achieved more than 90%. When integrating LiDAR with multispectral images, OBIA also produced better results. Tan and Johansen (2011) using integrated LiDAR data and aerial imagery evaluated OBIA and PBIA for two class groups which describe land cover at different levels. At the lower level which defines the objects on a coarser scale, the overall accuracy and the kappa coefficients of OBIA was 15.5% and 18.8% higher than that of PBIA. At the higher level, the overall accuracy increased by 5.2% and kappa coefficients grew by 10.4%.

2.4.2 OBIA - Image segmentation

Image segmentation is a vital process because objects are the basic classification units for OBIA and its quality can largely affect classification accuracy. The ideal segmentation level should result in each segmented object only containing one land cover class. In practical terms, however, images may be over or under segmented. If a ground object is divided into many image objects, it is over-segmented. By contrast, if an image object contains more than one ground object, it is under segmented (Drăguţ, Tiede, & Levick, 2010). Both these situations may affect the classification, but it should be noted that compared with under-segmentation, over-segmentation may lead to fewer errors because it can be fixed by merging objects. Liu and Xia (2010) evaluated the relationship between segmentation scale, segmentation accuracy and overall classification accuracy using multispectral images. The result showed that segmentation accuracy decreased with an increase in segmentation scale. This is because the negative effect of under-segmentation becomes more significant. However, the overall classification accuracy saw a significant increase when the scale increased from 0 to 12. After reaching the optimum scale, the classification accuracy decreased since the images were over-segmented. By comparing with the overall accuracy of the pixel-based classification, they also showed that object-based classification generated better results as long as the segmentation scale is in a reasonable range (Figure 2-1).

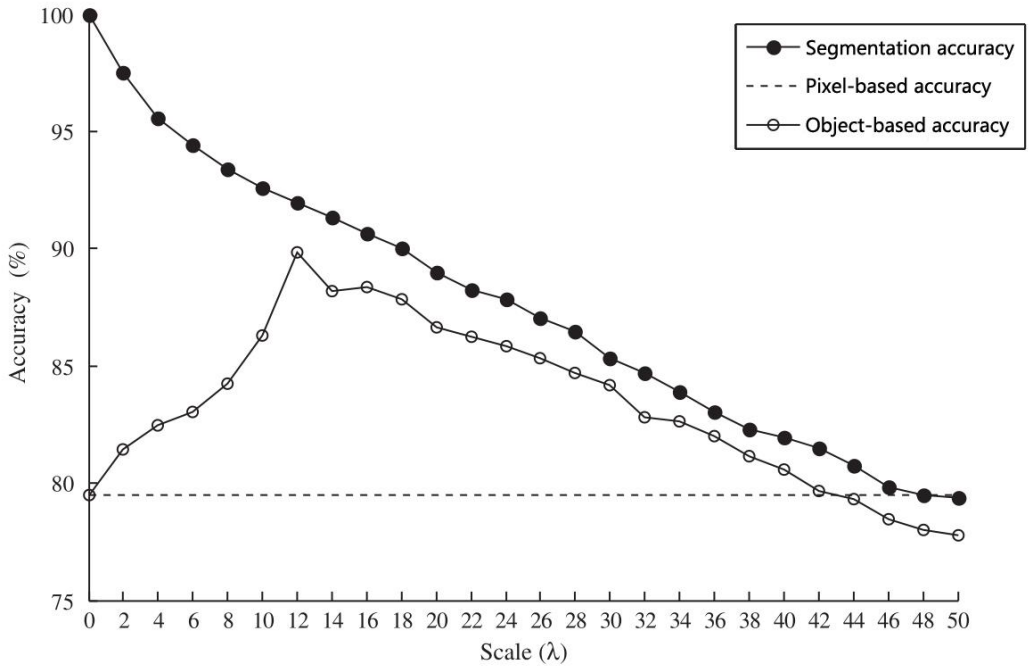

Figure 2-1: Segmentation and classification accuracies at different segmentation scales

[Adapted from ''Assessing object-based classification: advantages and limitations.'' by Liu, D., & Xia, F, 2010, Remote Sensing Letters, 1(4), 187-194.]

Finding the optimum scale for land cover classes in urban area is challenging because of the complexity of the landscape (Drăguţ, Tiede, & Levick, 2010). Hence, the segmentation scale should be at multi-scale to avoid over or under-segmentation for land entities of different sizes (Bruzzone & Carlin, 2006). Multi-scale segmentation has been applied in many studies for deriving man-made features (Liu, Wang, & Liu, 2005; Tian & Chen, 2007) as well as natural objects such as trees (Jing, Hu, Noland, & Li, 2012) and other landscape features (Clark & Pellikka, 2009). In a study conducted by Johnson (2013), RGB aerial imagery was classified into seven classes (grass, tree, building, other impervious surfaces, shadow, soil, and pool) in an urban area of Deerfield Beach, Florida, USA, using multi-scale segmentation. The overall accuracy was improved by 5% (from 78.1% to 82.1%) compared with single-scale segmentation. Kim, Warner, Madden, and Atkinson (2011) segmented RGB imagery of a salt marshland at Chatham County, Georgia, USA into three classes using both multi-scale and single-scale methods. The result of multi-scale method showed 6% improvement (from 76% to 82%) in overall accuracy.

2.4.3 Classifier comparison

For classifications of remote sensing data, numerous techniques have been developed to fulfil different analysis requirements. Among those techniques, supervised classifiers are most commonly used, for their flexibility in processing features of classification objects (Niemeyer, Rottensteiner, & Soergel, 2014). Random forest (RF) is a machine learning classifier which had been reported having relatively better performance compared with other classifiers (Belgiu & Drăguţ, 2016).

Myint et al. (2011) compared Random Forest (RF) classifier with single Classification Tree (CT) by evaluating the classification accuracies of 14 urban land cover classes. Among these classes, 13 Kappa indexes of RF are higher than that of CT. The accuracies improved by 0.11% to 30.17%. Four classes improved by over 20%. In the comparison made by Novack, Esch, Kux, and Stilla (2011), World-View and QuickBird-2 imagery covering a continuous metropolitan area were classified using an object-based approach with four classifiers: Support Vector Machine (SVM), DT, RF and Regression Tree. Their result showed that RF produced the highest overall accuracy as well as the Kappa coefficient of all 4 land covers.

Apart from higher classification accuracy, RF also has a good balance between accuracy and efficiency. In a study conducted by Chutia, Bhattacharyya, Sarma, Kalita, and Sudhakar (2016), four classifiers, support vector machine (SVM), maximum likelihood classifier (MLC), RF and object-based classifier were compared using hyperspectral imagery. The accuracies of object-based RF classifier were all slightly greater than that of SVM. MLC had the fastest processing speed but the lowest accuracies. RF by comparison, took nearly two to three times less than the other two classifiers and yielded greater accuracies at the same time. Miao, Heaton, Zheng, Charlet, and Liu (2012) compared RF with other four tree-based classifiers (bagging tree, Ababoost tree, Ababoost random forest and classification and regression tree). The accuracy of RF was close to other classifiers but its efficiency could be significantly improved by parallel processing. By contrast, this is not achievable with other classifiers which are similar in accuracy and computing time. Another dramatic increase of processing efficiency was reported in a study by Gan et al. (2015). They compared SVM and RF using the same datasets and yielded similar classification accuracies, with 86.52% and 86.16% respectively, but RF demonstrated approximately 15 times faster processing than SVM.

RF consists of many individual decision trees and the final classification result is generated by the 'votes' from those trees. As a result, RF is less affected by noises and outliers in the input data (Pal, 2005). Rodriguez-Galiano, Ghimire, Rogan, Chica-Olmo, and Rigol-Sanchez (2012) tested the impact of noise on classification accuracies of RF and decision tree (DT). When the percentage of noise in training dataset increased from 0-60%, RF produced fewer errors than DT. Similar results were also found in another study (Mellor, Boukir, Haywood, & Jones, 2015) which reported that less than 7.2% decrease occurred when 25% training samples were mislabelled. Overall, RF has fewer parameter settings (Gislason, Benediktsson, & Sveinsson, 2006), shorter processing time and insensitivity to noise. These merits have made RF more suitable for large dataset analysis with more feature inputs.

2.5 Individual tree crown detection and delineation (ITCD)

A growing field of application for remote sensing techniques is individual tree crown detection and delineation (ITCD). Tree crown information is important features for forest inventory because it can be used for stem volume estimation (Holmgren, 2004), canopy structure analysis (Lévesque & King, 2003), and tree species classification (Breidenbach, Næsset, Lien, Gobakken, & Solberg, 2010). Various remotely sensed data such as multispectral and LiDAR have been analysed to find tree locations and delineate crown boundaries.

Many studies used multispectral remote sensing data for ITCD (Culvenor, 2000; Pouliot, King, Bell, & Pitt, 2002; Wulder, Niemann, & Goodenough, 2000). For multispectral data, tree crowns are distinguished according to their spectral difference between background pixels (Ke & Quackenbush, 2011). The accuracy for tree crown delineation can, therefore, be affected by factors such as spatial resolution, spectral homogeneity, and illumination angle (Gulbe, 2015). The effect of these factors can be more significant when delineating tree crowns in urban areas because of varied land cover structures (Alonzo, Bookhagen, & Roberts, 2014). The lack of vertical information generally puts limits on improvements for ITCD using multispectral data.

LiDAR data, by comparison, provides more accurate information about the vertical structures of trees and is less affected by illumination conditions. A popular and efficient way of using LiDAR data is interpolating LiDAR points into raster surfaces (Zhen, Quackenbush, Stehman, & Zhang, 2015). Same as the calculation of nDSM, a normalized surface, canopy height model (CHM) can be produced through a subtraction of DSM and DEM in tree covered area. After that, several raster-based algorithms such as local maxima filter, region growth, and watershed segmentation can be adopted for finding treetops or crown delineations (Fang, Im, Lee, & Kim, 2016).

For ITCD, multispectral images can provide vital spectral information that is missed in LiDAR data and thereby achieve a more accurate classification of trees. Improvements have been found in research which integrated LiDAR and multispectral data (Heinzel, Weinacker, & Koch, 2008; McCombs, Roberts, & Evans, 2003; Suárez, Ontiveros, Smith, & Snape, 2005). With the advancing of LiDAR technologies, a fusion of these two datasets is also showing an increasing trend for different forest inventory tasks (Ke & Quackenbush, 2011).

2.6 Conclusion

The use of LiDAR data for urban land cover classification has been well researched in many studies. Fusion of LiDAR with aerial images has also proven beneficial for correcting LiDAR-based classification errors. Therefore, it is possible to accurately classify land cover types in Christchurch using these two datasets. Compared with pixel-based classification, object-based classification is more suitable for processing data in this study. Multi-level segmentation scales will be applied to different areas, as the land cover heterogeneity for Christchurch varies in the central areas and surrounding suburbs. Among the main classifiers, RF shows obvious advantages in dealing with large datasets, reaching a balance between accuracy and efficiency and insensitivity to noise. These characteristics make RF a preferable classifier for this study.

Using land cover classification results, ITCD can be finished using LiDAR data and provide important information for urban forest management. Several algorithms are available for conducting such tasks with raster surfaces derived from LiDAR data.

Chapter 3 - Land cover classification

3.1 Introduction

Nationwide Land cover classification in New Zealand has a history dating back to the mid-1990s. Using multispectral satellite imagery from SPOT and Landsat platforms, a national land cover map, the New Zealand land cover database (LCDB) has been produced. The datasets used for classification were from 1996/97, 2001/02, 2008/09 and 2012/03, respectively. At the time of the beginning of this study, the latest version was LCDB v4.1 and it contains 33 land cover classes (LRIS, 2015). While the LCDB cover both natural and urban environments, it is better suited for land cover mapping at a national scale. Within urban boundaries, land cover classes only include "Urban Parkland/Open Space", "Built-up Area", and various water land covers. Moreover, the coarse resolution (20 m for SPOT and 30 m for Landsat) of satellite imagery used to generate the LCDB can lead to errors for urban land cover classes such as individual buildings and urban forest (Jones, 2017). For these reasons, the LCDB cannot be used to effectively quantify land cover change within Christchurch resulting from the Canterbury Earthquake Sequence.

The acquisition of remote sensing data immediately following the 22 February 2011 earthquake and again in 2015 provided an opportunity for a more refined analysis of land cover change for Christchurch. Together, the Christchurch City Council (CCC) and the Environment Canterbury regional council acquired both aerial RGB imagery and LiDAR data in both 2011 and 2015 (Table 3-1 & Table 3-2). Compared with the satellite data used for the LCDB, fusion of RGB and LiDAR datasets could enable more accurate classification for urban environment (Bartels & Wei, 2006; Guan, Li, & Chapman, 2011; Hartfield et al., 2011; Rastiveis, 2015). Therefore, the purpose of this study was to achieve high accurate classification and change detection for land cover between 2011 and 2015 in Christchurch using a fusion of LiDAR and RGB aerial imagery.

3.2 Method

3.2.1 Study site

Christchurch (43° 31' 32.3400" S, 172° 38' 23.4492" E) is located on the east coast of Canterbury in New Zealand. It is the largest city in the South Island, covering 606 km² (excluding the Banks Peninsula ward) and the third most populous city in the country with 396,700 residents (2017, Stats New Zealand). According to data from the CCC, 49.48% of land area (299.85 km²) is considered as urban land use. The city has 792 city parks which are covered mostly by grass and trees, accounting for one-third of the city area (Chen, Colin, Maria, Glenn, & Wu, 2015).

The study area itself does not correspond to the official city boundary, instead, it is defined by the available remotely sensed data. The study area was bounded by the overlap between LiDAR data and RGB imagery acquired in 2011. It covers 368 km² and accounts for about 60% of Christchurch (Figure 3-1). The area spreads over various land environments, including both urban and rural parts of Christchurch.

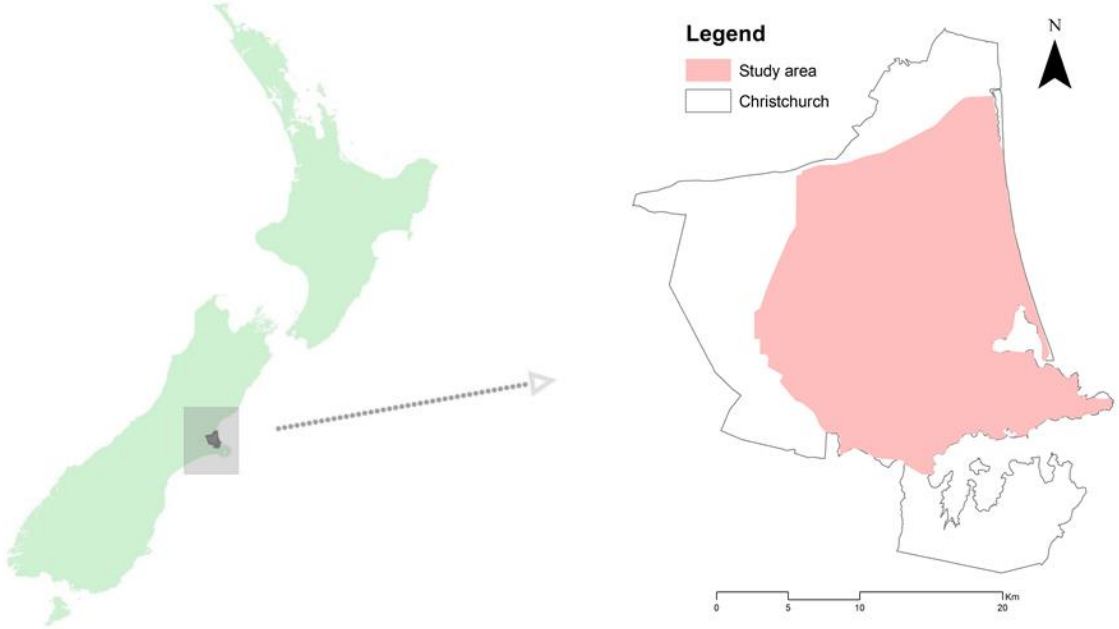

Figure 3-1. Christchurch location and study area

3.2.2 Data used

Aerial imagery and LiDAR point clouds from 2011 and 2015 were used for land cover change analysis. Both LiDAR datasets (Table 3-1) were acquired by AAM Pty Limited, Australia. The LiDAR dataset from 2011 was acquired from a fixed wing aircraft with the ALS50 system in autumn, between May 20th and May 30th, 2011. The main purpose of this survey was assessing the February 2011 earthquake damage extent. GPS base station support was provided by GeoSystems NZ. Ground check-points acquired by the CCC were used for accuracy assessment of the data.

LiDAR data from 2015 were acquired by the same aircraft but with upgraded sensors, AAM's Riegl LMS-Q1560 and Leica ALS60 LiDAR system. AAM conducted this survey during the spring season for Environment Canterbury Regional Council between 5th October and 7th November 2015. GPS base station support was sourced from Global Surveys Continuously Operating Reference Station (CORS) operating in Christchurch. The ground check-points were field surveyed by Sounds Surveying Limited and were used for data accuracy assessment.

Table 3-1. LiDAR data Information

Acquisition period	Pulse Rate	Point density	Returns	Footprint size	Vertical accuracy	Horizontal accuracy	Mosaic tiles
20/05-30/05,2011	127.5 kHz	4 pts m^{-2}	4	0.3 m	+/- 0.1 m	+/- 0.4 m	578
05/10-07/11,2015	145 kHz	4 pts m^{-2}	4	0.47 m	+/- 0.1 m	+/- 0.5 m	336

Aerial Red-Green-Blue (RGB) imagery from 2011 was captured by New Zealand Aerial Mapping (NZAM), while the imagery from 2015 was captured by AAM Pty Limited (Table 3-2). RGB imagery from 2011 has a resolution of 0.1 m. It was collected flying at 1,600 m above the ground using a Vexcel UCXp large format digital aerial camera. The photography was acquired in late summer on 24 February 2011 between 11 am and 6 pm. Images were provided with 1372 tiles which are 480m width ×720m height. Each tile was merged by individual aerial photos and this process was done by the data provider. However, as this photography was collected for a rapid response following the 22 February 2011 earthquake, NZAM used a simple photo merging algorithm and a number of shortcuts for image orthorectification which resulted in some errors. Correcting these errors was not feasible, as it would have required retrospectively collecting ground control points. The implications of these errors are considered in the discussion section of this chapter.

RGB imagery from 2015 has a resolution of 0.075 m. It was captured in spring and early summer between 2015 and 2016. Images were provided with 4810 tiles which are 240m width ×360m height Aerial photography over the Christchurch City central business district (CBD) was captured on 17th November 2015 and the surrounding parts of Christchurch City were captured on 22nd January 2016. Compared with the 2011 RGB imagery, the 2015 dataset has a greater quality in terms of orthorectification, photo merging and definition. A detailed comparison is shown in Table 3-2.

Table 3-2.RGB data Information

Acquisition period	Resolution	Mosaic image size	Coverage (Clipped)	Cloud cover	Spatial accuracy	Supplier	Mosaic tiles
24/02/2011	0.1 m	98.3 GB	368 km^2	Very small proportion	±0.2 m	NZ Aerial Mapping Ltd	4810
17/11/2015, 22/01/2016	0.075 m	195 GB	368 km^2	Cloud free	unknown	AAM	1372

3.2.3 Land cover classes

This research involved undertaking land cover classifications in 2011 and 2015. A critical component of land cover classification studies is defining the land cover classes to be included. In this study, land cover classes were selected and modified based on the Land Cover Database (LCDB) version 4.1. LCDB v 4.1 is the latest version and it was refined based on previous versions which derived land overs of New Zealand from satellite remote sensing data. The LCDB programme is led by Landcare Research, along with an associated research program. The project identified seven first-order land cover classes using satellite images and divided them into 33 mainland-classes. These classes represent 100% of the surface of New Zealand and are mutually exclusive. However, as the LCDB classes were defined for mapping land cover on a national scale, they were inappropriate for the city-wide scale needed in this study. As such, the seven first-order classes were modified to better represent land cover classes for Christchurch city.

With LiDAR and RGB imagery, some green croplands and grasslands are difficult to be distinguished due to their similarity in elevation and spectral information. Hence, cropland was then divided into two classes and merged with related classes. Green croplands were classified as grasses, while dry croplands were classified as lightly vegetated surfaces. Scrub and forest were combined into a tree class as both contain woody vegetation. Artificial surfaces were subdivided into buildings and roads. RGB images suffer from shadows, which alter the reflectance of light off the underlying land cover and result in uncertainty. Hence, shadow was added as a new class. The final modified land cover classes used are shown, and described, in Table 3-3:

Table 3-3. Land cover classes used in this study

LCDB	Classes used	Description
Artificial surfaces	Road	Including asphalt and cement surfaces such as roads and footpaths, pathways, airport runways and car parks.
	Roof	Buildings and other man-made structures that have higher elevation value than roads and exceed 1 m.
Water bodies	Water	Rivers, ponds, lakes and other surfaces covered by water.
Grass (Dry)	Grass	Including green cropland, grass and green artificial surfaces such as tennis courts.
Grass (Green)	Bare land	Dry grass areas where have similar colour as bare land and light vegetal area
Bare land	Bare land	Bare land with no vegetation coverage
Forest	Trees	Forests and shrubs
Shrub		
Crop land (Dry)	Bare land	Crop lands that have similar colour as bare land
Crop land (Green)	Grass	Crop lands that have similar colour as grass
	Shadow	All areas that are not able to be distinguished land cover type due to low brightness values corresponding to low surface reflectance and low image qualities. This Additional class is for reducing misclassifications.

3.2.4 Data pre-processing

A number of surfaces were produced from the LiDAR data for use in land cover classification. They include a digital elevation model (DEM), digital surface model (DSM), normalised digital surface model (nDSM), and a returns per pulse (RPP) surface. The LiDAR processing workflow is shown in Figure 3-2 and described below.

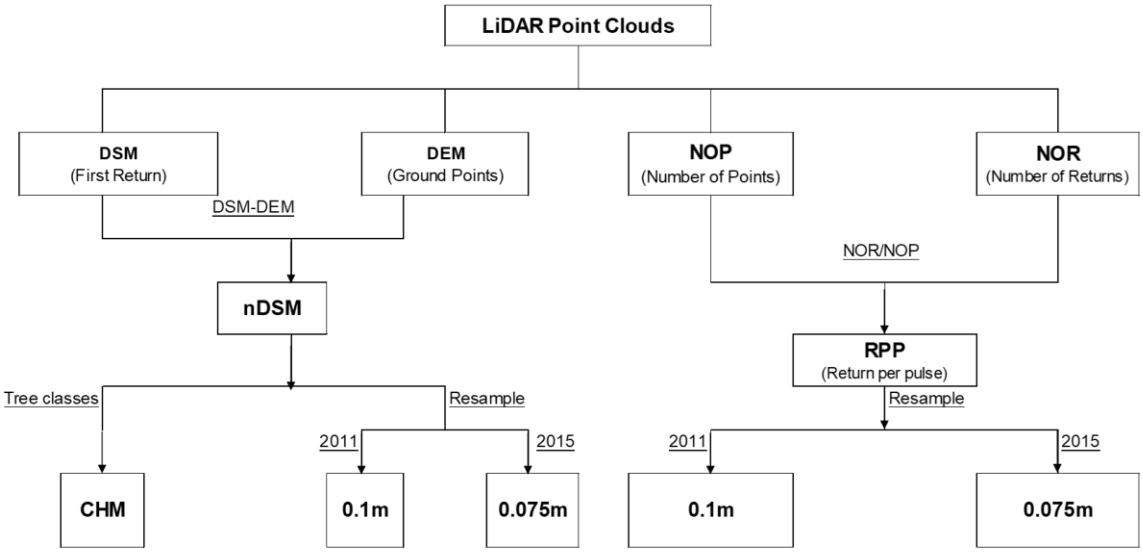

Figure 3-2. LiDAR data processing work flow

3.2.4.1 LiDAR-derived surface models

Two commonly used LiDAR processing packages, ArcGIS (ESRI, Redlands, CA) and LAStools (Rapidlasso, Friedrichshafen) have different interpolation algorithms and produce surfaces with different qualities. Therefore, the quality of the surfaces produced by the two packages was compared prior to digital surface generation. The comparison result showed that LAStools yielded better surfaces than ArcGIS and therefore it was used for deriving LiDAR surfaces. Detailed descriptions of surface interpolation with both LAStools and ArcGIS and a comparison of resulting surfaces can be found in Appendix A.

In LAStools, the interpolated pixel size was set at 1 m, as the average point spacing of these two datasets ranged between 0.5 m to 0.9 m. This theoretically allows for one LiDAR point inside each raster pixel; however, LiDAR point clouds are never completely regular, so areas with low point-density will not have points inside each pixel. For DEM interpolation, only points classified as ground were used. DSMs were then produced following the same process, except for using only points classified as first returns. By subtracting DSMs from DEMs, nDSM was produced for 2011 and 2015.

3.2.4.2 LiDAR-derived Return per pulse (RPP) surfaces

Surfaces were produced to quantify the number of returns from each pulse in each 1 m^2 cell. To calculate the number of returns for each pulse, the number of pulses within each pixel and the number of returns corresponding to each pulse were derived in the first instance. Then, the return per pulse (RPP) surface was computed by dividing the second surface by the first surface. RPP pixels corresponding to trees were generally greater than one because LiDAR pulses usually have multiple-returns when they hit trees. By comparison, pixels with values equal to or lower than one are more likely to be building or ground. An exception is when a pulse hits the edge of a building, which can result in multiple returns.

3.2.4.3 Tiles mosaic and Resampling LiDAR surfaces

After the LiDAR points in different tiles had been interpolated (Table 3-1), the raster tiles were merged and clipped to exactly fit the study extent. The same process was also applied for RGB imagery tiles. When merging tiles into one completed image, several algorithms could be used for deciding values for overlapping areas (Esri, 2016). However, both LiDAR tiles and RGB tiles were inputted with boundaries which are adjacent to each other so a simple merging and clip process was finished in ArcGIS for two types of dataset.

As RGB imagery had higher resolution than LiDAR-derived surfaces, the nDSM and RPP were resampled into 0.1 m and 0.075 m to better align with RGB imagery. The nearest neighbour algorithm was used in ArcGIS to resample LiDAR surfaces.

3.2.5 Object-based image analysis (OBIA)

OBIA classifies images by segmenting pixels into meaningful image-objects and assigning classes to objects based on their features such as texture, spectral information, and shape (Hay & Castilla, 2008). Compared with pixel-based analysis, OBIA can eliminate salt-and-pepper effect (Gao, Mas, Niemeyer, Marpu, & Palacio, 2007; Zhang, Li, Yang, Zhou, & Su, 2010) and have a better performance on high-resolution images (Cleve, Kelly, Kearns, & Moritz, 2008; Ghosh & Joshi, 2014). The first step of OBIA is image segmentation which groups pixels into objects with similar characteristics and the second step is classification (Cleve et al., 2008). A detailed workflow is shown in Figure 3-3. One of the most common OBIA software packages, eCognition (Trimble, CA), was used in this study for image classification. It integrates many OBIA functions which enabled accurate image segmentation and flexible extraction of object features (Walker & Blaschke, 2008).

3.2.5.1 Segmentation scale estimation with ESP tools

Image segmentation requires the user to specify a scale parameter, but optimising the scale parameter can be problematic (Ryherd & Woodcock, 1996). Drăguţ et al. (2010) developed a tool, estimation of

scale parameter (ESP), for optimal scale selection. This tool runs as an extension tool in eCognition packages. ESP calculates the local variance (LV) of object heterogeneity for each object and then compares the changes of LV across a range of scale parameter values. The rate of change of LV (ROC-LV) provides an indication of the optimal scale for image segmentation. After testing those indicated values, the user can narrow the range of selection and choose an appropriate scale.

The study area spans various land environments, such as urban settlements, city gardens, and rural croplands. Within such a varied landscape, objects vary in density, size or shape. Therefore, using a single scale can result in under-segmentation for small objects and over-segmentation for large objects. Over-segmentation indicates that too much detailed and small regions were segmented for a real object, while under-segmentation means segmented regions are too large and failed to perfect represent the object (Schiewe, 2002). Both these situations can result in misclassification in the later stage. Multi-level segmentation is a way to reduce those errors and has yielded good results in many studies (Almeida et al., 2007; Blaschke, 2010; Myint et al., 2011). In this study, two scale levels were explored and applied for segmentation.

Land cover objects with considerably different sizes exist between rural and built-up areas. For example, cropland and bare land in rural areas are often large in size, while residential areas and city centre areas usually contain small objects such as roofs and individual trees. Therefore, this study firstly divided Christchurch into rural and urban areas based on classes from LCDB. The urban area was defined by the built-up area class, a second-order class under artificial surfaces from LCDB. The other second order classes such as urban parklands, lake or pond, different types of cropland were defined as rural areas.

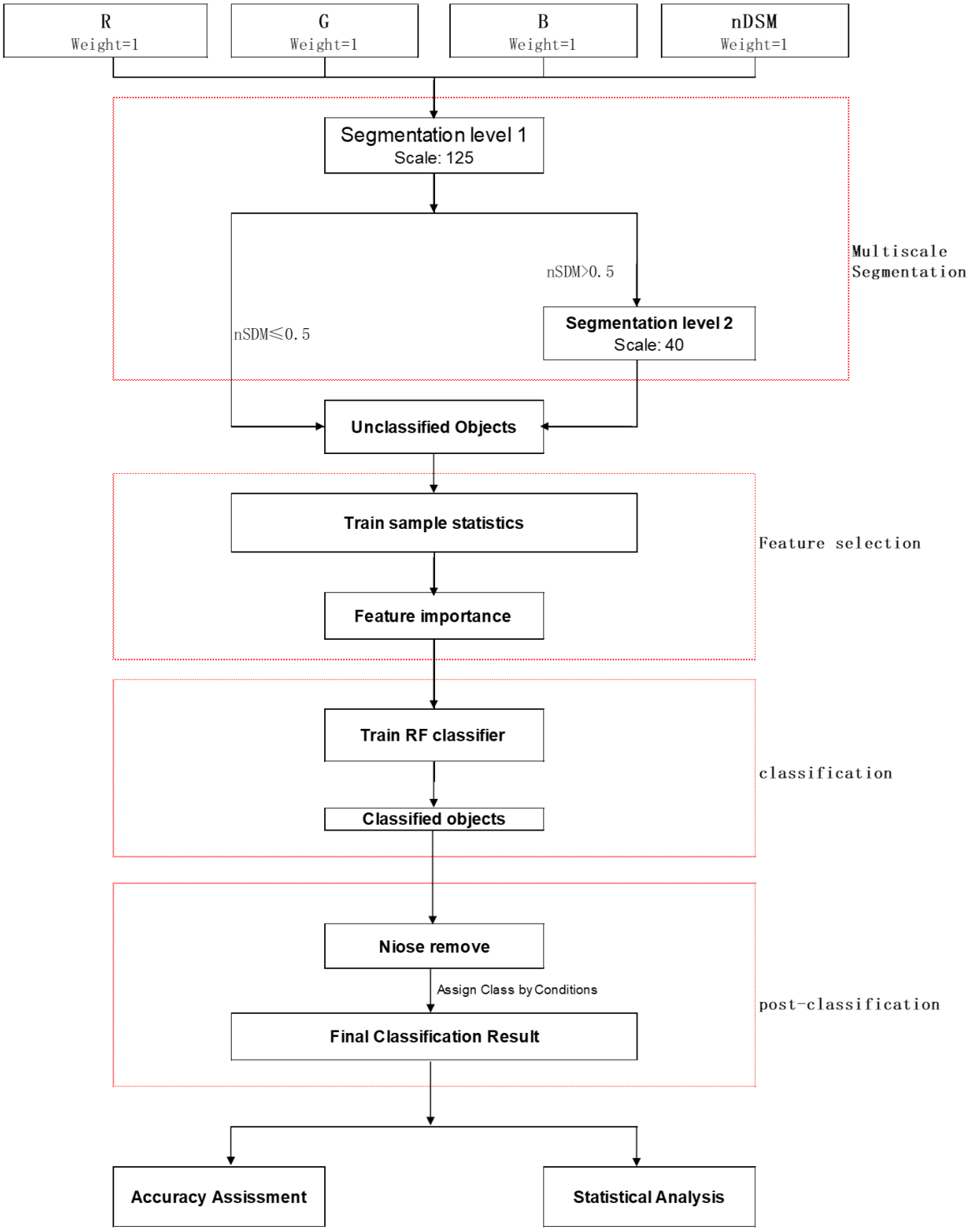

Figure 3-3.Classification flow

In this study, the ESP tool was implemented using the RGB imagery as its input. Considering the large size of RGB data (98.3 GB and 212.2 GB), it was impractical to run the ESP tool on the complete study area. Thus, 20 subsample areas were randomly identified in rural and built-up areas. To ensure they could representative wide range of land cover classes, these subsamples avoid areas which contain less than four land cover types. Subsamples in urban areas measured 240×360 m, while subsamples in rural areas measured 480×720 m because of the relatively large size of objects in rural areas. ESP was undertaken on subsample areas for both 2011 and 2015 datasets. The results of ESP led to selecting two scale values, 40 and 125, for a subsequent multi-level segmentation. The results of the ESP analysis are summarised in Table 3-4.

Table 3-4. The result of ESP Range analysis

	ESP Range for urban subsamples	ESP Range for rural subsamples
2011	35-48	121-200
2015	28-43	11-152

3.2.5.2 Segmentation

Having identified optimal scale parameter values using ESP, the images corresponding to the complete study area were segmented into two levels. Firstly, datasets were segmented coarsely (scale = 125) to delineate large objects such as grassland, road and cropland. Next, the large objects with a mean nDSM value greater than 0.5 m were subjected to finer segmentation (scale = 40). This is because most large objects such as grassland, cropland and car parks have lower elevations than 0.5 m while small objects, such as buildings and trees, generally exceed 0.5 m in height and would be under–segmented at a scale of 125. After the second segmentation, a visual inspection showed that objects such as roofs and trees, which were not well delineated in the first segmentation level, were better segmented.

3.2.5.3 Random Forest Classifier

In this study, five classifiers in eCognition package were compared using a sample area that accounted for 5% of the total study area. The results suggested that RF produced the highest classification accuracy in comparison with other classifiers. The details of this classifier comparison process is described in Appendix B.

RF is an ensemble algorithm which consists of multi-tree classifiers. It assigns classes according to the frequency of vote from each tree. Training RF is made up by training for a specified number of classification and regression trees (CART). Each training process used a bootstrapped sample of the complete training data, and the randomly chosen part of input features for creating tree nodes. When

applying classification, input data are classified through decision trees and the output class is assigned based on the majority result from those trees.

Two parameters, the number of decision trees (*n*) and the size of randomly selected features used for each tree nodes (*m*) need to be set before training the RF classifier. Since over-fitting is not an issue with RF, *n* can be as large as possible. However, considering the large size of datasets in this study, *n* needs to be in a reasonable range to avoid overloading computing resources. Rodriguez-Galiano et al. (2012) evaluated the influence of *n* selection on RF. Their result showed that the classifier's accuracy improved less than 10% once *n* is over 100. They also reported that changing *m* improved the classifier's accuracy less than 1% after *n* reaches 40. Belgiu and Drăguţ (2016) compared studies with different *n* number and suggested 500 is enough to reach a stable classification result. In other studies, 500 is also chosen as *n* value (Gislason et al., 2006; Pal, 2005; Zhu, 2013). For the selection of *m*, many previous studies used the square root of the total number of input features and found no significant difference when this value changed (Gan et al., 2015; Gislason et al., 2006; Stumpf & Kerle, 2011). It has also been reported that *m* value has little effect on RF classifier performance (Eisavi, Homayouni, Yazdi, & Alimohammadi, 2015; Ma, Zhou, & Li, 2017). Based on previous research, *n* and *m* were set as 500 and the square root of the number of input features (automated calculated when train classifier), respectively.

3.2.5.4 Sample selection

Once the classifier with the highest classification accuracy was selected, it was used to classify for the whole study area. The first step was to select the training and validation samples for the classification. Thanh Noi and Kappas (2017) compared five different training sample sizes for the RF classifier. By increasing the number of training sample points from 50 to 1250, the classification accuracy of RF classifier only improved by 3.26%, from 91.47% to 94.09%. Another study conducted by Rodriguez-Galiano et al. (2012) selected 2100 sample sites with 14 land cover classes and then divided them into training and validation sample sets by a ratio of 2:1. They then gradually reduced the training sample size by proportion and found that RF's classification accuracy had no significant change between 100% and 30% of the training samples. Na, Zhang, Li, Yu, and Liu (2010) also reported that RF is not sensitive to training sample size as long as it covers wide variability of land cover objects. Therefore, the size of training sample in this study was decided by the size of validation sample with a ratio of 4:1 (Training: Validation).

The validation sample size was determined by a rule regarding the study extent suggested by Congalton and Green (2008). For a classification with less than 12 classes and study area smaller than 1 million acres (about 40,469 km^2), each class should be allocated at least 50 samples. If the study area is larger, then 75 to 100 validation samples need to be selected. They also reported a multinomial distribution method to calculate validation sample number, equation (1):

$$N=B/4b^2 \qquad (1)$$

Where N is the number of validation samples, B is determined by chi-square table with 1 degree of freedom and 1-α/k， where α is the confidence interval and k is the number of classes. b is the desired precision.

According to equation (1), for the seven classes used in this study, N is equal to 529 (about 75 samples for each class). This value was used to inform the sampling strategy. In this study, sample points of each class were selected by visual inspection using RGB imagery in two different years. Based on the area of different land cover types, the size of sample points for each class were set between 300 and 500. This can ensure that each class has over 50 validation points after randomly divided with a ratio of 4:1 (Training:Validation). Then the total number of sample points were 3000 which contains 2400 training points and 600 validation points (Table 3-5).

Table 3-5. Number of sample points for 2011 and 2015

Land cover class	Number of training points	Number of validation points
Bare land	400	100
Grass	400	100
Road	320	80
Roof	400	100
Shadow	240	60
Tree	400	100
Water	240	60
Total	2400	600

3.2.5.5 Classification

OBIA allows objects to be classified based on spectral, textural, and contextual features of the input imagery. Furthermore, it allows features to be derived from aerial images and LiDAR surfaces. In this study, LiDAR-derived surfaces, nDSM and RPP were combined with red, green, and blue (RGB) bands from aerial imagery. Based on these five bands, numerous features were tested for their ability to discriminate classes. Table 3-6 lists the descriptions of the features included as inputs for the classification.

The first two feature groups, spectral features and textural features are the most commonly used for object-based classification with multispectral images (Feng, Liu, & Gong, 2015; Georganos et al., 2018; Novack et al., 2011; Voltersen, Berger, Hese, & Schmullius, 2014). For spectral features, this study chose mean band values, brightness, and maximum difference. Those features reflect the spectral information of an object from different perspectives. As LiDAR-derived surfaces were integrated as additional bands, the mean values of these surfaces were also calculated and added as LiDAR-derived features. For texture features, a common method, grey level co-occurrence matrix (GLCM) was used. It calculates the possibilities of the occurrence of different combinations of pixel grey levels. These possibilities reflect spatial relationships of grey level between adjacent pixels and record this information in a co-occurrence matrix (Haralick & Shanmugam, 1973). As the adjacent relationship of pixels can be considered from different directions (0°, 45°, 90°, 135° and all directions), GLCM values were also calculated from these directions. GLCM values can be evaluated with different parameters such as homogeneity and standard deviation. In this study, all directions of GLCM were calculated and evaluated by different parameters. In addition to classifying images with spectral, texture and LiDAR-derived features, shape features were included as the input features for classification (Table 3-6).

A RF classifier was trained using the four groups of feature for 2400 training samples. The importance of these features was then ranked according to Gini index. A complete comparison of feature importance for road and bare land classification is shown in Figure 3-4. The change of Gini index was used for assessing the feature importance. It reflects the purity and equity of nodes created in RF. When a node of RF algorithm is divided, a feature was used and therefore sub-nodes have lower Gini index values. If this decrease is significant, it means the used feature has a large effect on the classification and is more important (Qi, Bar-Joseph, & Klein-Seetharaman, 2006). LiDAR-derived features such as mean RPP and mean nDSM have low influence, while spectral features such as Mean R, brightness and Mean G ranked highly. Shape features including length/width, asymmetry and standard deviation of length of edges had high importance and ranked higher than some spectral features such as Mean G and brightness. Average length of edges also ranked at same level as some texture features. However, some shape features ranked after mean RPP were considered as no effect on classification and were not useful in reducing the error.

Table 3-6.Features used for classification

Feature Group	Feature name	Description
Spectral features	Mean R, G, B	This feature calculates the mean values of R G, B bands for each segmented object.
	Brightness	It is calculated by summing the mean value of each band within an object and dividing this value by the number of bands. In this study, only R, G, B bands were used for calculating brightness.
	Maximum difference	It is calculated by the determining the maximum difference value between bands and dividing this value by the object's brightness.
LiDAR derived features	Mean nDSM	Mean value of the normalized elevation of an object.
	Mean RPP	Mean number of returns for each object.
Texture features	GLCM Homogeneity	It calculates the similarity for rows and columns in GLCM. This value reflects the local homogeneity. High values mean that an object is locally homogeneous.
	GLCM Contrast	It reflects the contrast of textures and is the opposite of homogeneity. High values mean that an object is locally heterogeneous.
	GLCM Dissimilarity	Similar to contrast, but in linear value.
	GLCM Entropy	It measures the entropy within an object. High entropy means objects contain high information volume and the texture is more complicated.
	GLCM Ang. 2nd Moment	Sum of squares value of GLCM. It reflects the evenness of grey level distribution. A higher value means an object has more regular texture distribution.
	GLCM Mean	Mean value of GLCM.
	GLCM Correlation	It measures the linear dependency of grey levels of neighbouring pixels.
Shape features	Length/Width	Length of the object divided by the width of the object. Road objects usually have a higher value than bare land object due to long and narrow shape
	Asymmetry	It similar to length/width and calculates the ratio of ellipse axes which fit the object
	StdDev of length of edges	Standard deviation of edges. This value could be high for most road object because they contain more long edges.
	Average length of edges	This feature calculated the average length of an object. Road objects normally have higher values than bare land objects because road objects contain more long edges.

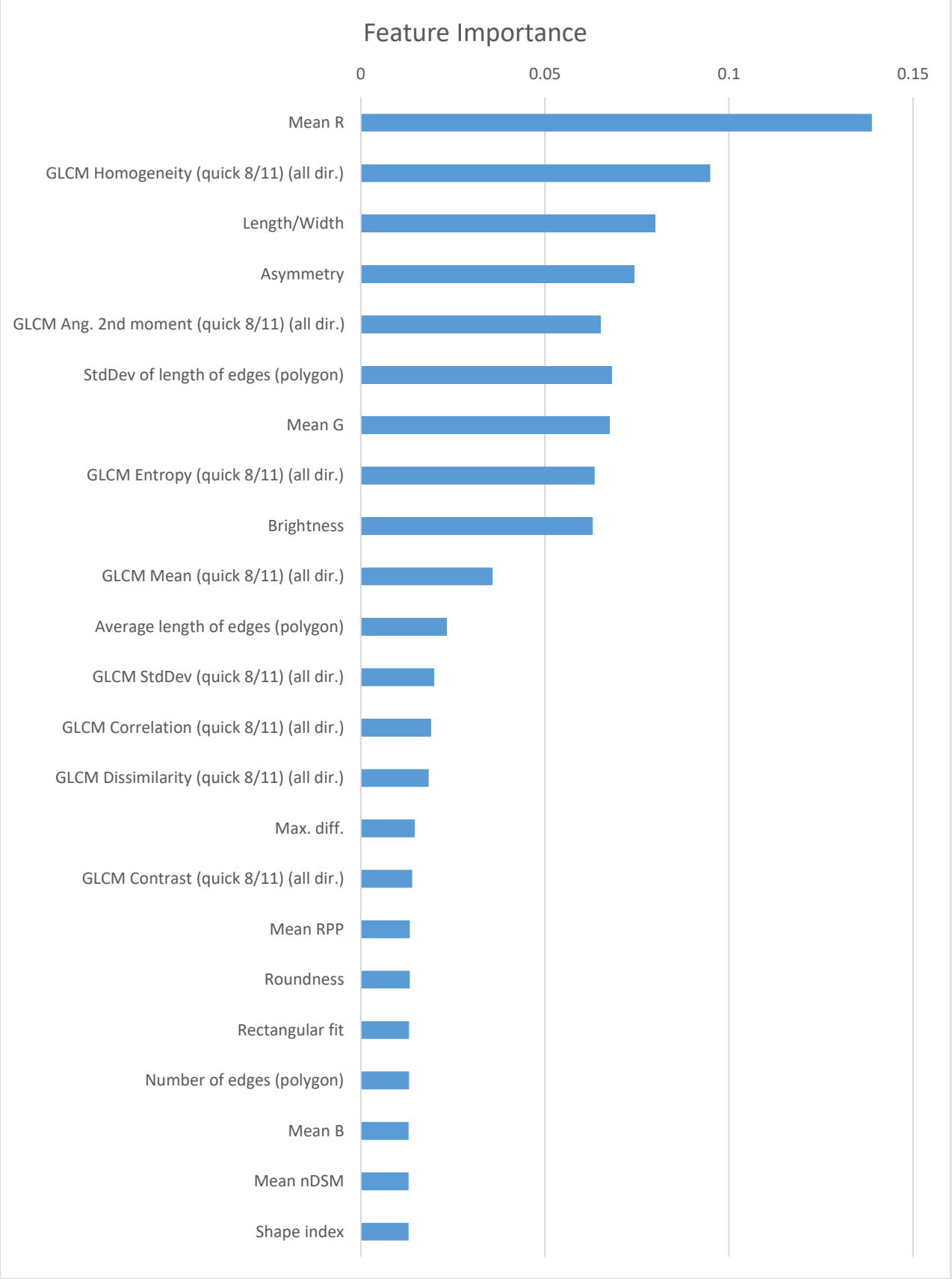

Figure 3-4.Feature importance for features by a decrease of Gini Index

3.2.5.6 Correcting misclassifications

After classification with RF, there were some consistent misclassifications. The following rules were applied to reassign misclassified objects into the correct classes:

1. Some blue-coloured roofs were misclassified as water. So, water objects with mean nDSM greater than 1 m were reassigned as roofs.
2. Some land-based objects obscured in shadow were misclassified as water. So, water objects with mean nDSM lower than 0.5 m and RPP greater than 0 were reassigned as shadow.
3. Some road objects were misclassified as grass or bare land. This occurred primarily for green or white painted areas on roads. So, grass or bare land objects that were 100% surrounded by road objects were reclassified as roads.
4. Some grass areas were misclassified as trees due to their colour similarity. Therefore, tree objects with an elevation lower than 1m were reclassified as grass.

3.2.5.7 Tile processing

Large data size means that classifying the complete scene in a single project would be time-consuming. eCognition server package provides a tiling and stitching method which splits one large project into separate tiles and processes them simultaneously. This can effectively improve processing efficiency. However, tiling can also introduce inaccuracies. The tile size was set as 1 km × 1 km as this size showed a good balance between processing time and accuracy.

3.2.6 Accuracy Analysis

Once the classification was complete, it was subjected to a formal accuracy assessment, using the error matrix approach (Congalton, 1991). The error matrix compares the classified value of 600 validation sample points to the assigned reference classes. It allows observation of the errors that occur in each class. Using the error matrix, overall accuracy was calculated by dividing the number of correctly classified samples by the total number of samples. The producer's accuracy was calculated by dividing the correct number of samples in a class by the total number of samples of that class. This value is correlated with omission errors. The user's accuracy was calculated by dividing the total number of correct samples in a class by the total number of samples that were classified in that classified. This value is correlated with commission errors (Congalton, 1991).

Kappa coefficient (κ) was also calculated. The κ is used for testing the level of agreement between the reference data and classification result. In the study conducted by Landis and Koch (1977), they classified the values for Kappa index into three levels. When the κ value is higher than 0.80, the agreement can be considered as strong. With values between 0.40 and 0.80, the agreement is moderate. When the value is lower than 0.40, the agreement is poor.

3.2.7 Land cover change analysis

Land cover change can be observed at the pixel level by comparing classification results from different years (Richards & Richards, 1999). A land cover change map and matrix are usually generated to describe change between classes (Gao et al., 2011; M. Liu et al., 2005; López et al., 2001). In this study, the comparison was made between the 2011 and 2015 land cover maps for Christchurch. There were seven land cover types in this study and each pixel on the ground had the potential to change from one land cover type to another, or remain the same.

Alberti, Weeks and Coe (2004) discussed problems associated with pixel-based change detection. Errors could be introduced because of poor image registration, misclassification and the complexity of urban land structure. To minimize those errors, they used a majority analysis method to filter the change detection image and received 85% overall accuracy. The same method was applied in this study. A 3×3 sized window was used to filter the image subtraction result. The majority value within this window was then assigned to each central pixel. After majority analysis, a land cover change map was produced.

Pixel statistics for the land cover change map were then summarised following three steps. Firstly, a change matrix with all classes was made. Secondly, figures correlated to shadow were excluded from statistics because the real land cover classes in shadow areas are hard to identify and the locations of areas affected by shadow from two years are varied. Including shadow will introduce errors for land cover comparison. After that, a total change statistic (TCS) table which calculates the net change in area for each class (excluded shadow area for two years) and a land cover transition (LCT) table which showed the area of transitions among different classes were produced (Alberti et al., 2004)

3.3 Result

3.3.1 Classification accuracy

Land cover classification maps for 2011 and 2015 are shown in Figure 3-5. The overall accuracy for the 2011 classification result is slightly lower than that of 2015, with 94.0% and 94.32% respectively (Table 3-7 & Table 3-8).

For the 2011 classification, the user's accuracies (related to omission errors) range from 98.33% to 86.67% (Table 3-7). Water has the highest user's accuracy followed by tree and roof with 98.0% and 96.0%. These three land cover classes are the most accurately represented land cover types in the classification map (Figure 3-5). Shadow is the only land cover type with user's accuracy less than 90%. The producer's accuracy (related to commission errors) ranges from 97.96% to 88.79%. Roof has the highest producer's accuracy, followed by water, road, trees and other classes. The producer's accuracies

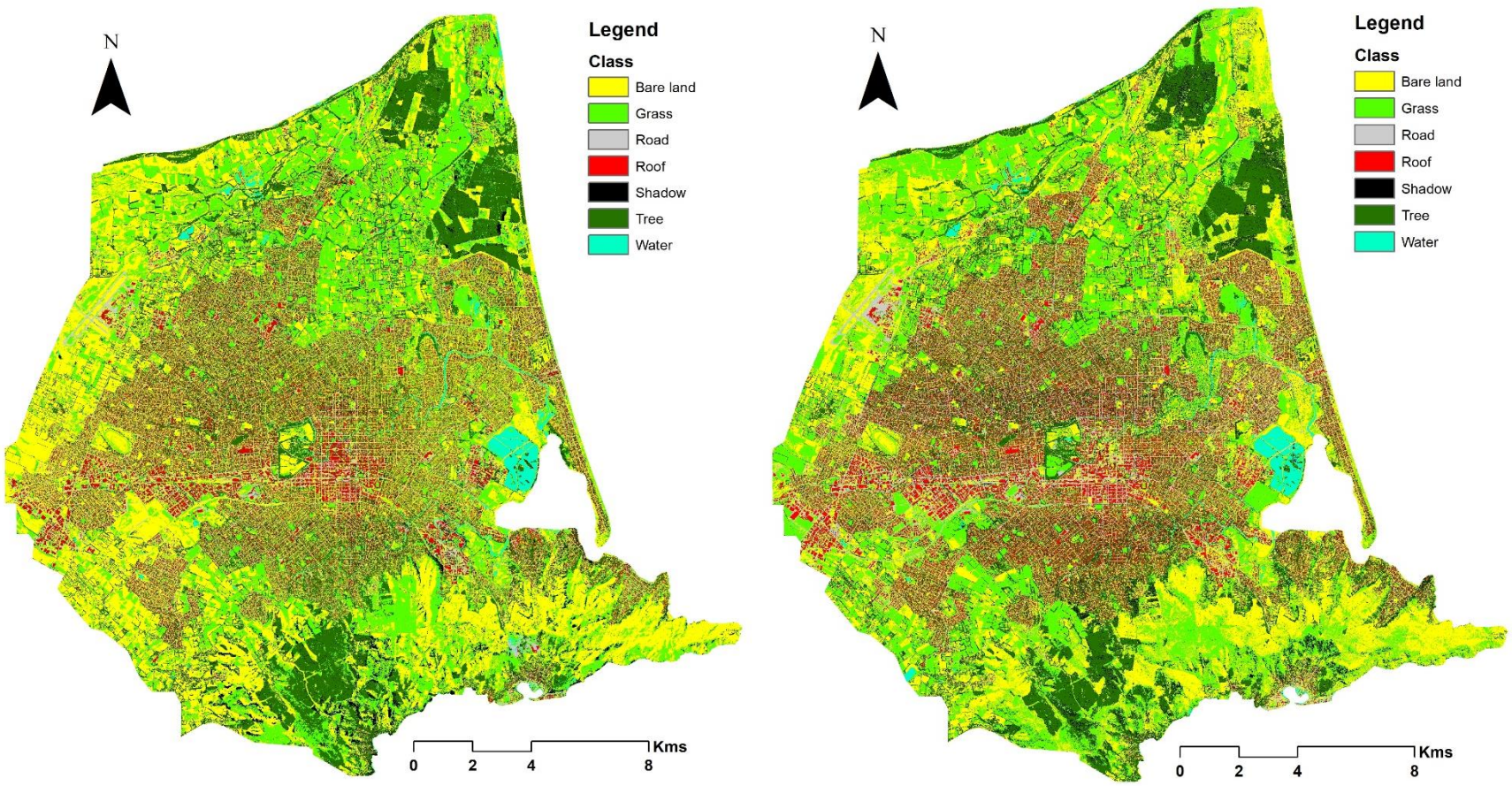

Figure 3-5. Land cover classification map for 2011 (left) and 2015 (right)

of these classes are all above 90% except for bare land. Kappa coefficients for individual and for overall classes are higher than 90% except for grassland.

For the classification of 2015, user's accuracies ranging from 97.0% to 88.33% (Table 3-8). Roof has the highest user's accuracy and followed by grass, bare land, tree, road, and shadow. Water is the only class that has a user's accuracy less than 90%. The producer's accuracies range from 98.96% to 88.07%. Bare land and shadow are the two classes with figures lower than 90%. Kappa coefficients in the result of individual and overall classes also show high agreement.

Figure 3-6 illustrates the difference of user's and producer's accuracies for both years. Roof, tree, and grass are three classes that have high user's accuracy in both years. The producer's accuracies of roof, tree, water, and road are higher than 95% in both years. Bare land, grass, and shadow are classes that contain more errors in the classification. Results from the error matrix indicate that the classification attained high accuracy, which was necessary for land cover change analysis.

3.3.2 Total change statistic (TCS) and land cover transition (LCT)

TCS and LCT measured the land cover change at two different levels. TCS summarises a net change including both negative and positive change for a specific land cover type. It provides general information about the area change. LCT, by comparison, shows the directions of land transition and their contribution to the net change. Figure 3-7 summarised the TCS and LCT statistics showed the land cover change from two perspectives (details of the statistics are shown in Appendix E). The bar chart illustrates the gains and losses for each land cover type between 2011 and 2015. Negative values indicate the area transitioned out to other classes, while positive values indicate the input of area from other classes.

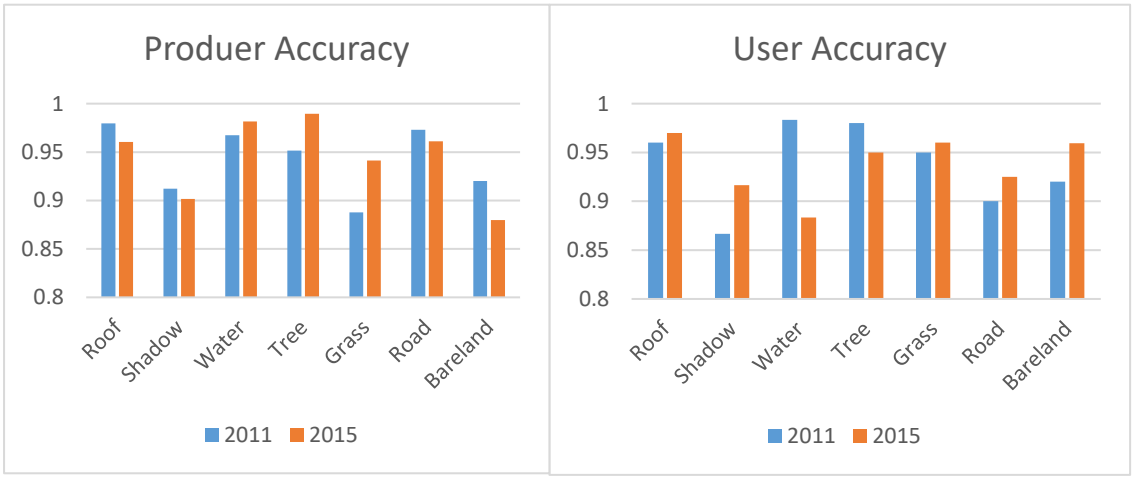

Figure 3-6. Comparison of accuracy change

Table 3-7. Error matrix of land cover map derived from 2011 datasets

User's Class \ Sample	Roof	Shadow	Water	Tree	Grass	Road	Bare land	Sum
Roof	96	1	0	2	1	0	0	100
Shadow	1	52	1	3	2	0	1	60
Water	0	0	59	0	1	0	0	60
Tree	1	1	0	98	0	0	0	100
Grass	0	3	1	0	95	0	1	100
Road	0	0	0	0	2	72	6	80
Bare land	0	0	0	0	6	2	92	100
Sum	98	57	61	103	107	74	100	
Producer's	97.96%	91.23%	96.72%	95.15%	88.79%	97.30%	92.00%	
User's	96.00%	86.67%	98.33%	98.00%	95.00%	90.00%	92.00%	
Kappa (Per Class)	97.55%	90.25%	96.36%	94.17%	86.54%	96.88%	90.40%	
Overall Accuracy	94.00%							
Kappa	92.95%							

Table 3-8. Error matrix of land cover map derived from 2015 datasets

User's Class \ Sample	Roof	Shadow	Water	Tree	Grass	Road	Bare land	Sum
Roof	97	0	0	1	1	1	0	100
Shadow	1	55	1	0	2	0	1	60
Water	0	2	53	0	1	0	4	60
Tree	2	3	0	95	0	0	0	100
Grass	0	0	0	0	96	2	2	100
Road	0	0	0	0	0	74	6	80
Bare land	1	1	0	0	2	0	96	100
Sum	101	61	54	96	102	77	109	
Producer's	96.03%	90.16%	98.15%	98.96%	94.12%	96.10%	88.07%	
User's	97.0%	91.67%	83.33%	95.00%	96.00%	92.50%	96.00%	
Kappa (Per class)	95.25%	89.07%	97.94%	98.75%	92.94%	95.50%	85.58%	
Overall Accuracy	94.32%							
Kappa	93.33%							

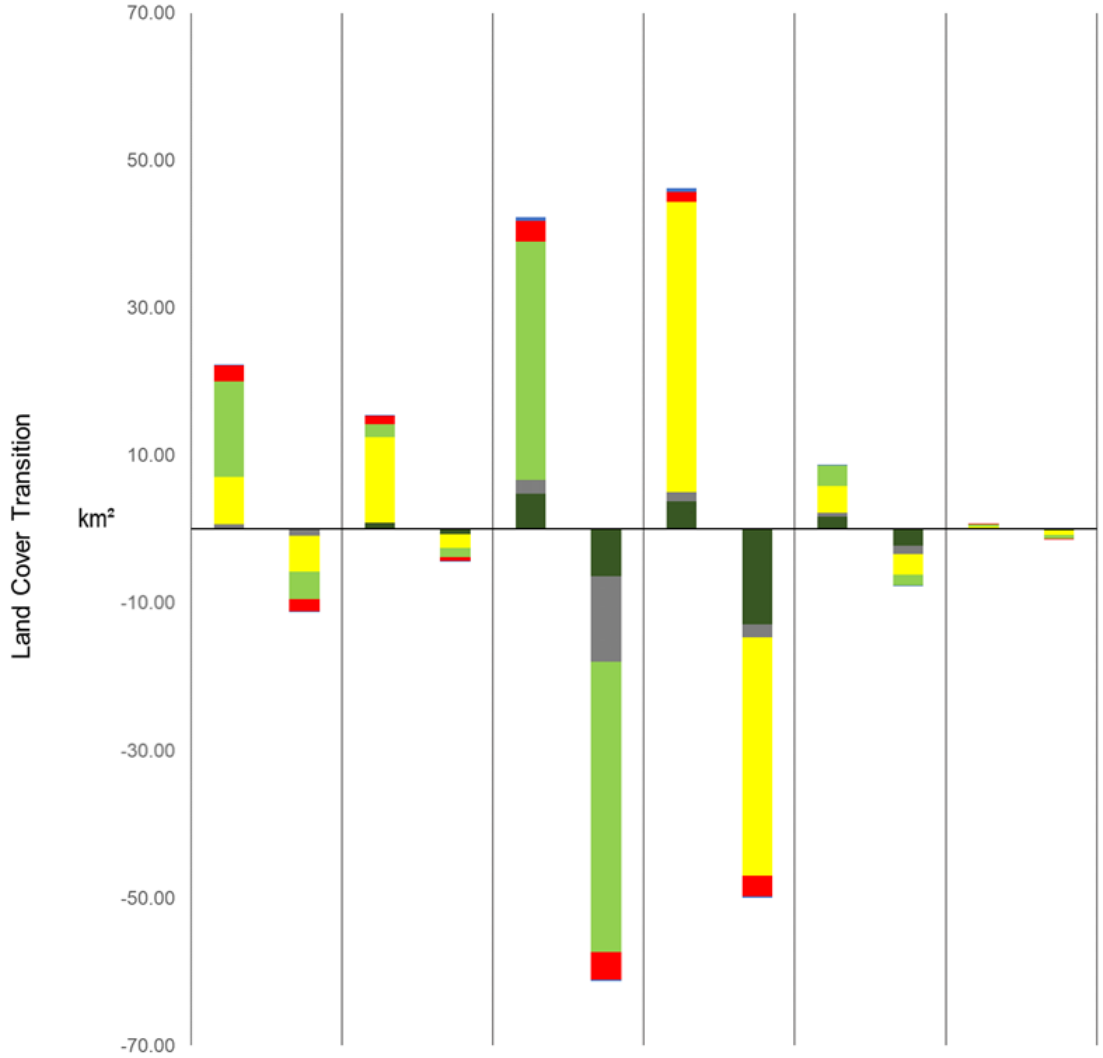

TCS (km²)	Tree	Road	Bare land	Grass	Roof	Water
Net change	11.06	11.16	-18.93	-3.71	1.09	-0.66
2011(without shadow)	51.81	21.33	119.61	100.14	33.61	4.54
2015(without shadow)	62.87	32.49	100.67	96.43	34.69	3.87

Figure 3-7. Land Cover Transition from 2011 to 2015

Table 3-9. Percentage of land cover change using data from 2011 as reference

		2015					
		Tree	Road	Bare land	Grass	Roof	Water
2011	Tree	78.22%	1.74%	9.26%	7.26%	3.31%	0.21%
	Road	3.30%	79.85%	8.75%	5.68%	2.28%	0.13%
	Bare land	5.33%	9.69%	48.77%	32.92%	3.08%	0.21%
	Grass	12.89%	1.78%	32.24%	50.07%	2.77%	0.24%
	Roof	6.56%	3.35%	8.49%	4.12%	77.38%	0.10%
	Water	3.35%	1.00%	12.03%	12.09%	0.52%	71.01%

For TCS, road and tree increased dramatically by 11.16 km² and 11.06 km², respectively. Roof had a slight growth of 1.09 km². Bare land had a significant decrease of 18.93 km² and then followed by grass with 3.71 km² of decrease. Water showed minimum change among the seven classes.

Nearly 80% of roads did not change compared with 2011 data (Table 3-9). The largest increase of road was from bare land, with 11.59 km². Most of this transition occurred in urban areas, where the road boundary became more continuous and clear in 2015.

During this period, 78.22% of tree area remained the same (Table 3-9). The increase of tree cover was contributed the most by grass, with 12.91 km². The second and the third ones are bare land and tree (mainly caused by tree crown growth), with 6.37 km² and 2.20 km² respectively (Figure 3-7). Most of the increase occurred at Styx suburb in the north-east of Christchurch (Appendix C). A large area of bare land and grass areas in this suburb such as in the Bottle Lake forest and Travis wetland nature heritage Park had been planted with trees during the 4 year period. For the losses, most parts of the tree was harvested or deforested as bare land with 4.80 km² and followed by grass with 3.76 km². Plantation areas in Styx and Cashmere West were two places where these transitions occurred the most.

There were 75.14% of roofs with no change within the study period (Table 3-9). Most roofs were replaced by bare land (2.85 km²). This is followed by trees (2.20 km²) and grass (1.38 km²). The decrease of roof may indicate that the corresponding building was demolished and had not been rebuilt. A large area of roof loss occurred in the Brooklands suburb and alongside the Avon River. About 3.69 km²and 2.78km² of the roof areas were built on bare land and grassland, respectively. These new buildings concentrated in south-west and north-east of the study area at Wigram, Halswell, Islington, Aidanfield and part of Styx suburbs.

Both grass and bare land had dramatic gains and losses, with only 48.77% and 50.07% of their area undergoing no change (Table 3-9). Most bare land (39.38 km²) was converted into grassland. The second highest loss was to the road, which was the main source of road increase. Grass experienced large areas of gain and loss to bare land within the study period but ended up with slightly decreases in

total area. The gain and loss of these two land cover types occurred mostly in rural places consisting mainly of cropland, grassland and natural parks.

Water had nearly 30% area lost (71.01% of no change) from 2011 despite the small decrease in area (Table 3-9). About 1.1 km² of water became grass and bare land in 2015. These transitions contributed largely to the loss and mainly existed in river and pond shores.

3.3.3 Exploring tree cover in Christchurch

After classification, tree covers for 2011 and 2015 were extracted for further analysis. Tree class was defined as both trees and shrubs in the classification process, so the analysis in this section includes both of these two types of vegetation. Tree cover maps for 2011 and 2015 were first produced and provided in Appendix E. Tree cover was then described for Christchurch's wards, which are a boundary created by the CCC for the purpose of enhancing community recognition and involvement for local governments (Stats, 2001). There are 15 out of Christchurch's 16 wards that had overlap with the study area, so only these wards were included (Figure 3-8). Figure 3-9 provides the percentage of tree cover for fifteen wards in Christchurch.

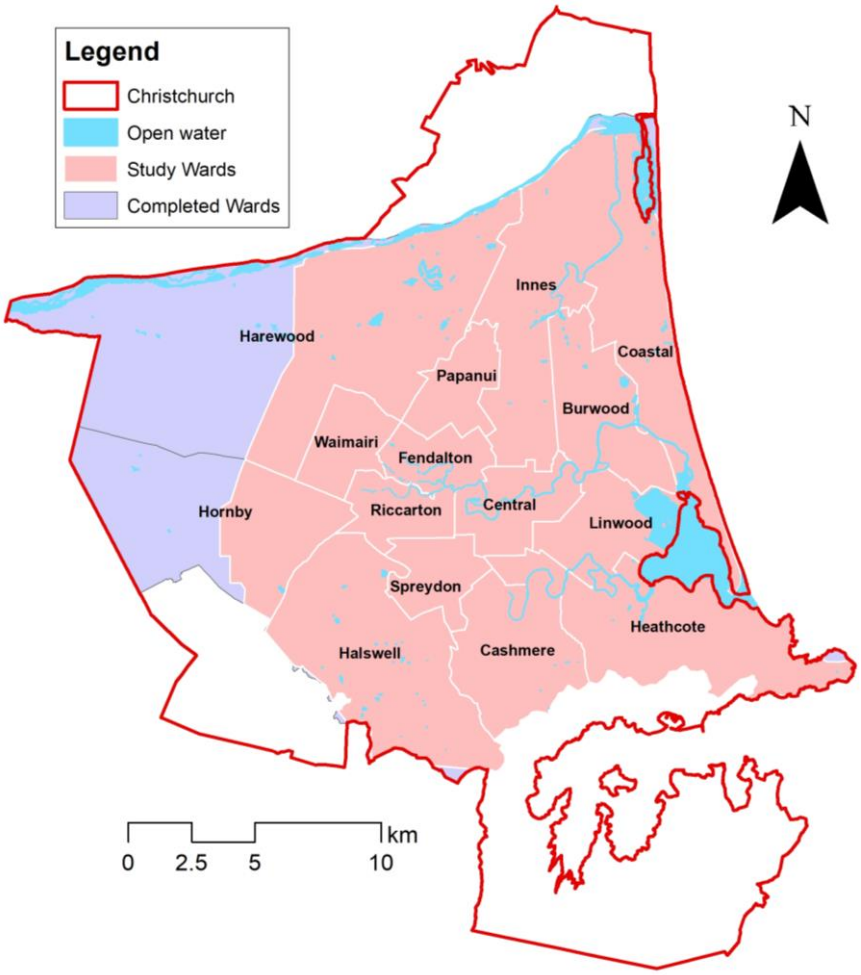

Figure 3-8. Overlapped wards for tree cover study

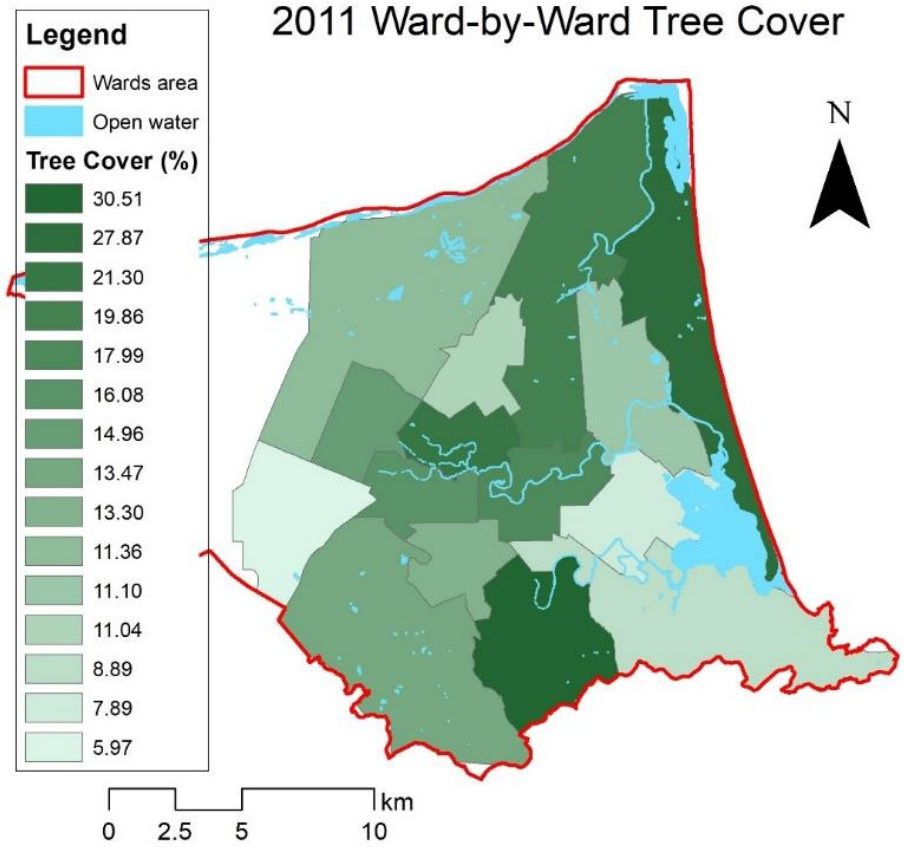

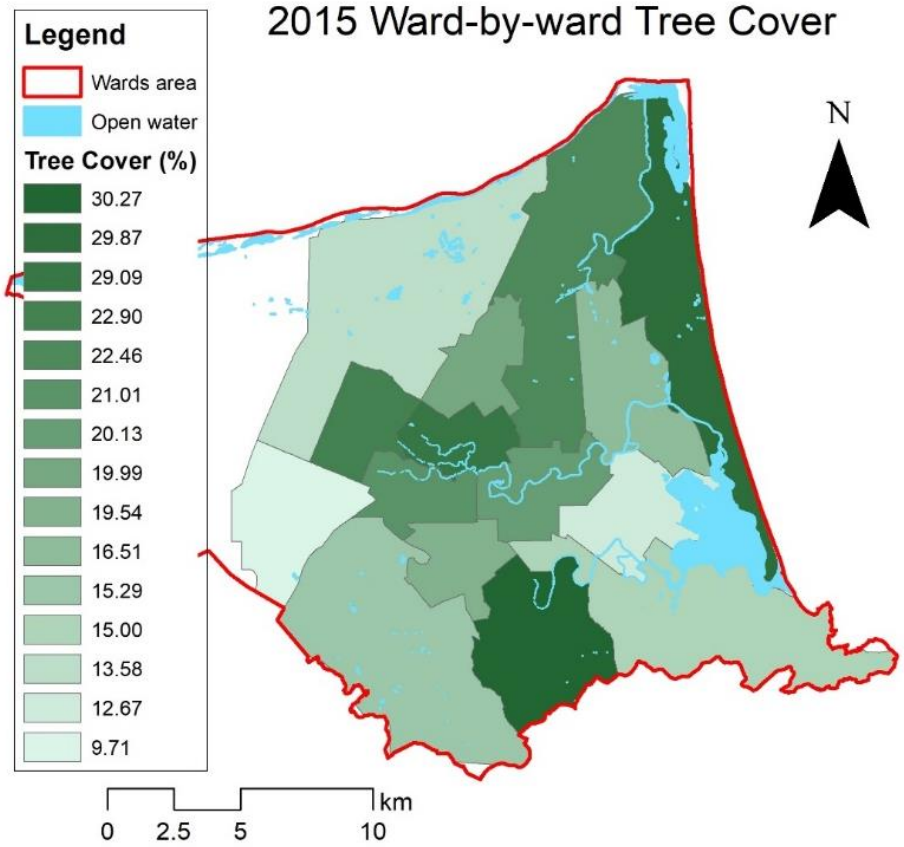

Figure 3-9. Ward by ward tree cover of 2011 (left) and 2015(right)

Table 3-10 shows the percentages of tree cover in different wards. Between 2011 and 2015, the total tree cover percentage increased by 3.54% (from 15.46% to 19.00%) in the study area. For different wards, tree cover in 2015 increased over 2011 values by 1.82% to 8.95%. Cashmere was an exception, showing a 0.24% decrease in tree cover between 2011 and 2015. The most significant increase in tree cover occurred in Papanui ward.

Table 3-10. Ward by ward tree cover change by area and percentage

Ward name	Ward area (ha)	2011 tree cover		2015 tree cover		Change	
		ha	%	ha	%	ha	%
Burwood	2050.07	227.51	11.10%	338.39	16.51%	110.88	5.41%
Cashmere	2390.44	729.22	30.51%	723.5	30.27%	-5.72	-0.24%
Central	1322.36	237.87	17.99%	266.2	20.13%	28.33	2.14%
Coastal	3118.03	868.97	27.87%	931.31	29.87%	62.34	2.00%
Fendalton	908.213	193.43	21.30%	264.24	29.09%	70.81	7.79%
Halswell	4533.19	610.66	13.47%	693.26	15.29%	82.6	1.82%
Harewood	5272.71	599.23	11.36%	716.14	13.58%	116.91	2.22%
Heathcote	3785.53	336.46	8.89%	567.75	15.00%	231.29	6.11%
Hornby	1843.54	110.13	5.97%	178.94	9.71%	68.81	3.74%
Innes	4049.17	804.3	19.86%	909.6	22.46%	105.3	2.60%
Linwood	1645.81	129.84	7.89%	208.54	12.67%	78.7	4.78%
Papanui	1050.31	115.91	11.04%	209.91	19.99%	94	8.95%
Riccarton	962.063	154.69	16.08%	202.1	21.01%	47.41	4.93%
Spreydon	1007.83	134.02	13.30%	196.92	19.54%	62.9	6.24%
Waimairi	1047.6	156.68	14.96%	239.93	22.90%	83.25	7.94%
Total	**34986.87**	**5408.92**	**15.46%**	**6646.72**	**19.00%**	**1237.8**	**3.54%**

3.4 Discussion

3.4.1 Classification accuracy

For other previous studies which use a data fusion approach, classification accuracies have ranged between 89.40% and 95.97% (Brennan & Webster, 2006; Chen, Su, Li, & Sun, 2009; Huang, Zhang, & Gong, 2011; Li et al., 2007). Like previous results, the classification result in this study also reached comparably high overall accuracies for both 2011 and 2015.

While the overall accuracy did not vary markedly between 2011 and 2015, the accuracies for individual classes did vary considerably. When the user accuracy is larger than the producer accuracy, there is a higher proportion of omission errors compared with that of commission errors, which means this class is under-classified. On the other hand, a higher percentage of commission errors exist when the user accuracy is lower than the producer accuracy. This indicates that this class is over-classified (Wilson & Sader, 2002; Xu, Morgenroth, & Manley, 2017).

For seven land cover classes in 2011, user accuracies of grass, tree, and water are higher than the producer accuracies. This means the proportions of omission errors are higher than that of commission errors and these classes were under-classified. The main source of omission errors for three classes are misclassifications to shadow. Producer accuracies of road and shadow are much lower than the user accuracies. For these two classes, the main sources of commission errors are from bare land and grass, respectively. This means pixels of bare land and grass tend to be classified into road and shadow. The under-classification and over-classification in 2011 can mostly be explained by the low brightness of RGB images. Due to poor weather and illumination conditions, brightness differences between pixels in images from 2011 are minor. Grass, trees, and water can contain many dark pixels (low brightness) which can be identified as other classes, for example, some dark green grassland were classified as shadow (Figure 3-10). Consequently, these classes tend to be under classified. Similarly, road and shadow are over classified because low brightness pixels have higher possibilities to be assigned to these two classes.

Figure 3-10. Misclassification between grass (light green) and shadow (black) caused by poor illumination in 2011 imagery.

For the classes in 2015, the user accuracies of bare land, grass, shadow, and roof are higher than the producer accuracies. Apart from bare land, the gaps between two types of accuracy are minor, within 2%. Omission errors in bare land are significant, 8% higher than the figure of commission and this means the classifier tend to assign pixels of bare land into road. The producer accuracies of water, road and tree are higher than the user accuracies. This indicates tree, water, and road classes were over classified and contain more misclassified pixels that should belong to other classes. Tree class was over classified mainly because of errors from shadow. Water and road class was over classified mainly caused by commission errors from bare land. The brightness of RGB images from 2015 has been significantly improved. However, the spectral similarity becomes the main reason for under- and over-classification. For example, bare land class was well classified in 2011 (92% in both producer and user accuracy) but became under classified in 2015. With the improvement of illumination conditions, some bare land surfaces could have higher spectral similarity with road (close in colour) and they are also difficult to distinguish using elevation data. Figure 3-11 shows that a bare land area which had lower brightness in 2011 was classified into road at 2015.

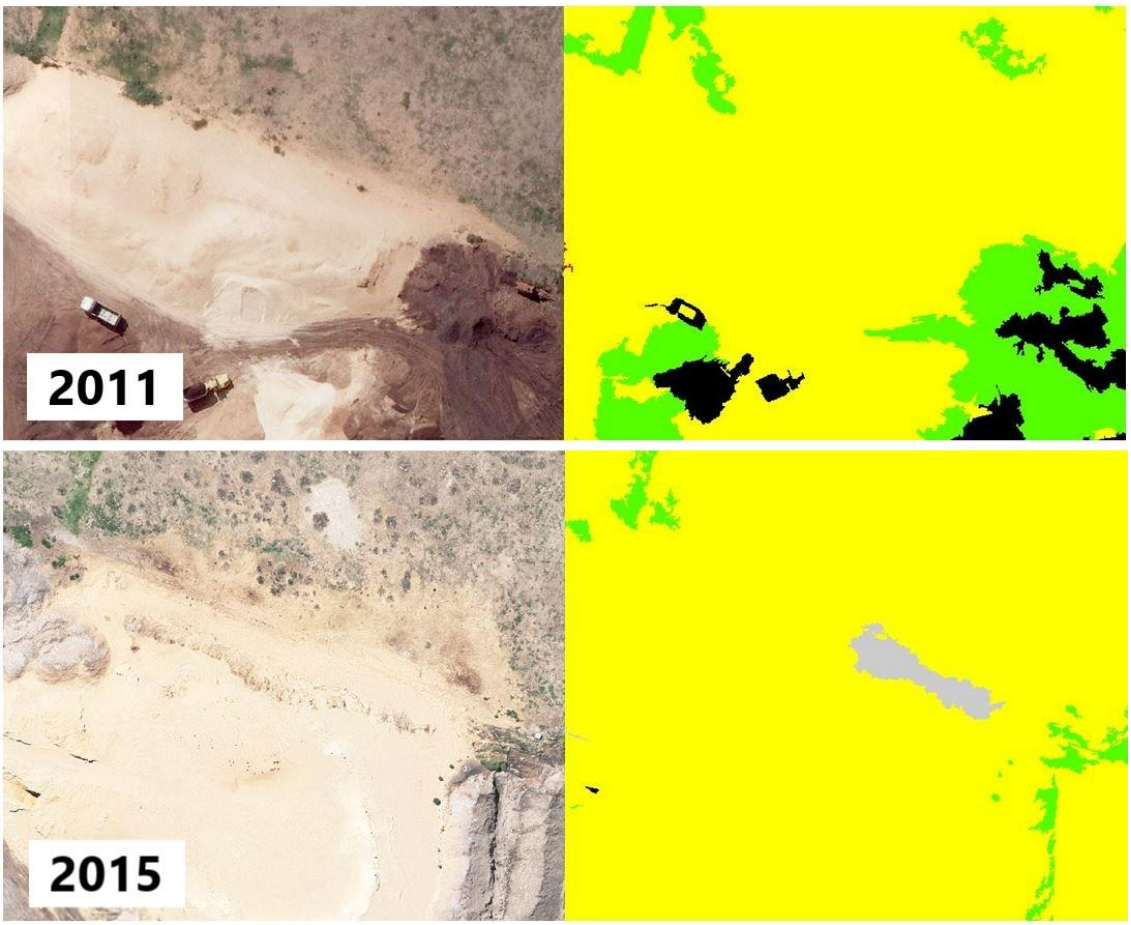

Figure 3-11. Misclassification between bare land (yellow) and road (grey) caused by spectrally similar brightness

To summarise, two main reasons that caused errors of under- and over-classification are the low brightness of RGB images from 2011and spectral similarity for classes with comparable elevation values. Some of these errors were eliminated by adding LiDAR features, for example, roofs were effectively distinguished with trees with similar colour using different values of LiDAR returns (RPP), while some errors were reduced by adding shape features, for example, using standard deviation of edges of objects, road objects which contain long edges were effectively distinguished with bare lands which have more short edges, despite their similarity in both spectral and elevation values.

When considering the changes of user accuracy within this period, the figures were varied. Apart from water and tree, all other classes showed improvements of between 1% and 4%. Potential reasons for the decreases in water and misclassification from algae covered surfaces for water and tree including poor orthorectification qualities. The reasons for those misclassifications are further discussed in section 3.4.2. The highest improvement existed in shadow because shadow areas were easier to identify under better light conditions using 2015 RGB images as opposed to 2011 images. As discussed previously, brighter sunlight can result in higher reflectance for the classes apart from shadow and this will provide more significant spectral differences that allow better differentiation between classes. Also, the higher spatial resolution and better orthorectification quality of the 2015 RGB images also produced more clearly segmented objects, which helps to avoid misclassification caused by seeing the sides of buildings (orthorectification issues) and enabled clearer delineation for classification objects.

As far as producer accuracies are concerned, roof, water, and road did not change significantly and were all greater than 95%. This is because these classes have obvious differences in vertical structure, allowing LiDAR features such as return per pulse and elevation, to classify them correctly. Using these features the classifier can effectively identify their classes with less information from RGB images. In 2011, the tree class had a producer's accuracy of 95.0% but this increased to 98.96% in 2015. It's possible that better quality RGB images from 2015 contributed to this improvement and resulted in the same change within the grass class. Compared with data from 2011, 2015 images have higher quality in both spatial and spectral perspectives. A higher spatial resolution allows clearer segmentation for individual trees in heterogeneous environments, for example one small tree adjacent to a roof (Chen, Stow, & Gong, 2004). The weather conditions when acquiring aerial imagery in 2015 were better than in 2011. The cloud cover was minute in 2015 and therefore sun illumination is stronger. This yielded higher quality images with brighter colour and higher contrast, which means more sufficient spectral information could be used to improve classification accuracy for vegetation (Myeong, Nowak, Hopkins, & Brock, 2001).

Overall, a fusion of RGB imagery and LiDAR resulted in high classification accuracy for land cover classes that are different in elevations and LiDAR pulse returns. When there is no sufficient spectral

information, it also yielded more stable classifications. A higher spatial resolution of RGB images from 2015 generally increased the user's accuracies for most classes, except for tree and water.

3.4.2 Explanations for land cover change

The land cover change map (Figure C-1) illustrates the spatial distribution of land transitions. By analysing where land cover changes occurred and identifying land transitions, this study further discussed reasons for those changes. The CES caused serious damage to the built-up areas in Christchurch. These damages including surface rupture, surface deformation, liquefaction, lateral effect and subsidence effects, mass movements, river avulsion, river gradient change and flooding (Quigley et al., 2016). With four years of rebuilding and redeveloping, many consequences of the damage had been repaired, which also resulted in noticeable land cover changes. Apart from the CES effects, many other reasons such as government policies, forest plantation and seasonal difference also contributed to the transitions between classes.

Tree cover increased by 11.06 km² between the two time periods. The increased area of trees is likely caused by two primary reasons. Firstly, due to annual growth, the size of tree crowns increased during the study period, thus resulting in a cumulative increase in tree canopy cover. With nearly five years of growth, most tree canopies had increased significantly in crown area (Figure 3-12). Another reason for increased canopy cover is misclassifications for the tree canopies. These errors are further discussed in section 3.5.3.

The tree cover result from 2015 was similar to the result from a study conducted by Morgenroth (2017), in which he analysed tree cover in all of Christchurch's wards. Given the study areas are different, a direct comparison with the present study is difficult. However, within the ward boundaries that have the same extent, tree cover figures from this study are generally 2-5% higher than the figures from Morgenroth (2017). The likely reason for this is the height threshold used to define trees in each study. Morgenroth (2017) only included trees that were greater than 3.5 m tall, while this study used a height threshold of 1 m. As a consequence, more small trees and shrubs would have been included in this study and resulted in higher tree cover estimates.

When observing tree cover changes within each ward, Cashmere was the only ward that showed a decrease between 2011 and 2015. The reason could cause by large-scale plantation forests being harvested (Figure 3-13). For the increases in other areas, the reasons could also be summarised as tree growth and misclassifications.

	2015 crown	2011 crown	Growth	Removed tree
Area (m²)	409.71	186.56	223.15	32.79

Figure 3-12. Tree crown growth. *Despite a tree being removed (green polygon), the growth in crown area was still considerable.*

Road has the second highest increase in area and mostly transited from bare land. As mentioned before, most road boundaries expanded and became clearer in 2015. This change was caused by the damages of CES and the recovery processes. Liquefactions from the earthquake resulted in a considerable amount of ejection of water, silt and sand on the surface (Potter, Becker, Johnston, & Rossiter, 2015) and converted the land cover type of those areas. Besides, rock fall and landslides also caused damages of roads in Lyttelton areas (Cubrinovski et al., 2010; Kaiser et al., 2012). As a result, road surfaces which were affected by liquefaction or damaged by landslides were misclassified as bare land in 2011. After reconstruction, these surfaces transitioned back to roads and resulted in a significant growth of road area. For example, transitions from bare land to road occurred extensively along the banks of Avon River where roads had been severely covered with sand and flooding (Figure 3-14). This problem has

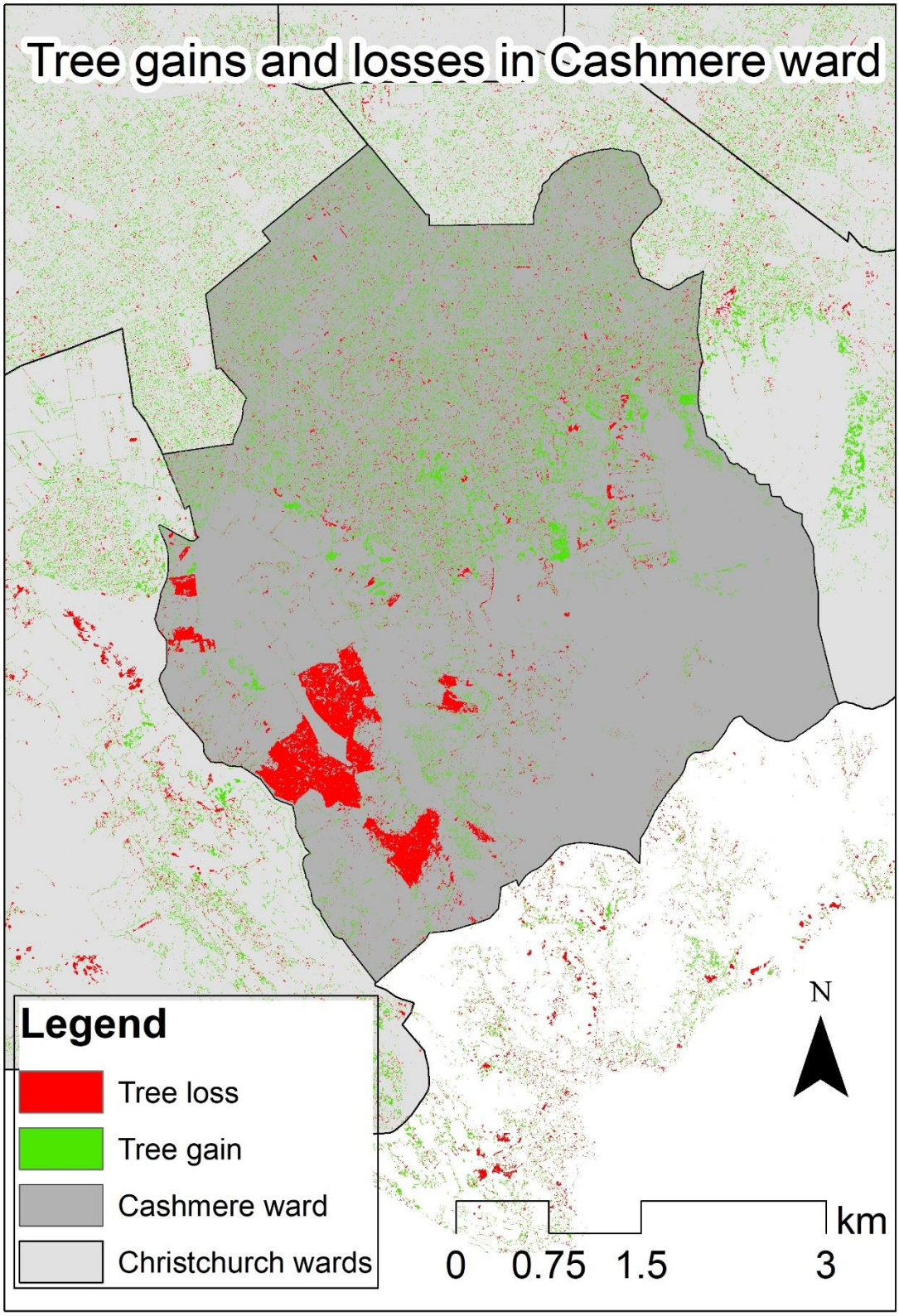

Figure 3-13. Tree gains and losses in Cashmere ward

previously affected the accuracy of object-based image analysis land cover studies in Christchurch (Morgenroth, Hughes, & Cubrinovski, 2016). This limited the detection of real road network change (such as the area of new roads or the increase in asphalt covered surface), as the base data of 2011 is poorly quantified. On the other hand, however, this analysis provides more information for the road damage assessment. Many studies and reports assessed the number of damaged roads and bridges (Chouw & Hao, 2012; Cubrinovski et al., 2010; Eidinger & Tang, 2012), but the affected area was less recorded. Canterbury Regional Council, Christchurch, NZ (2013) reported that the recovery programme of Christchurch involved 900,000 tonnes of liquefaction silt removal. With such a huge amount of work, this remote sensing based method could provide damages estimations in terms of area and work-load with less time and cost. This idea was first suggested by Morgenroth et al. (2016) in their case study of a small area in east Christchurch.

Figure 3-14 Flooded area caused difficult identification of road

The greatest loss of roof cover occurred in the residential red zone areas that were marked by the New Zealand government after the CES. The land and infrastructure in those areas were seriously damaged in the earthquakes and was no longer suitable for residential usage over a short to medium term. Thousands of residential homes were demolished in the red zone areas (LINZ, 2016). By comparison, the city centre experienced both demolitions and reconstructions. About 1240 buildings had been demolished in central Christchurch due to the damage caused by CES (CERA, 2016), while some of the buildings were rebuilt or redeveloped. New buildings, which contributed to increasing roof cover, were distributed primarily in two areas of Christchurch, replacing areas that used to be cropland or bare land. Halswell and Wigram which are under the South-West Christchurch Area Plan, are anticipated to be the largest population growth suburb in Christchurch through to 2031 (CCC, 2014). The urban growth had been in high rate in these areas after the earthquake and this trend is expected to continue.

Transitions from bare land to grass occurred mainly at cropland and dry grassland in rural areas. Part of the reason for this transition was the damage caused by CES such as liquefaction and surface rupture.

In 2017, the land was covered in liquefaction, resulting in a classification of ‘bare land’. These places were later recovered as grassland in 2015. Besides, the growth of grass in 2015 was generally better than that in 2011. An extensive area of dry grassland turned into green grassland at 2015. This is likely related to the season of image acquisition. In 2011, the imagery was captured in late summer, by which time grass had dried out and turned yellow or brown. In contrast, in 2015, the imagery was captured in late spring when new grass was green.

Most loss of water surfaces in 2011 transitioned into grass or bare land. During the CES, water environment had been seriously affected by liquefaction and groundwater change. The hydrological effects including the formation of new springs, expulsion of groundwater, and surface flooding, resulted in a widespread surface flooding (Quigley et al., 2016). Some of these flooded areas later turned into other land cover types such as marshland, which is also the main reason for water-grass and water-bare land transitions (Figure 3-15). Besides, some water surface was covered by algae in 2015 also contributed to water-grass transition (Figure 3-16).

Figure 3-15. Flooded area to bare land, 2011 (left) vs. 2015 (right).

Overall, most land cover decreases between 2011 and 2015, such as buildings, bare land, grassland and water surfaces were related to the damages caused by CES. The changes of different land cover types are caused by various reasons such as government policy, seasonal differences or vegetation growth, and reconstruction processes. By analysing those transitions, the extent of some damage such as liquefaction and flooding is also available for more detailed evaluations. Compared with human surveys, this remote-sensing based method is more time and resource efficient and suitable for large extent analysis.

Figure 3-16. Algae covers water surface in 2015 (right), but not in 2011 (left).

3.5 Limitations

3.5.1 Aerial image difference

Different qualities of aerial imagery have led to some errors. The imagery from 2015 has higher resolution (0.075 m) as well as a better orthorectification quality. As introduced in the methods section, several shortcuts were used for orthorectifying 2011 images, which led to misalignment of raster layers. An obvious consequence is that some building edges were segmented and misclassified as trees or other land cover types (Figure 3-17). Because of the poor orthorectification, some building sides were segmented into objects. These objects can have same feature values such as return per pulse with tree objects and therefore have possibilities to be misclassified into tree. As mentioned in the previous

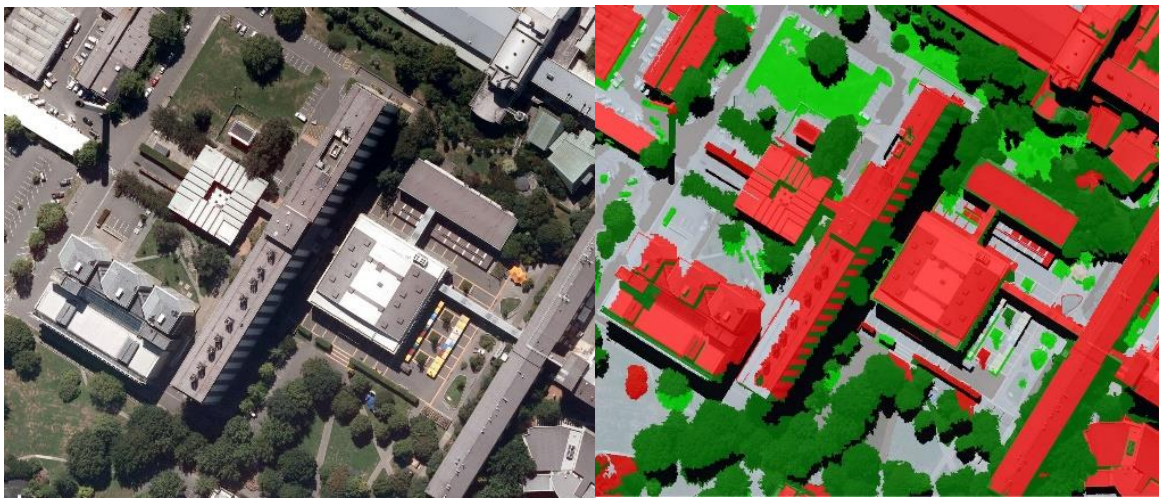

Figure 3-17. Errors caused by poor orthorectification

section, the errors from orthorectification issues could contribute most on the decrease of user accuracy for trees.

Imagery tiles were originally merged by individual aerial photos. For 2011 data, a simple 'most nadir' algorithm was used for this process. This algorithm generated many seam lines between tiles and caused errors in both segmentation and classification steps. As shown in Figure 3-18, a roof was segmented into different objects between tiles and some parts were misclassified. Considering difficulties of reference data collection and limited research time, correction of these errors is impractical and this became a limitation of this study.

Figure 3-18. Errors caused by seamlines

3.5.2 Some misclassifications

High-resolution RGB imagery provides very detailed information which enables more accurate segmentations on heterogeneous land cover types such as urban environment (Chen et al., 2004). However, this also increases the difficulty in selecting optimum scales that can work effectively for all land cover types. For example, ventilation installations, air conditioners, skylights and other structures on the top of roofs were segmented into individual objects and then classified into different land cover types. Some roof edges were also segmented and misclassified into trees. This is because that roof edges have similar attributes in terms of LiDAR returns (RPP) and elevation (nDSM). Those issues are common in urban land cover classifications using remote sensing data (Awrangjeb, Zhang, & Fraser, 2012). Some corrects can be finished with more spectral bands such as near-infrared band (Awrangjeb, Ravanbakhsh, & Fraser, 2010; Meng, Currit, Wang, & Yang, 2012) or full-waveform LiDAR data (Tseng, Wang, Chu, & Hung, 2015), which are not available for this study. For the 2015 datasets, these errors were more common due to a higher resolution of RGB images and led to a decrease for user's accuracy of tree class in 2015. However, the misclassification from roofs to trees only have a minimal effect for the overall accuracy statistic and the producer and user accuracies for roof and trees did not

show significant differences. According to the final classification result, the overall accuracies were also at a reasonable level compared with previous studies (Brennan & Webster, 2006; Chen et al., 2009; Huang et al., 2011; Li et al., 2007). Those segmentation errors were therefore accepted. Nevertheless, some potential solutions are discussed below.

One solution to reduce errors is increasing the segmentation scale parameter value, but this will lead to under segmentation for small roofs. Adding more area divisions (such as dividing urban areas into residential areas where have small roofs and central business districts where have large roofs) with different segmentation scales could be a potential solution. However, selecting those area divisions required large amounts of manual work, which is not suitable for the time period in this study. Thus, dividing study area into two divisions is reasonable. Likewise, post-processing the land cover classes resulting from RF classification could minimise these misclassifications. However, post-processing would increase the manual processing required and render results less generalisable.

Another limitation of the study is limited spectral bands. For example, misclassification between roof edges and trees could be reduced with the introduction of near-infrared (NIR) band for both land covers have multiple LiDAR pulse returns and are similar in elevation. The NIR band, and its use in common vegetation indices like the normalized difference vegetation index (NDVI) could have been able to better differentiate between those two land cover classes. Many previous studies have shown the utility of the NIR band or NDVI to identify vegetation (Al-Kofahi et al., 2012; Malinverni et al., 2011; Moskal et al., 2011). Figure 3-16 illustrates misclassification for algae covered water surfaces. Both LiDAR data and RGB bands have limitation for identifying these surfaces. It also results in a significant decrease of user's accuracy of water class in 2015.

3.5.3 Pixel-based land cover transition analysis

Issues associated with pixel-based change detection (PBCD) had been discussed in many studies (Alberti et al., 2004; Chen, Hay, Carvalho, & Wulder, 2012; Im, Jensen, & Tullis, 2008). Errors from image registration and salt-and-pepper noise are two main problems that affected the accuracy of PBCD. In this study, these problems also occurred and introduced errors for change analysis. One alternative for PBCD is object-based change detection (OBCD). However, the limited computing capacity makes using OBCD for this study unachievable. With high-resolution RGB images, each scene could contain millions of objects for a single class. The small pixel size (0.075m/1m) also generates objects with a large number of vertices and edges. Extracting and processing these objects require massive computing power which is not available in this study. As a result, PBCD was applied, and its limitations were accepted.

3.6 Conclusion

After the CES, Christchurch experienced a dramatic land cover change due to the rebuild of the city. As a result, monitoring urban land cover change is crucial for urban management and development. Compared with other survey methods, remote sensing is an efficient way to acquire land cover information to a large extent. The availability of high-resolution RGB imagery and LiDAR data five years apart provided a possibility to accurately analyse the land cover change in Christchurch during this period. To overcome the limitations of a single data source, this study explored an OBIA by fusing these two datasets and yielded an accurate classification result.

Based on the classification results, the land cover change of Christchurch city between 2011 and 2015 was analysed. The statistics showed that the area of tree, road, and roof had increased, while bare land, grass and water decreased. To better understand the reasons for those changes, land cover transitions were calculated. Canopy growth, seasonal differences and forest plantation establishment were the main reasons for tree area increase. Reconstruction and recovery after the earthquake was the main reason for road area growth. Liquefaction and other damage caused by CES had led to dramatic transitions between bare land and grass. By comparing the spatial distribution of these transitions, this study also identified Halswell and Wigram as the fastest developing suburbs in Christchurch. These data provided quantity information for the effects of CES and allowed a better understanding for the current status of Christchurch. Much information such as road damage, building demolishment and reconstruction, and tree canopy change could be accurately provided for decision makers in a short time.

In this study, a fusion of RGB imagery and LiDAR data had been proved as an effective tool for monitoring land cover change. With more available data in the future, this method could be applied for datasets with longer time spans to derive land cover information for different purposes. For future acquisitions of remote sensing data, some recommendations include: 1. Improve the quality of pre-processing for RGB imagery in terms of orthorectification, image mosaic and acquisition conditions. 2. Using sensors that can acquire wider spectral bands, such as NIR. 3. Minimise the time span between LiDAR data acquisition and spectral imagery acquisition to achieve better time consistency of two datasets. Using datasets with better quality, future studies could focus on areas such as exploring optimal classification process with fusion data or analysing land cover change for specific types (e.g. tree species, building change).

Chapter 4 - Individual tree crown detection and delineation

4.1 Introduction

The previous chapter provided insights into changes in land cover in Christchurch, between 2011 and 2015. The increase in tree cover was significant. In this chapter, the tree land cover is studied in greater detail using an individual tree crown delineation (ITCD) approach. Tree crown information plays a vital role in forest inventory and management as it is related to various forest attributes (Liu, Im, & Quackenbush, 2015). This is true in both natural forests, planted forests, and urban forests, like in Christchurch. When extracting crown information with remote sensing data, a land cover classification, followed by ITCD are the initial steps for deriving such information (Jing, Hu, Noland, et al., 2012). Among different data types, passive data including multispectral imagery is widely used (Ke & Quackenbush, 2011). However, the lack of vertical information can introduce significant errors when conducting ITCD in urban areas. By comparison, LiDAR data provide accurate tree structure information and various approaches have been developed for ITCD with LiDAR data. Both multispectral and LiDAR data have limitations, but a fusion of these two datasets can overcome shortages and achieve higher accuracy (Gulbe, 2015).

4.1.1 ITCD approaches

ITCD approaches assume that there is one highest point in each individual tree and the surrounding heights around this top gradually decrease until it reaches the edge of crown (Wulder et al., 2000). As a result, most ITCD approaches extract tree tops first and then use different algorithms such as watershed segmentation or region growing to detect edges of crown. Based on formats and usages of LiDAR data, approaches for tree crown delineation were divided into four types: raster-based approaches, point cloud based approaches, fusion approach and tree crown reproduction (Maltamo, Næsset, & Vauhkonen, 2014). Zhen, Quackenbush, and Zhang (2016) summarised 136 studies of individual tree count and crown delineation from 2001 to 2015. They reported that raster-based approaches accounted for the highest proportion among those studies and it also showed the fastest growth rate. Compared with other approaches, raster-based approaches have several advantages. Firstly, many LiDAR-derived features such as return numbers, intensity, and canopy maximum model can be exported as raster format, which allows fusion of LiDAR data with raster imagery. Secondly, it is more efficient and available for large datasets. Thirdly, a large number of raster-based algorithms have been developed and optimised for different tree cover environments (Maltamo et al., 2014).

4.1.2 ITCD accuracy assessment

The accuracy assessment for ITCD can be assessed by using plots or individual trees as units. When plots are used, only the number of detected trees within each plot will be considered, which ignores location information between delineated trees and reference data (Lamar, McGraw, & Warner, 2005) When considering accuracy based on individual trees, each delineated crown will be considered as an object. This allows detailed comparison of correspondence of trees and includes commission and omission errors that are missed in plot-based assessment (Ke & Quackenbush, 2011). If two or more tree crowns were detected within a referenced tree crown or the delineated object is not a tree, then there are commission errors. If a reference crown was missed, then there is an omission error. However, the definition of correct detection can be difficult because it is hard to find a perfect match between objects from delineation and reference data. Some studies considered the location of detected trees and specified that if there is only one tree inside a reference crown then it is a match (Dalponte & Coomes, 2016; González-Ferreiro et al., 2013; Pouliot et al., 2002). This method failed to consider the shape of delineated tree crowns but focused mainly on location accuracies. Several area-based comparisons were made to overcome this shortcoming. Lamar et al. (2005) used a 50% overlap as a threshold for identifying a complete match. Jing, Hu, Li, and Noland (2012) defined four types of correspondence between the delineated and reference crown. Similar criteria was also adopted. Liu et al. (2015) took both the tree tops and crown area into consideration and defined a crown with only one tree top and 50% overlap as a correct detection. Previous ITCD studies in urban environment used different accuracy assessment methods and were tested on different tree species. The overall accuracies of these studies ranged between 53% and 83% (Alonzo et al., 2014; Ardila, Tolpekin, Bijker, & Stein, 2011; Chang, Linb, Linc, & Liu, 2016; Iovan, Boldo, & Cord, 2008).

The main objective of this study is to assess the potential to count trees and delineate individual tree crowns for the urban forest in Christchurch, using automatic ITCD and a combination of LiDAR and aerial. No attempt was made to compare the number of trees in Christchurch in 2011 with the number in 2015 as this was beyond the scope of this study. However, should that be a future goal, this research will provide a workflow and guidance on the accuracy that can be expected.

4.2 Method

4.2.1 Canopy height model

In this study, LiDAR data and aerial imagery from 2015 were used because the higher resolution of aerial imagery allowed clearer selection of reference data. Using the classification result produced in previous chapters, the LiDAR point cloud was clipped using the raster extent of pixels classified as trees. A DEM, DSM, and CHM were interpolated from the clipped point clouds, using the same

methods described in section 3.2.4. When interpolating DSM from only points within the tree cover boundary, LiDAR pulses which penetrate through canopies and hit ground or substructures of trees can cause "holes" on the CHM raster surface. These "holes" will interrupt the continuity of tree crowns and result in errors on tree top detections (Khosravipour, Skidmore, Isenburg, Wang, & Hussin, 2014; Suárez et al., 2009). To address this problem, the CHM needed to be smoothed before tree top detection. Following the method used in the study conducted by Chang et al. (2016), a smoothing function called "subcircle" was applied. This function increases the size of a single LiDAR point by expanding its area and therefore fewer pits or empty pixels are generated in the CHM.

4.2.2 Plot selection and reference data

It was not feasible to test tree delineation for the entire study area, so 30 sample plots that contained tree cover were randomly established within the study area to assess the performance of tree crown delineation. All plots are circular with a fixed radius of 50 m. The boundaries of reference tree crowns within those plots were manually delineated by visually inspecting RGB imagery from 2015. After ITCD, the delineated crown polygons were clipped by the plots and then compared with those manually delineated tree crowns to assess accuracies.

4.2.3 ITCD approach

The raster-based approaches for tree delineation can be divided into two steps, tree top detection and crown delineation (Ke & Quackenbush, 2011). The first step produces "seeds" required for crown detection and the second step uses different algorithms to find the edge of crown.

4.2.3.1 Tree top detection using local maxima filter

Local maxima filter had been used in many studies for tree top and location detection (Chang, Eo, Kim, & Kim, 2013; Silva et al., 2016; Wu et al., 2016). For a crown of an individual tree, there is normally one highest point (tree top) and local maxima filter is used for detecting the highest point by filtering pixels with a fixed window (Brandtberg & Walter, 1998). If the central pixel within the window has the highest value, it will be identified as a tree top. Due to this reason, the window size can affect detection accuracy and should be set according to image resolutions and crown sizes (Ke & Quackenbush, 2011). To find the appropriate window size, three settings, 5×5 m, 7×7 m and 9×9 m, were tested in sample plots. Then, numbers of detected tree tops were compared with reference data.

Figure 4-1 showed a detailed comparison between 5×5 m, 7×7 m, and 9×9 m windows. Comparing with reference numbers of trees in 30 plots, both 5×5 m and 7×7 m windows yielded higher numbers of trees. A 9×9 m window yielded the closest estimations for a large majority of plots and, overall, detected 905

trees compared with 915 reference trees. As this estimation is close to the reference number, a larger window size was not tested, and the 9×9m window size was used for tree top detection and tree delineation.

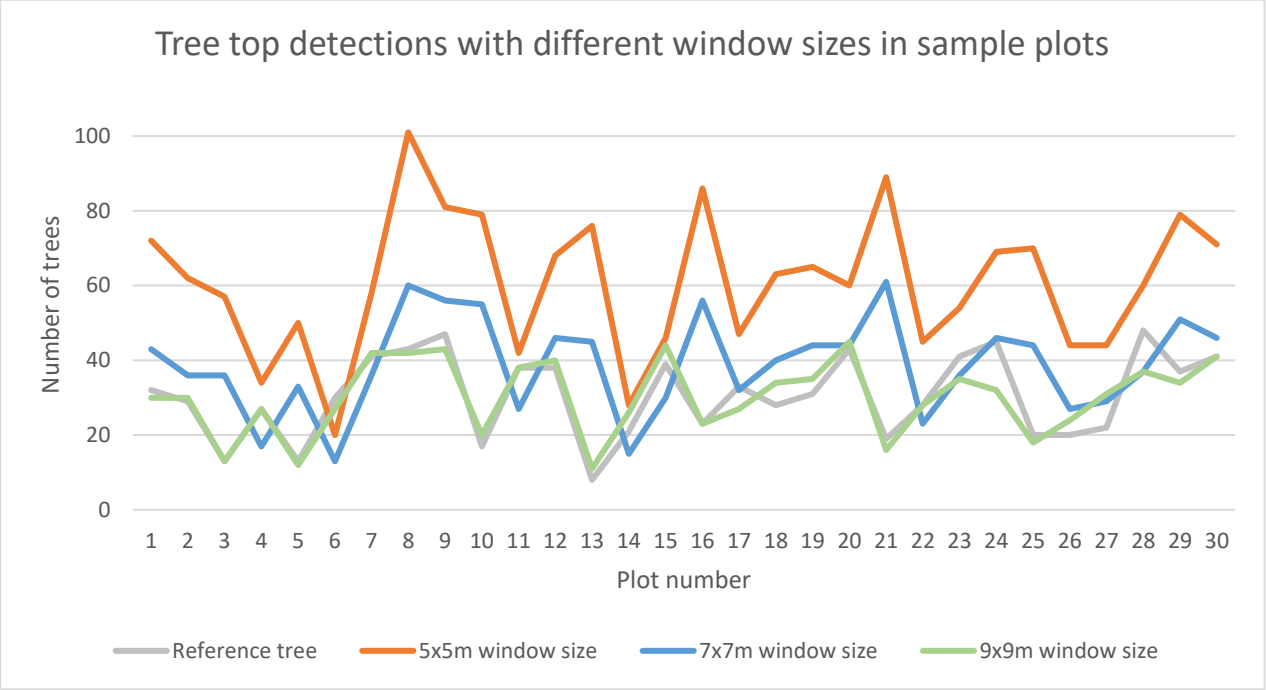

Figure 4-1. Comparison of tree top detections with 5×5m, 7×7m and 9×9m window sizes

4.2.3.2 Tree crown delineation

This study used a region growth algorithm proposed by Dalponte and Coomes (2016) for crown delineation. The method is performed in R using the lastree function from lidR package. Region growth is a pixel-based algorithm. It uses a central pixel as the seed to group surrounding pixels that have similar attributes and makes the region "grow". When significant differences in elevation are detected, the region growing will be stopped (Ke & Quackenbush, 2011). Using the tree tops which were detected with local maxima filter as seeds, tree crowns were delineated by this algorithm.

4.2.4 Accuracy assessment

Following the experience from previous studies (Jing, Hu, Li, et al., 2012; Lamar et al., 2005; Liu et al., 2015), 50% overlap was used as a threshold for identification of completed matches. The definition of errors was followed from the method in the research of Lamar et al. (2005). The omission errors referred to reference crowns which were not detected (less than 50% overlap of delineated crowns) and they

were represented by producer's accuracy (1), while the commission errors referred to two or more delineated crowns corresponding to one reference crown (less than 50% overlap of reference crown) and these errors were represented by user's accuracy (2):

$$\text{Producer's accuracy} = \frac{\text{Number of matched reference crowns (NoMR)}}{\text{Number of reference trees (NoR)}} \quad (1)$$

$$\text{User's accuracy} = \frac{\text{Number of matched delineated crowns (NoMD)}}{\text{Number of delineated trees (NoD)}} \quad (2)$$

Producer's accuracy and user's accuracy evaluated the overlap area from reference crown and delineated crown perspectives but they cannot provide a general view of accuracy. Therefore, an overall accuracy which evaluates both omission and commission errors were further calculated (3):

$$\text{Overall accuracy} = \frac{\text{NoMR+NoMD}}{\text{NoR+NoD}} \quad (3)$$

4.3 Result

For the 30 plots, the overall tree identification accuracy is 75.40%. Among 915 reference trees, the ITCD algorithm detected 905 tree crowns and 741 reference tree crowns overlapped more than 50% with delineated tree crowns. The user's accuracy was 70.17% and producer's accuracy was 80.98% (Table 4-1).

Table 4-1. Overall ITCD accuracies

Reference trees	Delineated trees	Matched reference trees	Matched delineated trees	User's accuracy	Producer's accuracy	Overall accuracy
915	905	635	741	70.17%	80.98%	75.40%

Accuracies for each individual plot were also analysed (Table 4-2). The overall accuracies range between 56.47% and 92.11%. There are ten plots that have overall accuracy higher than 80% and two plots that have overall accuracy lower than 50%. The producer's accuracies within 24 plots are higher than user's accuracies. On the other hand, the user's accuracies within 6 plots showed a higher value.

Table 4-2. ITCD accuracies in individual plots, sorted in declining order by overall accuracy.

Plot number	User's accuracy	Producer's accuracy	Overall accuracy
25	100.00%	85.00%	92.11%
21	93.75%	89.47%	91.43%
9	93.02%	89.36%	91.11%
17	92.59%	84.85%	88.33%
2	93.33%	82.76%	88.14%
22	82.14%	89.29%	85.71%
5	75.00%	92.86%	84.62%
13	72.73%	100.00%	84.21%
6	74.07%	86.67%	80.70%
30	78.05%	82.93%	80.49%
11	73.68%	84.21%	78.95%
16	69.57%	86.96%	78.26%
8	76.19%	79.07%	77.65%
7	69.05%	85.37%	77.11%
10	60.00%	94.12%	75.68%
23	74.29%	75.61%	75.00%
26	66.67%	85.00%	75.00%
19	62.86%	87.10%	74.24%
24	90.63%	62.22%	74.03%
14	61.54%	85.71%	72.34%
15	56.82%	89.74%	72.29%
29	64.71%	78.38%	71.83%
27	61.29%	86.36%	71.70%
1	60.00%	81.25%	70.97%
4	66.67%	74.07%	70.37%
18	52.94%	85.71%	67.74%
3	61.54%	69.23%	65.38%
12	55.00%	71.05%	62.82%
20	40.00%	74.42%	56.82%
28	54.05%	58.33%	56.47%

4.4 Discussion

Compared with other studies which yield overall accuracies between 53% and 83% (Chang et al., 2016; Shojanoori & Shafri, 2016; Zhang et al., 2015), the overall accuracy for this study reached 75.60%. From the perspective of reference data, most tree crowns within the study area were detected by the proposed method (80.98% producer's accuracy), but the ITCD also created considerable commission errors (75.40% user's accuracy), which indicates incorrectly delineated crowns. A lower user accuracy, relative to producer accuracy, means tree crowns were over-counted and delineated. On the other hand,

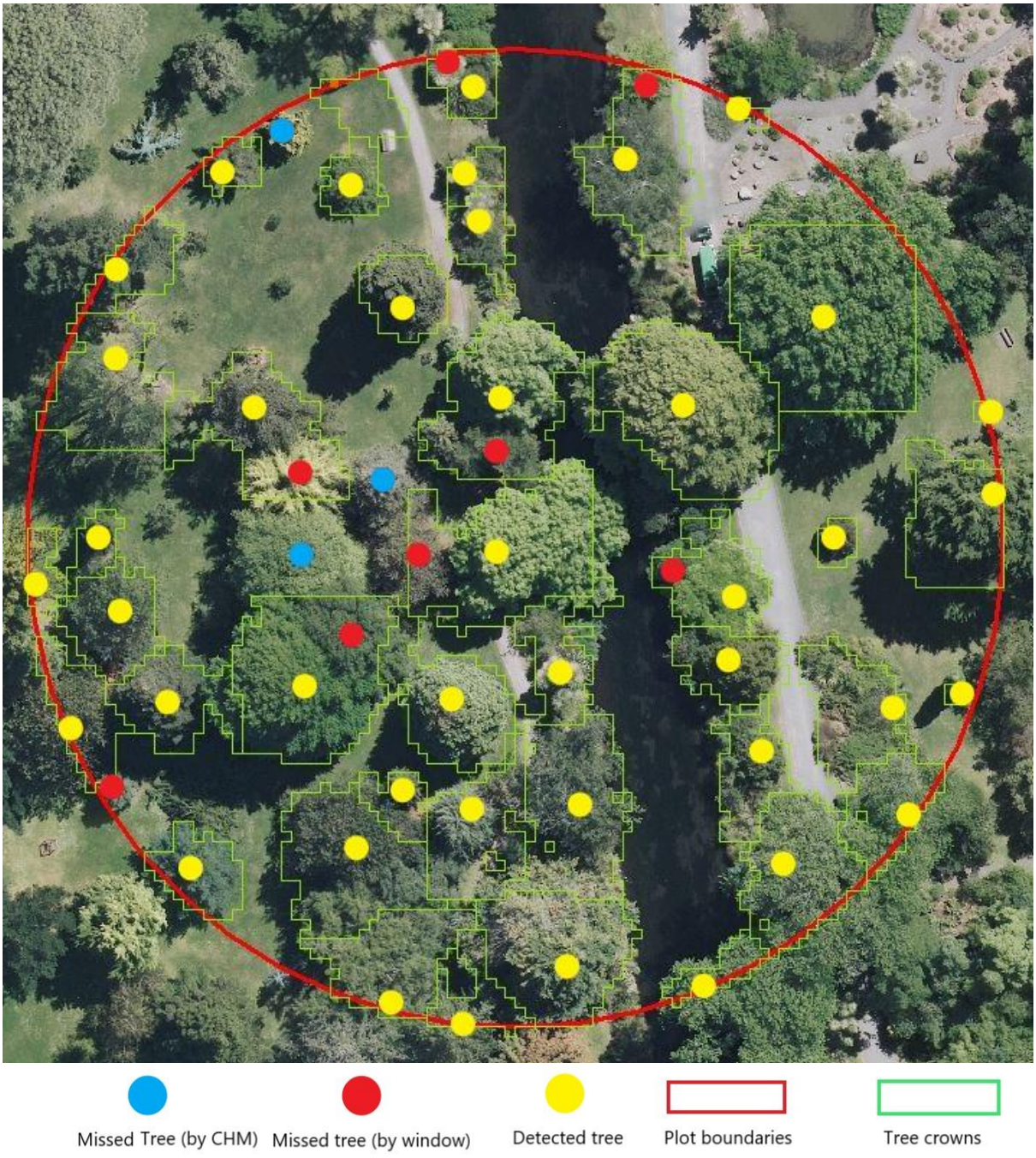

Figure 4-2. Missed tree caused by large widow size and errors from CHM

underestimated tree count and delineation exists when producer accuracies are lower than user accuracies (Lamar et al., 2005). One reason that can cause under-counted trees is relatively large window size. If the window size is much larger than a tree crown, small tree crowns that adjacent to large crowns could be missed (Wulder et al., 2000). For the 6 plots in which trees were under-counted, the fixed window size successfully identified large crowns and small trees, but only if they were spatially separated from larger trees. Small crowns that were adjacent to large crowns generally failed to be detected (Figure 4-2). One possible solution for such an error would be to adopt a variable window size based on tree conditions. However, variable size windows require field survey data to explore the relationship between crown sizes and other conditions (Silva et al., 2016). This was unachievable in this study but could be undertaken in future studies.

Compared with under-counted plots, there are 24 plots where trees were over-counted. One reason for over-counts could be a relatively small window size when detecting large trees. It was thought that large trees may have been split into two or more trees due to the window size. However, after checking plot by plot, this type of error was not commonly observed. For most commission errors, the main source is from misclassifications in the land cover map. In Figure 4-2, three trees were missed because they were not classified as trees by the land cover classification described in Chapter 3. As such, they were not included in the CHM boundary that was exported for use in ITCD in this chapter. Apart from missed data, some pixels in the CHM actually belonged to buildings – they were also not perfectly excluded from CHM due to land cover misclassification. These building pixels were later identified as trees during ITCD, resulting in over-counting the number of trees. Plots with fewer buildings appeared to have fewer of these kinds of error Figure 4-3. There were five plots that had no building coverage and all of them had overall accuracies higher than 80%. For two plots that had accuracies lower than 60%, the proportions of building coverage were high (over 40%). Clearly, this is problematic for ITCD in urban areas where buildings are very common (Awrangjeb et al., 2012; Gomes & Maillard, 2013; Zhen et al., 2016). One solution for this problem is refined the classification result and remove building edge points before interpolating raster surfaces. However, this may not be feasible, particularly for large areas.

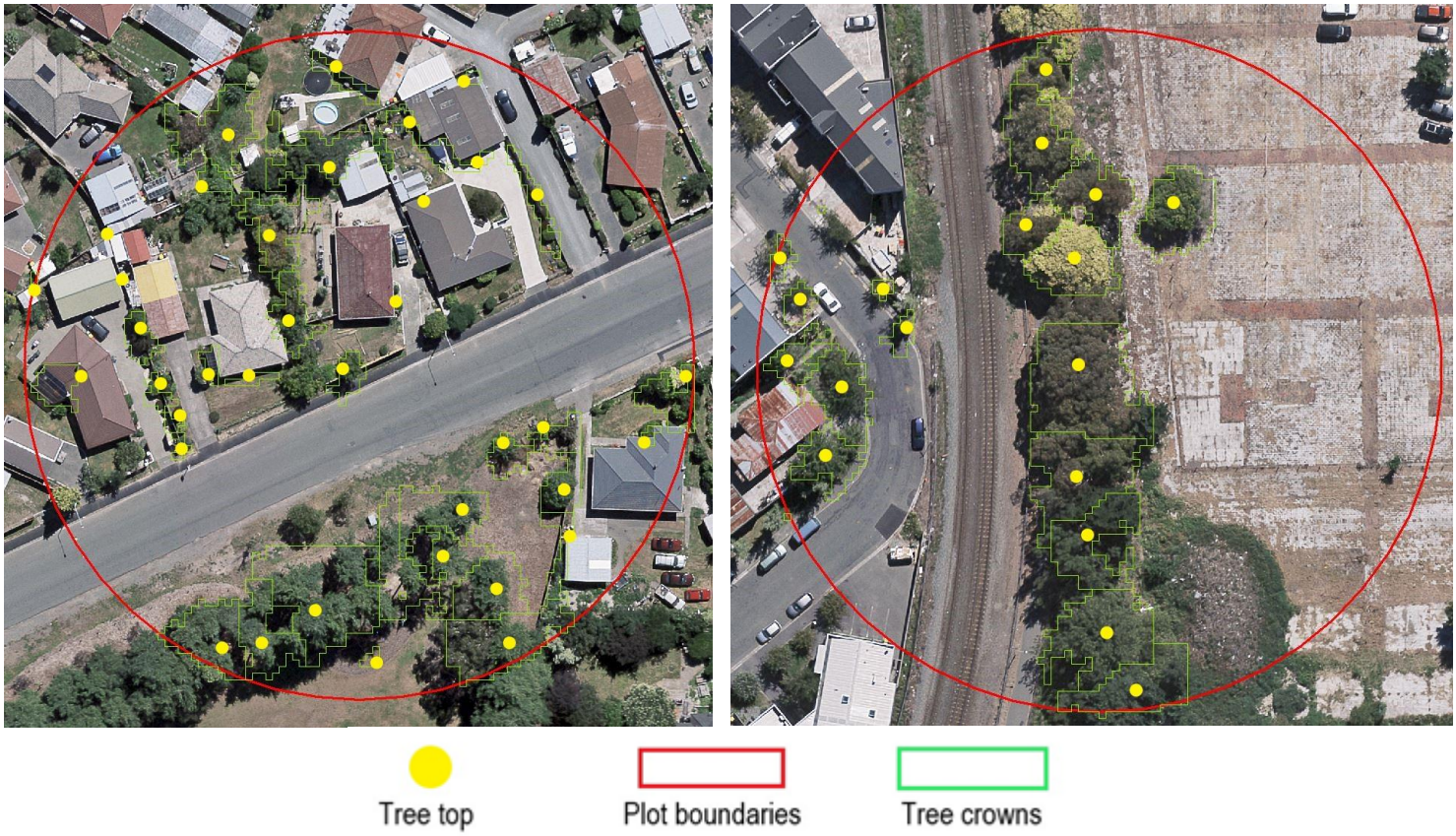

Figure 4-3. Plots with lowest overall accuracy, with 56.47% (left), and highest overall accuracy, with 92.11% (right).

Due to the lack of historical crown reference data, this study used RGB imagery to manually create reference tree crowns. This can introduce some errors where tree boundaries cannot be clearly distinguished from the aerial imagery. For those areas where trees existed in high densities, visually identifying individual tree crowns can only rely on their colour difference. Therefore, to more accurately evaluate the result of ITCD, some field measured data should be included in future studies.

To summarise, delineation accuracy was largely affected by window size, CHM quality and land cover types within the study area. The difficulty of reference data collection also restricted a detailed comparison between the ITCD result and real tree crowns. Visually delineated crowns may also be less accurate than field survey data. However, the high producer's accuracies have shown the potential that accurate automatic ITCD could be achievable by fusion of LiDAR and aerial imagery.

4.5 Conclusion

Overall, this study explores a workflow for using LiDAR and aerial imagery for automated ITCD in Christchurch. In most plots with low building cover, the proposed method produced accurate tree delineations. However, the result could still be refined if a variable window size could be adopted and using a CHM with fewer classification errors. For future study, some suggestions include: 1. Improving classification by focussing more on accurate tree cover extraction. 2. Adopt flexible window size or used different window size for the specific area. 3. Collecting field data if possible to conduct a better assessment for delineation results.

Chapter 5 - Thesis Conclusion

Land cover classification in Christchurch between 2011 and 2015 was conducted using an OBIA approach with a fusion of LiDAR and RGB data. By adding spectral data to LiDAR-derived and shape features, advantages from both datasets were combined effectively and yielded overall land cover classification accuracies of 94.00% (2011) and 94.32% (2015). After comparing two land cover maps, considerable changes for seven land cover classes were found within the study area. According to the spatial distributions and transitions between classes, causes for land cover changes likely include: the damage caused by the CES, such as surface liquefaction and flooding; the rebuilding activities such as red zone redevelopment and newly built properties to replace buildings demolished after the earthquakes; and finally tree growth over a 5 year period.

Based on the classification result, tree cover change in this study area had aroused particular interest due to the importance of urban forests and the significant area of change. Percentages of tree cover in Christchurch's fifteen wards were analysed in order to provide a general idea of tree cover change in the city extent. Following this, the study undertook an automatic ITCD approach in the urban environment of Christchurch to determine the feasibility of tree counting using existing methods. The accuracies of the proposed approach ranged between 56.47% and 92.11% in different sample plots and had an overall accuracy of 75.60%. Such varied accuracies were later found caused by fixed tree detection window size and misclassifications from the land cover classification that affected the quality of the CHM. Such variable accuracy means that automated tree counting may not be appropriated given existing methods. However, directions for further study for ITCD in Christchurch cloud be exploring ITCD approaches with variable window size or optimize classification approach to focus more on producing CHMs.

During the classification process, some methods and parameters were tested to achieve optimised classifications. Two popular LiDAR surface interpolation algorithm triangulation and binning interpolation were compared. The result indicated triangulation method produced more accurate surface than another. Five different popular classifiers RF, SVM, KNN, DT, and Bayes were also assessed after testing on sample datasets and RF was identified as the most suitable classifier for this study.

However, the different aerial imagery qualities and limited spectral bands put limitations to further improve accuracies in both land cover classification and ITCD. Therefore, future studies can focus on reducing the effects caused by these limitations and improving data acquisition standards to collect more accurate datasets.

References

Al-Kofahi, S., Steele, C., VanLeeuwen, D., & Hilaire, R. S. (2012). Mapping land cover in urban residential landscapes using very high spatial resolution aerial photographs. *Urban forestry & urban greening, 11*(3), 291-301.

Alberti, M., Weeks, R., & Coe, S. (2004). Urban land-cover change analysis in central Puget Sound. *Photogrammetric Engineering & Remote Sensing, 70*(9), 1043-1052.

Alexander, C., Tansey, K., Kaduk, J., Holland, D., & Tate, N. J. (2010). Backscatter coefficient as an attribute for the classification of full-waveform airborne laser scanning data in urban areas. *ISPRS Journal of Photogrammetry and Remote Sensing, 65*(5), 423-432.

Almeida, C. M., Souza, I. M., Alves, C. D., Pinho, C., Pereira, M. N., & Feitosa, R. Q. (2007). *Multilevel object-oriented classification of quickbird images for urban population estimates.* Paper presented at the Proceedings of the 15th annual ACM international symposium on Advances in geographic information systems.

Alonzo, M., Bookhagen, B., & Roberts, D. A. (2014). Urban tree species mapping using hyperspectral and lidar data fusion. *Remote Sensing of Environment, 148*, 70-83.

Alqurashi, A. F., Kumar, L., & Sinha, P. (2016). Urban land cover change modelling using time-series satellite images: A case study of urban growth in five cities of Saudi Arabia. *Remote Sensing, 8*(10), 838.

Ardila, J. P., Tolpekin, V. A., Bijker, W., & Stein, A. (2011). Markov-random-field-based super-resolution mapping for identification of urban trees in VHR images. *ISPRS journal of photogrammetry and remote sensing, 66*(6), 762-775.

Awrangjeb, M., Ravanbakhsh, M., & Fraser, C. S. (2010). Automatic detection of residential buildings using LIDAR data and multispectral imagery. *ISPRS Journal of Photogrammetry and Remote Sensing, 65*(5), 457-467.

Awrangjeb, M., Zhang, C., & Fraser, C. S. (2012). Building detection in complex scenes thorough effective separation of buildings from trees. *Photogrammetric Engineering & Remote Sensing, 78*(7), 729-745.

Bandyopadhyay, M., van Aardt, J. A., & Cawse-Nicholson, K. (2013). Classification and extraction of trees and buildings from urban scenes using discrete return LiDAR and aerial color imagery. *SPIE Defense, Security, and Sensing*, 873105-873105.

Bartels, M., & Wei, H. (2006). *Maximum likelihood classification of LIDAR data incorporating multiple co-registered bands.* Paper presented at the Proceedings of 4th International Workshop on Pattern Recognition in Remote Sensing/18th International Conference on Pattern Recognition.

Belgiu, M., & Drăguţ, L. (2016). Random forest in remote sensing: A review of applications and future directions. *ISPRS Journal of Photogrammetry and Remote Sensing, 114*, 24-31.

Benz, U. C., Hofmann, P., Willhauck, G., Lingenfelder, I., & Heynen, M. (2004). Multi-resolution, object-oriented fuzzy analysis of remote sensing data for GIS-ready information. *ISPRS Journal of photogrammetry and remote sensing, 58*(3-4), 239-258.

Berezowski, T., Chormański, J., Batelaan, O., Canters, F., & Van de Voorde, T. (2012). Impact of remotely sensed land-cover proportions on urban runoff prediction. *International Journal of Applied Earth Observation and Geoinformation, 16*, 54-65.

Blaschke, T. (2001). What's wrong with pixels? Some recent developments interfacing remote sensing and GIS. *GeoBIT/GIS, 6*, 12-17.

Blaschke, T. (2010). Object based image analysis for remote sensing. *ISPRS journal of photogrammetry and remote sensing, 65*(1), 2-16.

Brandtberg, T., & Walter, F. (1998). Automated delineation of individual tree crowns in high spatial resolution aerial images by multiple-scale analysis. *Machine Vision and Applications, 11*(2), 64-73.

Breidenbach, J., Næsset, E., Lien, V., Gobakken, T., & Solberg, S. (2010). Prediction of species specific forest inventory attributes using a nonparametric semi-individual tree crown approach based on fused airborne laser scanning and multispectral data. *Remote Sensing of Environment, 114*(4), 911-924.

Brennan, R., & Webster, T. (2006). Object-oriented land cover classification of lidar-derived surfaces. *Canadian journal of remote sensing, 32*(2), 162-172.

Bruzzone, L., & Carlin, L. (2006). A multilevel context-based system for classification of very high spatial resolution images. *IEEE transactions on Geoscience and Remote Sensing, 44*(9), 2587-2600.

Caccetta, P., Collings, S., Devereux, A., Hingee, K., McFarlane, D., Traylen, A., . . . Zhou, Z.-S. (2016). Monitoring land surface and cover in urban and peri-urban environments using digital aerial photography. *International Journal of Digital Earth, 9*(5), 457-475.

Casals-Carrasco, P., Kubo, S., & Madhavan, B. B. (2000). Application of spectral mixture analysis for terrain evaluation studies. *International Journal of Remote Sensing, 21*(16), 3039-3055.

CCC. (2014). *Community board and ward profiles.* Retrieved from https://www.ccc.govt.nz/culture-and-community/christchurch/statistics-and-facts/community-profiles/

CERA. (2016). Public geospatial data.

Chang, A., Eo, Y., Kim, Y., & Kim, Y. (2013). Identification of individual tree crowns from LiDAR data using a circle fitting algorithm with local maxima and minima filtering. *Remote sensing letters, 4*(1), 29-37.

Chang, K., Linb, C., Linc, Y., & Liu, J. (2016). Accuracy Assessment of Crown Delineation Methods for the Individual Trees Using LIDAR Data. *ISPRS-International Archives of the Photogrammetry, Remote Sensing and Spatial Information Sciences*, 585-588.

Charaniya, A. P., Manduchi, R., & Lodha, S. K. (2004). *Supervised parametric classification of aerial lidar data.* Paper presented at the Computer Vision and Pattern Recognition Workshop, 2004. CVPRW'04. Conference on.

Chen, C. D., Colin, M. D., Maria, I. E., Glenn, S. H., & Wu, S. J. (2015). Identifying and evaluating functional connectivity for building urban ecological networks. *Shengtai Xuebao/ Acta Ecologica Sinica, 35*(19), 6414-6424.

Chen, D., & Stow, D. (2002). The effect of training strategies on supervised classification at different spatial resolutions. *Photogrammetric Engineering and Remote Sensing, 68*(11), 1155-1162.

Chen, D., Stow, D., & Gong, P. (2004). Examining the effect of spatial resolution and texture window size on classification accuracy: an urban environment case. *International Journal of Remote Sensing, 25*(11), 2177-2192.

Chen, G., Hay, G. J., Carvalho, L. M. T., & Wulder, M. A. (2012). Object-based change detection. *International Journal of Remote Sensing, 33*(14), 4434-4457.

Chen, Y., Su, W., Li, J., & Sun, Z. (2009). Hierarchical object oriented classification using very high resolution imagery and LIDAR data over urban areas. *Advances in Space Research, 43*(7), 1101-1110.

Chen, Z., & Gao, B. (2014). An object-based method for urban land cover classification using airborne lidar data. *IEEE Journal of Selected Topics in Applied Earth Observations and Remote Sensing, 7*(10), 4243-4254.

Chouw, N., & Hao, H. (2012). Pounding damage to buildings and bridges in the 22 February 2011 Christchurch earthquake. *International Journal of Protective Structures, 3*(2), 123-139.

Chutia, D., Bhattacharyya, D., Sarma, K. K., Kalita, R., & Sudhakar, S. (2016). Hyperspectral remote sensing classifications: a perspective survey. *Transactions in GIS, 20*(4), 463-490.

Clark, B., & Pellikka, P. (2009). Landscape analysis using multiscale segmentation and object orientated classification. *Recent advances in remote sensing and geoinformation processing for land degradation assessment, 8*, 323.

Cleve, C., Kelly, M., Kearns, F. R., & Moritz, M. (2008). Classification of the wildland–urban interface: A comparison of pixel-and object-based classifications using high-resolution aerial photography. *Computers, Environment and Urban Systems, 32*(4), 317-326.

Cole, G. L., Dhakal, R. P., & Turner, F. M. (2012). Building pounding damage observed in the 2011 Christchurch earthquake. *Earthquake Engineering & Structural Dynamics, 41*(5), 893-913.

Congalton, R. G. (1991). A review of assessing the accuracy of classifications of remotely sensed data. *Remote sensing of environment, 37*(1), 35-46.

Congalton, R. G., & Green, K. (2008). *Assessing the accuracy of remotely sensed data: principles and practices*: CRC press.

Cox, C. (1992). Satellite imagery, aerial photography and wetland archaeology: an interim report on an application of remote sensing to wetland archaeology: the pilot study in Cumbria, England. *World Archaeology, 24*(2), 249-267.

Cubrinovski, M., Green, R., Allen, J., Ashford, S., Bowman, E., Bradley, B., . . . Orense, R. (2010). Geotechnical reconnaissance of the 2010 Darfield (New Zealand) earthquake.

Culvenor, D. S. (2000). *Development of a tree delineation algorithm for application to high spatial resolution digital imagery of Australian native forest.*

Dalponte, M., & Coomes, D. A. (2016). Tree‐centric mapping of forest carbon density from airborne laser scanning and hyperspectral data. *Methods in ecology and evolution, 7*(10), 1236-1245.

Dare, P. M. (2005). Shadow analysis in high-resolution satellite imagery of urban areas. *Photogrammetric Engineering & Remote Sensing, 71*(2), 169-177.

Dewan, A. M., & Corner, R. J. (2012). *The impact of land use and land cover changes on land surface temperature in a rapidly urbanizing megacity.* Paper presented at the Geoscience and Remote Sensing Symposium (IGARSS), 2012 IEEE International.

Drăguţ, L., Tiede, D., & Levick, S. R. (2010). ESP: a tool to estimate scale parameter for multiresolution image segmentation of remotely sensed data. *International Journal of Geographical Information Science, 24*(6), 859-871.

Eidinger, J., & Tang, A. K. (2012). Christchurch, New Zealand Earthquake Sequence of Mw 7.1 September 04, 2010 Mw 6.3 February 22, 2011 Mw 6.0 June 13, 2011: Lifeline Performance. *American Society of Civil Engineers, Reston, VA*.

Eisavi, V., Homayouni, S., Yazdi, A. M., & Alimohammadi, A. (2015). Land cover mapping based on random forest classification of multitemporal spectral and thermal images. *Environmental monitoring and assessment, 187*(5), 291.

Esri. (2016). Mosaic To New Raster.

Fang, F., Im, J., Lee, J., & Kim, K. (2016). An improved tree crown delineation method based on live crown ratios from airborne LiDAR data. *GIScience & Remote Sensing, 53*(3), 402-419.

Feng, Q., Liu, J., & Gong, J. (2015). UAV Remote Sensing for Urban Vegetation Mapping Using Random Forest and Texture Analysis. *Remote Sensing, 7*(1), 1074.

Foody, G. M. (2004). Thematic map comparison. *Photogrammetric Engineering & Remote Sensing, 70*(5), 627-633.

Gan, Z., Zhong, L., Li, Y., & Guan, H. (2015). *A random forest based method for urban object classification using lidar data and aerial imagery.* Paper presented at the Geoinformatics, 2015 23rd International Conference on.

Gao, F., Masek, J., Schwaller, M., & Hall, F. (2006). On the blending of the Landsat and MODIS surface reflectance: Predicting daily Landsat surface reflectance. *IEEE Transactions on Geoscience and Remote sensing, 44*(8), 2207-2218.

Gao, X., Feng, S., Kang, J., Wu, G., Guo, L., Zou, C., . . . Zhang, Y. (2011). *Using remote sensing and GIS to analyze land use/cover change and urban expansion in Xining City of Qinghai province, China.* Paper presented at the Geoinformatics, 2011 19th International Conference on.

Gao, Y., Mas, J., Niemeyer, I., Marpu, P., & Palacio, J. (2007). *Object-based image analysis for mapping land-cover in a forest area.* Paper presented at the Proc. of 5th International Symposium on Spatial Data Quality.

Georganos, S., Grippa, T., Vanhuysse, S., Lennert, M., Shimoni, M., & Wolff, E. (2018). Very High Resolution Object-Based Land Use-Land Cover Urban Classification Using Extreme Gradient Boosting. *IEEE Geoscience and Remote Sensing Letters*.

Ghosh, A., & Joshi, P. (2014). A comparison of selected classification algorithms for mapping bamboo patches in lower Gangetic plains using very high resolution WorldView 2 imagery. *International Journal of Applied Earth Observation and Geoinformation, 26*, 298-311.

Gislason, P. O., Benediktsson, J. A., & Sveinsson, J. R. (2006). Random forests for land cover classification. *Pattern Recognition Letters, 27*(4), 294-300.

Gomes, M. F., & Maillard, P. (2013). *Identification of urban tree crown in a tropical environment using WorldView-2 data: Problems and perspectives.* Paper presented at the Earth Resources and Environmental Remote Sensing/GIS Applications IV.

González-Ferreiro, E., Diéguez-Aranda, U., Barreiro-Fernández, L., Buján, S., Barbosa, M., Suárez, J. C., . . . Miranda, D. (2013). A mixed pixel-and region-based approach for using airborne laser scanning data for individual tree crown delineation in Pinus radiata D. Don plantations. *International journal of remote sensing, 34*(21), 7671-7690.

Guan, H., Li, J., & Chapman, M. A. (2011). Urban Thematic Mapping by Integrating Lidar Point Cloud with Colour Imagery. *GEOMATICA, 65*(4), 375-385.

Gulbe, L. (2015). *Identification and delineation of individual tree crowns using Lidar and multispectral data fusion.* Paper presented at the Geoscience and Remote Sensing Symposium (IGARSS), 2015 IEEE International.

Haack, B., & Mahabir, R. (2018). Relative value of radar and optical data for land cover/use mapping: Peru example. *International Journal of Image and Data Fusion, 9*(1), 1-20.

Haralick, R. M., & Shanmugam, K. (1973). Textural features for image classification. *IEEE Transactions on systems, man, and cybernetics*(6), 610-621.

Hartfield, K. A., Landau, K. I., & Van Leeuwen, W. J. (2011). Fusion of high resolution aerial multispectral and LiDAR data: land cover in the context of urban mosquito habitat. *Remote Sensing, 3*(11), 2364-2383.

Hay, G. J., & Castilla, G. (2008). Geographic Object-Based Image Analysis (GEOBIA): A new name for a new discipline *Object-based image analysis* (pp. 75-89): Springer.

Heinzel, J. N., Weinacker, H., & Koch, B. (2008). Full automatic detection of tree species based on delineated single tree crowns–a data fusion approach for airborne laser scanning data and aerial photographs. *Proceedings of SilviLaser, 2008*(8th).

Hepinstall‐Cymerman, J. (2011). Ecological Modeling in Urban Environments: Predicting Changes in Biodiversity in Response to Future Urban Development. *Urban Remote Sensing: Monitoring, Synthesis and Modeling in the Urban Environment, 250*, 359-370.

Holmgren, J. (2004). Prediction of tree height, basal area and stem volume in forest stands using airborne laser scanning. *Scandinavian Journal of Forest Research, 19*(6), 543-553.

Huang, X., Zhang, L., & Gong, W. (2011). Information fusion of aerial images and LIDAR data in urban areas: vector-stacking, re-classification and post-processing approaches. *International Journal of Remote Sensing, 32*(1), 69-84.

Im, J., Jensen, J., & Tullis, J. (2008). Object‐based change detection using correlation image analysis and image segmentation. *International Journal of Remote Sensing, 29*(2), 399-423.

Iovan, C., Boldo, D., & Cord, M. (2008). Detection, characterization, and modeling vegetation in urban areas from high-resolution aerial imagery. *IEEE Journal of Selected Topics in Applied Earth Observations and Remote Sensing, 1*(3), 206-213.

Jensen, J. (2007). Remote sensing of the environment: an earth resource perspective: Pearson Prentice Hall. *Upper Saddle River, NJ*.

Jing, L., Hu, B., Li, J., & Noland, T. (2012). Automated delineation of individual tree crowns from LiDAR data by multi-scale analysis and segmentation. *Photogrammetric Engineering & Remote Sensing, 78*(12), 1275-1284.

Jing, L., Hu, B., Noland, T., & Li, J. (2012). An individual tree crown delineation method based on multi-scale segmentation of imagery. *ISPRS Journal of Photogrammetry and Remote Sensing, 70*, 88-98.

Johnson, B. A. (2013). High-resolution urban land-cover classification using a competitive multi-scale object-based approach. *Remote Sensing Letters, 4*(2), 131-140.

Jones, H. (2017). *Factsheet: Monitoring land cover in New Zealand.* Retrieved from https://www.lawa.org.nz/learn/factsheets/monitoring-land-cover-in-new-zealand/

Kaiser, A., Holden, C., Beavan, J., Beetham, D., Benites, R., Celentano, A., . . . Dellow, G. (2012). The Mw 6.2 Christchurch earthquake of February 2011: preliminary report. *New Zealand journal of geology and geophysics, 55*(1), 67-90.

Ke, Y., & Quackenbush, L. J. (2011). A review of methods for automatic individual tree-crown detection and delineation from passive remote sensing. *International Journal of Remote Sensing, 32*(17), 4725-4747.

Khorram, S. (2012). *Remote sensing*. New York: Springer.

Khosravipour, A., Skidmore, A. K., Isenburg, M., Wang, T., & Hussin, Y. A. (2014). Generating pit-free canopy height models from airborne lidar. *Photogrammetric Engineering & Remote Sensing, 80*(9), 863-872.

Kim, M., Warner, T. A., Madden, M., & Atkinson, D. S. (2011). Multi-scale GEOBIA with very high spatial resolution digital aerial imagery: scale, texture and image objects. *International Journal of Remote Sensing, 32*(10), 2825-2850.

Kim, Y. (2016). Generation of Land Cover Maps through the Fusion of Aerial Images and Airborne LiDAR Data in Urban Areas. *Remote Sensing, 8*(6), 521.

Koetz, B., Morsdorf, F., Van der Linden, S., Curt, T., & Allgöwer, B. (2008). Multi-source land cover classification for forest fire management based on imaging spectrometry and LiDAR data. *Forest Ecology and Management, 256*(3), 263-271.

Lamar, W. R., McGraw, J. B., & Warner, T. A. (2005). Multitemporal censusing of a population of eastern hemlock (Tsuga canadensis L.) from remotely sensed imagery using an automated segmentation and reconciliation procedure. *Remote Sensing of Environment, 94*(1), 133-143.

Lambin, E. F., Turner, B. L., Geist, H. J., Agbola, S. B., Angelsen, A., Bruce, J. W., . . . Folke, C. (2001). The causes of land-use and land-cover change: moving beyond the myths. *Global environmental change, 11*(4), 261-269.

Landis, J. R., & Koch, G. G. (1977). The measurement of observer agreement for categorical data. *biometrics*, 159-174.

Lévesque, J., & King, D. J. (2003). Spatial analysis of radiometric fractions from high-resolution multispectral imagery for modelling individual tree crown and forest canopy structure and health. *Remote Sensing of Environment, 84*(4), 589-602.

Li, H., Gu, H., Han, Y., & Yang, J. (2007). *Fusion of high-resolution aerial imagery and lidar data for object-oriented urban land-cover classification based on svm.* Paper presented at the ISPRS Workshop on Updating Geo-spatial Databases with Imagery & The 5th ISPRS Workshop on DMGISs.

LINZ. (2016). *Demolitions and clearances.* Retrieved from https://www.linz.govt.nz/crown-property/types-crown-property/christchurch-residential-red-zone/demolitions-and-clearances

LINZ. (2017). *Residential red zone areas.* Retrieved from https://www.linz.govt.nz/crown-property/types-crown-property/christchurch-residential-red-zone/residential-red-zone-areas

Liu, D., & Xia, F. (2010). Assessing object-based classification: advantages and limitations. *Remote Sensing Letters, 1*(4), 187-194.

Liu, M., Qi, Q., Liu, J., Su, S., Jun, C., Zou, X., . . . Li, J. (2005). Monitoring land cover changes with remote sensing in transboundary area of southwest china.

Liu, T., Im, J., & Quackenbush, L. J. (2015). A novel transferable individual tree crown delineation model based on Fishing Net Dragging and boundary classification. *ISPRS Journal of Photogrammetry and Remote Sensing, 110*, 34-47.

Liu, Z., Wang, J., & Liu, W. (2005). *Building extraction from high resolution imagery based on multi-scale object oriented classification and probabilistic Hough transform.* Paper presented at the Geoscience and Remote Sensing Symposium, 2005. IGARSS'05. Proceedings. 2005 IEEE International.

López, E., Bocco, G., Mendoza, M., & Duhau, E. (2001). Predicting land-cover and land-use change in the urban fringe: a case in Morelia city, Mexico. *Landscape and urban planning, 55*(4), 271-285.

LRIS. (2015). *LCDB v4.1 Version Trace, Mainland New Zealand.* Retrieved from https://lris.scinfo.org.nz/layer/48423-lcdb-v41-land-cover-database-version-41-mainland-new-zealand/

Lu, D., Hetrick, S., & Moran, E. (2010). Land cover classification in a complex urban-rural landscape with QuickBird imagery. *Photogrammetric Engineering & Remote Sensing, 76*(10), 1159-1168.

Ma, L., Zhou, M., & Li, C. (2017). LAND COVERS CLASSIFICATION BASED ON RANDOM FOREST METHOD USING FEATURES FROM FULL-WAVEFORM LIDAR DATA. *ISPRS-International Archives of the Photogrammetry, Remote Sensing and Spatial Information Sciences*, 263-268.

MacFaden, S. W., O'Neil-Dunne, J. P., Royar, A. R., Lu, J. W., & Rundle, A. G. (2012). High-resolution tree canopy mapping for New York City using LIDAR and object-based image analysis. *Journal of Applied Remote Sensing, 6*(1), 063567.

Malinverni, E. S., Tassetti, A. N., Mancini, A., Zingaretti, P., Frontoni, E., & Bernardini, A. (2011). Hybrid object-based approach for land use/land cover mapping using high spatial resolution imagery. *International Journal of Geographical Information Science, 25*(6), 1025-1043.

Maltamo, M., Næsset, E., & Vauhkonen, J. (2014). Forestry applications of airborne laser scanning. *Concepts and case studies. Manag For Ecosys, 27*, 2014.

Marshall, M., & Thenkabail, P. (2015). Advantage of hyperspectral EO-1 Hyperion over multispectral IKONOS, GeoEye-1, WorldView-2, Landsat ETM+, and MODIS vegetation indices in crop biomass estimation. *ISPRS Journal of Photogrammetry and Remote Sensing, 108*, 205-218.

McCombs, J. W., Roberts, S. D., & Evans, D. L. (2003). Influence of fusing lidar and multispectral imagery on remotely sensed estimates of stand density and mean tree height in a managed loblolly pine plantation. *Forest Science, 49*(3), 457-466.

Mellor, A., Boukir, S., Haywood, A., & Jones, S. (2015). Exploring issues of training data imbalance and mislabelling on random forest performance for large area land cover classification using the ensemble margin. *ISPRS Journal of Photogrammetry and Remote Sensing, 105*, 155-168.

Meng, X., Currit, N., Wang, L., & Yang, X. (2012). Detect residential buildings from lidar and aerial photographs through object-oriented land-use classification. *Photogrammetric Engineering & Remote Sensing, 78*(1), 35-44.

Miao, X., Heaton, J. S., Zheng, S., Charlet, D. A., & Liu, H. (2012). Applying tree-based ensemble algorithms to the classification of ecological zones using multi-temporal multi-source remote-sensing data. *International journal of remote sensing, 33*(6), 1823-1849.

Miliaresis, G., & Kokkas, N. (2007). Segmentation and object-based classification for the extraction of the building class from LIDAR DEMs. *Computers & Geosciences, 33*(8), 1076-1087.

Morgenroth, J. (2017). *Tree Canopy Cover in Christchurch, New Zealand. Prepared for the Christchurch City Council* Retrieved from https://cccgovtnz.cwp.govt.nz/assets/Documents/Environment/Trees/Tree-cover-in-Christchurch-final-report.pdf

Morgenroth, J., & Armstrong, T. (2012). The impact of significant earthquakes on Christchurch, New Zealand's urban forest. *Urban forestry & urban greening, 11*(4), 383-389.
Morgenroth, J., Hughes, M. W., & Cubrinovski, M. (2016). Object-based image analysis for mapping earthquake-induced liquefaction ejecta in Christchurch, New Zealand. *Natural Hazards, 82*(2), 763-775.
Morgenroth, J., O'Neil-Dunne, J., & Apiolaza, L. A. (2017). Redevelopment and the urban forest: A study of tree removal and retention during demolition activities. *Applied geography, 82*, 1-10.
Moskal, L. M., Styers, D. M., & Halabisky, M. (2011). Monitoring urban tree cover using object-based image analysis and public domain remotely sensed data. *Remote Sensing, 3*(10), 2243-2262.
Myeong, S., Nowak, D. J., Hopkins, P. F., & Brock, R. H. (2001). Urban cover mapping using digital, high-spatial resolution aerial imagery. *Urban Ecosystems, 5*(4), 243-256.
Myint, S. W., Gober, P., Brazel, A., Grossman-Clarke, S., & Weng, Q. (2011). Per-pixel vs. object-based classification of urban land cover extraction using high spatial resolution imagery. *Remote sensing of environment, 115*(5), 1145-1161.
Na, X., Zhang, S., Li, X., Yu, H., & Liu, C. (2010). Improved land cover mapping using random forests combined with landsat thematic mapper imagery and ancillary geographic data. *Photogrammetric Engineering & Remote Sensing, 76*(7), 833-840.
Niemeyer, J., Rottensteiner, F., & Soergel, U. (2014). Contextual classification of lidar data and building object detection in urban areas. *ISPRS journal of photogrammetry and remote sensing, 87*, 152-165.
Nordbo, A., Karsisto, P., Matikainen, L., Wood, C. R., & Järvi, L. (2015). Urban surface cover determined with airborne lidar at 2 m resolution–implications for surface energy balance modelling. *Urban Climate, 13*, 52-72.
Novack, T., Esch, T., Kux, H., & Stilla, U. (2011). Machine learning comparison between WorldView-2 and QuickBird-2-simulated imagery regarding object-based urban land cover classification. *remote sensing, 3*(10), 2263-2282.
Ossola, A., & Hopton, M. E. (2018). Measuring urban tree loss dynamics across residential landscapes. *Science of The Total Environment, 612*, 940-949.
Pal, M. (2005). Random forest classifier for remote sensing classification. *International Journal of Remote Sensing, 26*(1), 217-222.
Phiri, D., & Morgenroth, J. (2017). Developments in Landsat land cover classification methods: A review. *Remote Sensing, 9*(9), 967.
Potter, S., Becker, J., Johnston, D., & Rossiter, K. (2015). An overview of the impacts of the 2010-2011 Canterbury earthquakes. *International Journal of Disaster Risk Reduction, 14*, 6-14.
Pouliot, D., King, D., Bell, F., & Pitt, D. (2002). Automated tree crown detection and delineation in high-resolution digital camera imagery of coniferous forest regeneration. *Remote sensing of environment, 82*(2-3), 322-334.
Qi, Y., Bar‐Joseph, Z., & Klein‐Seetharaman, J. (2006). Evaluation of different biological data and computational classification methods for use in protein interaction prediction. *Proteins: Structure, Function, and Bioinformatics, 63*(3), 490-500.
Quigley, M. C., Hughes, M. W., Bradley, B. A., van Ballegooy, S., Reid, C., Morgenroth, J., . . . Pettinga, J. R. (2016). The 2010–2011 Canterbury earthquake sequence: Environmental effects, seismic triggering thresholds and geologic legacy. *Tectonophysics, 672*, 228-274.
Rastandeh, A., Pedersen Zari, M., & Brown, D. K. (2018). Land cover change and management implications for the conservation of a seabird in an urban coastal zone under climate change. *Ecological Management & Restoration*.
Rastiveis, H. (2015). Decision level fusion of LIDAR data and aerial color imagery based on Bayesian theory for urban area classification. *The International Archives of Photogrammetry, Remote Sensing and Spatial Information Sciences, 40*(1), 589.
Richards, J. A., & Richards, J. (1999). *Remote sensing digital image analysis* (Vol. 3): Springer.

Rodriguez-Galiano, V. F., Ghimire, B., Rogan, J., Chica-Olmo, M., & Rigol-Sanchez, J. P. (2012). An assessment of the effectiveness of a random forest classifier for land-cover classification. *ISPRS Journal of Photogrammetry and Remote Sensing, 67*, 93-104.

Roy, S., Byrne, J., & Pickering, C. (2012). A systematic quantitative review of urban tree benefits, costs, and assessment methods across cities in different climatic zones. *Urban Forestry & Urban Greening, 11*(4), 351-363.

Ryherd, S., & Woodcock, C. (1996). Combining spectral and texture data in the segmentation of remotely sensed images. *Photogrammetric engineering and remote sensing*.

Samadzadegan, F., Bigdeli, B., & Ramzi, P. (2010). *A Multiple Classifier System for Classification of LIDAR Remote Sensing Data Using Multi-class SVM.* Paper presented at the MCS.

Schiewe, J. (2002). Segmentation of high-resolution remotely sensed data-concepts, applications and problems. *International Archives of Photogrammetry Remote Sensing and Spatial Information Sciences, 34*(4), 380-385.

Schiewe, J., Tufte, L., & Ehlers, M. (2001). Potential and problems of multi-scale segmentation methods in remote sensing. *GeoBIT/GIS, 6*(01), 34-39.

Shackelford, A. K., & Davis, C. H. (2003). A hierarchical fuzzy classification approach for high-resolution multispectral data over urban areas. *IEEE transactions on geoscience and remote sensing, 41*(9), 1920-1932.

Shafri, H. Z. M., & Hamedianfar, A. (2015). *Mapping of intra-urban land covers using pixel-based and object-based classifications from airborne hyperspectral imagery.* Paper presented at the Information Science and Security (ICISS), 2015 2nd International Conference on.

Shaker, A., & El-Ashmawy, N. (2012). Land cover information extraction using lidar data. *International Archives of the Photogrammetry, Remote Sensing and Spatial Information Sciences (ISPRS), 39*, 167-172.

Shojanoori, R., & Shafri, H. Z. (2016). Review on the use of remote sensing for urban forest monitoring. *Arboric Urban For, 42*(6), 400-417.

Short, N. (2010). The remote sensing tutorial [web site]. *National Aeronautics and Space Administration (NASA), Goddard Space Flight Center*.

Sifakis, N., & Deschamps, P.-Y. (1992). Mapping of air pollution using SPOT satellite data. *Photogrammetric Engineering and Remote Sensing, 58*, 1433-1433.

Silva, C. A., Hudak, A. T., Vierling, L. A., Loudermilk, E. L., O'Brien, J. J., Hiers, J. K., . . . Falkowski, M. J. (2016). Imputation of individual Longleaf Pine (Pinus palustris Mill.) Tree attributes from field and LiDAR data. *Canadian journal of remote sensing, 42*(5), 554-573.

Singh, K. K., Vogler, J. B., Shoemaker, D. A., & Meentemeyer, R. K. (2012). LiDAR-Landsat data fusion for large-area assessment of urban land cover: Balancing spatial resolution, data volume and mapping accuracy. *ISPRS Journal of Photogrammetry and Remote Sensing, 74*, 110-121.

Stats. (2001). *Ward definition.* Retrieved from http://archive.stats.govt.nz/methods/classifications-and-standards/classification-related-stats-standards/ward/definition.aspx

Stefanov, W. L., Ramsey, M. S., & Christensen, P. R. (2001). Monitoring urban land cover change: An expert system approach to land cover classification of semiarid to arid urban centers. *Remote sensing of Environment, 77*(2), 173-185.

Stumpf, A., & Kerle, N. (2011). Object-oriented mapping of landslides using Random Forests. *Remote sensing of environment, 115*(10), 2564-2577.

Suárez, J., Di Lucca, M., Goudie, J., Polsson, K., Xenadis, G., Gardiner, B., & Perks, M. (2009). An individual canopy delineation algorithm based on Object-Oriented segmentation and classification. *Silvilaser. Texas A&M University, College Station, Texas. http://forestry. oxfordjournals. org/Downloaded from*.

Suárez, J. C., Ontiveros, C., Smith, S., & Snape, S. (2005). Use of airborne LiDAR and aerial photography in the estimation of individual tree heights in forestry. *Computers & Geosciences, 31*(2), 253-262.

Tan, Q., & Johansen, S. (2011). Evaluation of urban vegetation mapping using high spatial resolution image: pixel versus object classification comparison [J]. *Journal of Basic Science and Engineering, 3*, 011.

Tang, S., Dong, P., & Buckles, B. P. (2012). A new method for extracting trees and buildings from sparse LiDAR data in urban areas. *Remote sensing letters, 3*(3), 211-219.

Thanh Noi, P., & Kappas, M. (2017). Comparison of Random Forest, k-Nearest Neighbor, and Support Vector Machine Classifiers for Land Cover Classification Using Sentinel-2 Imagery. *Sensors, 18*(1), 18.

The World Bank. (2016). *Urban population.* Retrieved from https://data.worldbank.org/indicator/SP.URB.TOTL?end=2017&start=1960&view=chart

Tian, J., & Chen, D. M. (2007). Optimization in multi‐scale segmentation of high‐resolution satellite images for artificial feature recognition. *International Journal of Remote Sensing, 28*(20), 4625-4644.

Tseng, Y.-H., Wang, C.-K., Chu, H.-J., & Hung, Y.-C. (2015). Waveform-based point cloud classification in land-cover identification. *International Journal of Applied Earth Observation and Geoinformation, 34*, 78-88.

Voltersen, M., Berger, C., Hese, S., & Schmullius, C. (2014). Object-based land cover mapping and comprehensive feature calculation for an automated derivation of urban structure types at block level. *Remote Sensing of Environment, 154*, 192-201.

Walker, J., & Blaschke, T. (2008). Object‐based land‐cover classification for the Phoenix metropolitan area: Optimization vs. transportability. *International Journal of Remote Sensing, 29*(7), 2021-2040.

Wang, Z., & Schenk, T. (2000). Building extraction and reconstruction from lidar data. *International Archives of Photogrammetry and Remote Sensing, 33*(B3/2; PART 3), 958-964.

Wentz, E. A., Stefanov, W. L., Gries, C., & Hope, D. (2006). Land use and land cover mapping from diverse data sources for an arid urban environments. *Computers, Environment and Urban Systems, 30*(3), 320-346.

Wilson, E. H., & Sader, S. A. (2002). Detection of forest harvest type using multiple dates of Landsat TM imagery. *Remote Sensing of Environment, 80*(3), 385-396.

Wu, B., Yu, B., Wu, Q., Huang, Y., Chen, Z., & Wu, J. (2016). Individual tree crown delineation using localized contour tree method and airborne LiDAR data in coniferous forests. *International Journal of Applied Earth Observation and Geoinformation, 52*, 82-94.

Wulder, M., Niemann, K. O., & Goodenough, D. G. (2000). Local maximum filtering for the extraction of tree locations and basal area from high spatial resolution imagery. *Remote Sensing of environment, 73*(1), 103-114.

Xiubin, L. (1996). A review of the international researches on land use/land cover change [J]. *Acta Geographica Sinica, 6*.

Xu, C., Morgenroth, J., & Manley, B. (2017). Mapping Net Stocked Plantation Area for Small-Scale Forests in New Zealand Using Integrated RapidEye and LiDAR Sensors. *Forests, 8*(12), 487.

Yan, W. Y., Shaker, A., Habib, A., & Kersting, A. P. (2012). Improving classification accuracy of airborne LiDAR intensity data by geometric calibration and radiometric correction. *ISPRS Journal of Photogrammetry and Remote Sensing, 67*, 35-44.

Yang, L., Xian, G., Klaver, J. M., & Deal, B. (2003). Urban land-cover change detection through sub-pixel imperviousness mapping using remotely sensed data. *Photogrammetric Engineering & Remote Sensing, 69*(9), 1003-1010.

Yoon, J.-S., Shin, J.-I., & Lee, K.-S. (2008). Land cover characteristics of airborne LiDAR intensity data: A case study. *IEEE Geoscience and Remote Sensing Letters, 5*(4), 801-805.

Yu, Q., Gong, P., Clinton, N., Biging, G., Kelly, M., & Schirokauer, D. (2006). Object-based Detailed Vegetation Classification with Airborne High Spatial Resolution Remote Sensing Imagery. *Photogrammetric Engineering & Remote Sensing, 72*(7), 799-811.

Yuan, F. (2008). Land‐cover change and environmental impact analysis in the Greater Mankato area of Minnesota using remote sensing and GIS modelling. *International Journal of Remote Sensing, 29*(4), 1169-1184.

Yuan, F., Sawaya, K. E., Loeffelholz, B. C., & Bauer, M. E. (2005). Land cover classification and change analysis of the Twin Cities (Minnesota) Metropolitan Area by multitemporal Landsat remote sensing. *Remote sensing of Environment, 98*(2-3), 317-328.

Zhang, C., Zhou, Y., & Qiu, F. (2015). Individual tree segmentation from LiDAR point clouds for urban forest inventory. *Remote Sensing, 7*(6), 7892-7913.

Zhang, L., Huang, X., Huang, B., & Li, P. (2006). A pixel shape index coupled with spectral information for classification of high spatial resolution remotely sensed imagery. *IEEE Transactions on Geoscience and Remote Sensing, 44*(10), 2950-2961.

Zhang, T., Li, Q., Yang, X., Zhou, C., & Su, F. (2010). *Automatic mapping aquaculture in coastal zone from TM imagery with OBIA approach.* Paper presented at the Geoinformatics, 2010 18th International Conference on.

Zhang, W., Tan, G., Zheng, S., Sun, C., Kong, X., & Liu, Z. (2018). Land Cover Change Detection in Urban Lake Areas Using Multi-Temporary Very High Spatial Resolution Aerial Images. *Water, 10*(2), 1.

Zhen, Z., Quackenbush, L. J., Stehman, S. V., & Zhang, L. (2015). Agent-based region growing for individual tree crown delineation from airborne laser scanning (ALS) data. *International Journal of Remote Sensing, 36*(7), 1965-1993.

Zhen, Z., Quackenbush, L. J., & Zhang, L. (2016). Trends in automatic individual tree crown detection and delineation—evolution of lidar data. *Remote Sensing, 8*(4), 333.

Zhou, W. (2013). An object-based approach for urban land cover classification: Integrating LiDAR height and intensity data. *IEEE Geoscience and Remote Sensing Letters, 10*(4), 928-931.

Zhu, X. (2013). Land cover classification using moderate resolution satellite imagery and random forests with post-hoc smoothing. *Journal of Spatial Science, 58*(2), 323-337.

Zhu, X., & Toutin, T. (2013). Land cover classification using airborne LiDAR products in Beauport, Québec, Canada. *International Journal of Image and Data Fusion, 4*(3), 252-271.

Appendix A: nDSM comparison

This appendix provided detailed information for the comparison between two algorithms for LiDAR surface interpolations. The purpose of this comparison is to test which algorithm can produce better LiDAR surface for this study. According to the final result, triangulate interpolation was adopted.

ArcGIS is one of the most popular GIS tools

When creating LiDAR-derived surfaces, two interpolation approaches, binning and triangulation were compared. The binning approach is available in ArcGIS 10.4 package. It uses cell assignment and void fill method to create raster surfaces. In this study, the average value of LiDAR points fell within the specified pixel size (1×1 m) was assigned to the DEM pixels while the maximum value was assigned to the DSM pixels. When there is no point in a pixel, the value was interpolated by natural neighbour algorithm.

The triangulation approach interpolates points temporarily into a triangular irregular network (TIN), and then samples the TIN onto a raster. In LAStools, this approach was achieved with LAS2DEM function. When interpolating raster surfaces, 50 meter buffers around the TIN in each tile were created. This can eliminate boundary errors by sampling raster surface from a TIN with a larger size. Another parameter of LAS2DEM,'thin with grid' was set as 0.5, which only keeps points within every 0.5 m^2 to save processing time and computing memory.

After that, nDSMs generated with these two approaches were compared by subtraction. For most area, the values were close. Significant differences only existed in high density tree and roof areas. Intersections were then made across those places to further assess qualities of two raster surfaces. Figure A-1 shows that some small gaps between tree crowns were filled in the nDSM produced by the binning approach. In another the surface, by comparison, vertical structures of individual tree were better delineated. The same differences also occurred in high density roof areas. Small gaps between roofs were missed by the binning approach but detected with the triangulation approach. In summary, the binning approach produced smoother surfaces, while the triangulation approach provided more detailed information and have a higher accuracy. Therefore, nDSM produced by triangulation approach was used for the classification in this study.

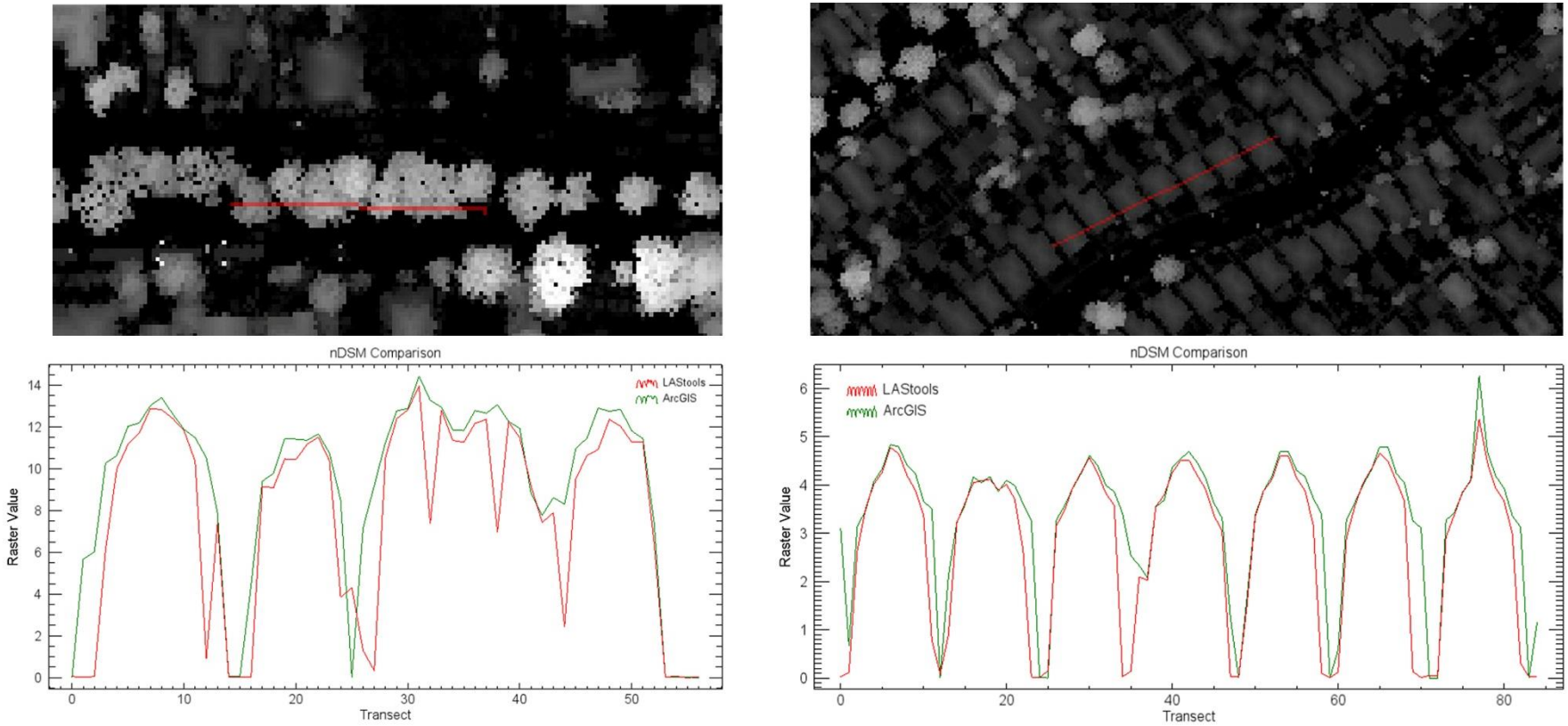

Figure A-1. nDSM comparison for dense tree areas (left) and dense roof areas (right)

Appendix B: Classifier comparison

This Appendix provide detailed information for all the classifiers that are available in eCognition packages. The purpose for this test is to choose a classifier that is both efficient and accurate in finishing the tasks in this study.

For this study, several factors needed consideration when selecting a classifier:

1. Large data size (hundreds of GBs).
2. A considerable number of features (spectral, texture, shape)
3. Heterogeneity of the urban landscape and high-resolution data, both of which can introduce noise.

Based on these requirements, RF is likely to be the best classifier because it has advantages such as quick processing time, available for large feature inputs, less affected by noise and have no overfitting issues, etc (Belgiu & Drăguţ, 2016; Gislason et al., 2006; Pal, 2005). Some studies also discussed advantages of RF by comparing with various classifiers using different datasets. However, no single study has compared SVM (support vector machine), RF, KNN (K-nearest neighbour), Bayes and DT (decision tree) classifiers at the same time. These are five classifiers that are available in the eCognition software for the OBIA. From a methodological perspective, it is worth comparing RF with other four classifiers to choose the most suitable one for this study.

A sample area that accounts for 5% of total study area was used to test the performance of these five classifiers. In an attempt to ensure that this area was representative of the complete study area, it was set as a narrow rectangular and covers an area spanning from the city centre to the edge of the city. Other steps such as sample selection and image segmentation were followed as same criteria in the final classification. Parameters setting for RF was discussed in Method part and for other four classifier, default settings were used because these values are most commonly used and set by empirical tests (Table B-1).

Table B-1. Parameter setting of classifiers

Classifier	Parameter Settings
RF	number of trees: 500 selected features for each node: square root of total features
SVM	kernel type: linear C parameter: 2
KNN	k value: 1
DT	Maximum categories: 16 Tree not pruned
Bayes	not available

Table B-2. Classifier comparison

Classifier	RF	SVM	KNN	DT	Bayes
Overall accuracy	91.05%	90.22%	84.55%	80.77%	79.11%

Considering overall accuracy (described in section 3.2.6 Accuracy Analysis), the result of the subsample classification showed that RF has the highest overall accuracy (91.05%) compared with other classifiers (Table B-2). KNN, DT, and Bayes produced much lower accuracies, ranging from 79.11-85.55%. SVM produced nearly as high an accuracy as RF accuracy, but its parameterization is more complex than that of RF (Foody, 2004). In this experiment, the processing time of RF also showed faster than that of SVM (about 2 times).As a result of high accuracy, simple parameterisation, and rapid processing, RF was selected as the classifier for the complete study area.

Appendix C: Land cover change maps

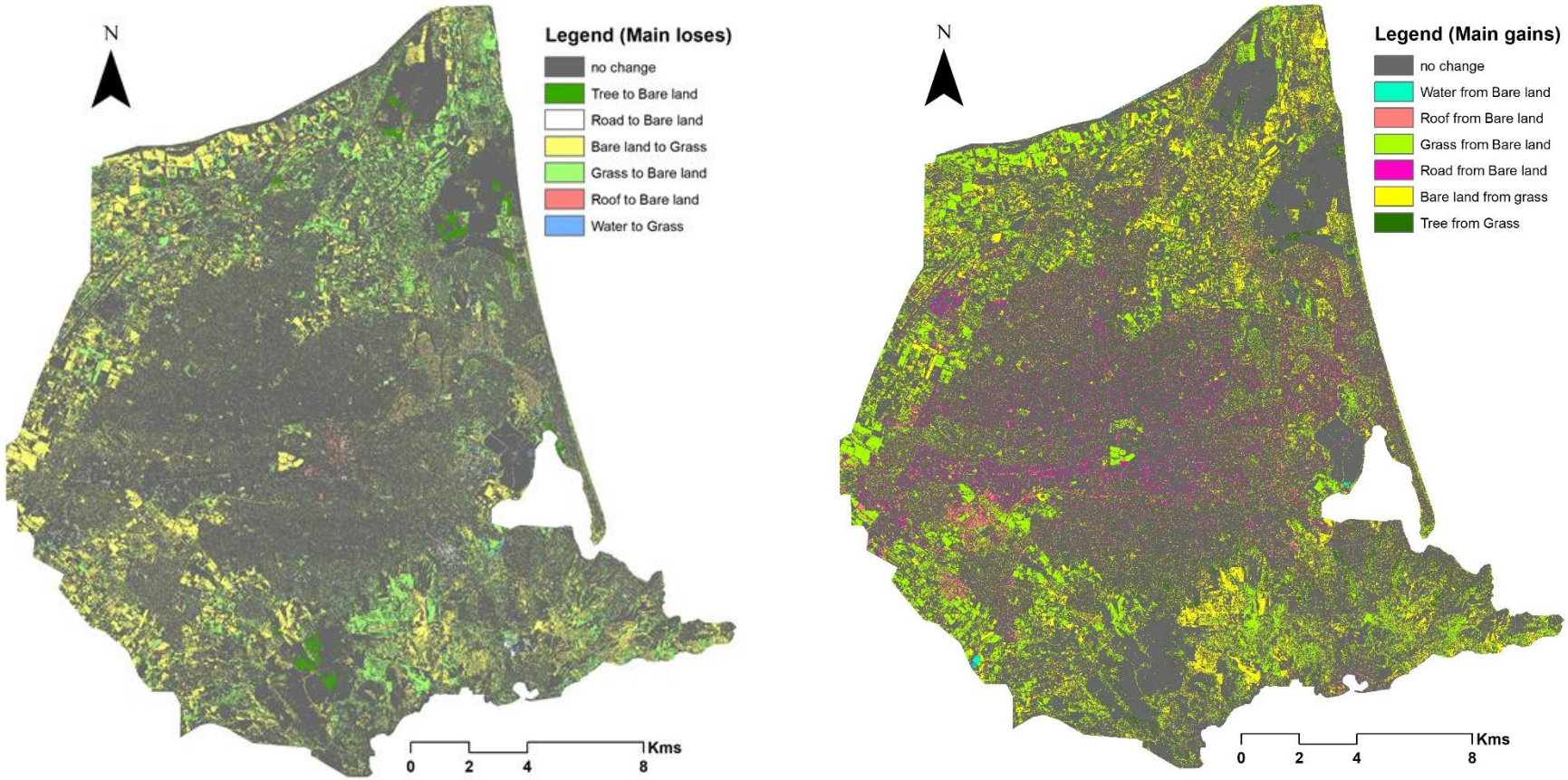

Figure C-1. Land cover change maps

Appendix D: TCS and LCT tables

Table D-1. Total change statistics (km²)

(Shadow excluded)	Tree	Road	Bare land	Grass	Roof	Water
Net change	11.06	11.16	-18.93	-3.71	1.09	-0.66
2011 Statistics	51.81	21.33	119.61	100.14	33.61	4.54
2015 Statistics	62.87	32.49	100.67	96.43	34.69	3.87

Table D-2. Land cover transitions between 2011 and 2015

		2015(km²)							
		Shadow	Tree	Road	Bare land	Grass	Roof	Water	Sum
2011 (km²)	Shadow	4.07	6.23	0.88	3.17	4.03	0.96	0.08	19.42
	Tree	5.92	40.53	0.90	4.80	3.76	1.71	0.11	57.74
	Road	0.68	0.70	17.03	1.87	1.21	0.49	0.03	22.00
	Bare land	3.57	6.37	11.59	58.33	39.38	3.69	0.25	123.18
	Grass	5.65	12.91	1.79	32.28	50.15	2.78	0.24	105.79
	Roof	1.14	2.20	1.13	2.85	1.39	26.01	0.03	34.74
	Water	0.17	0.15	0.05	0.55	0.55	0.02	3.22	4.71
	Sum	21.20	69.10	33.37	103.84	100.46	35.65	3.96	

Appendix E: Tree cover maps

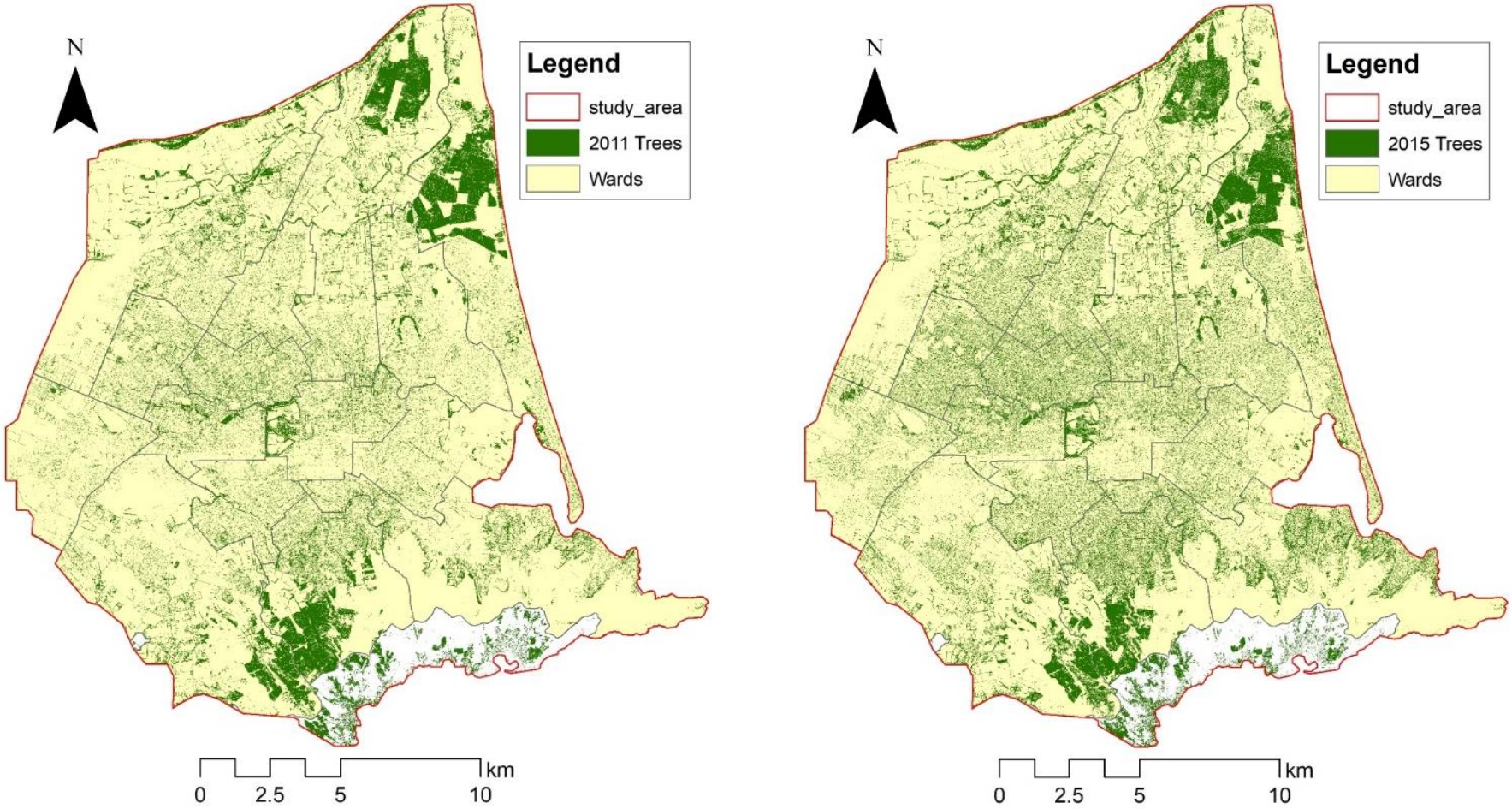

Figure E-1 Tree cover maps of 2011 (left) and 2015 (right)